Conversion of Carbon Dioxide and Biomass for Fuels and Chemicals Precursor through Gasification: Experimental and Modeling Approach

by

Narendra Sunil Sadhwani

A Dissertation submitted to the Graduate Faculty of
Auburn University
in partial fulfillment of the
requirements for the Degree of
Doctor of Philosophy

Auburn, Alabama
May 6, 2017

Keywords: Gasification, carbon dioxide, biomass,
fluidized bed, kinetics, ASPEN plus

Approved by

Mario R. Eden, Co-Chair, Professor, Department of Chemical Engineering
Sushil Adhikari, Co-Chair, Associate Professor, Department of Biosystems Engineering
Xinyu Zhang, Associate Professor, Department of Chemical Engineering
Allan David, Assistant Professor, Department of Chemical Engineering

Abstract

In the current scenario, the entire planet immensely depends on coal and petroleum based fuels for fulfilment of their power and liquid fuel needs. The consumption of these energy sources in such humongous amounts has led to a tremendous increase in environmental pollution. This not only affects human health but adds greatly to global warming by the release of greenhouse gases specially carbon dioxide (CO_2), which is a major component of flue gases from many industries. The ever- increasing energy demand coupled with environmental concerns has led to the development of alternate and renewable sources of energy. Renewable resources for power production like solar and wind have gained massive attention over the years. Biomass is an attractive option to fulfil not only our electric power needs but also liquid fuel demands. In addition to being renewable, biomass has the potential to recycle carbon dioxide (CO_2) into plant material. Power and fuel production from biomass is well adapted to the southeastern United States due to its abundant lignocellulosic biomass resources. Of the woody biomass feedstock, pine is the most likely feedstock for large-scale production as it accounts for 83 % of tree species in the aforementioned states. Biomass can be converted to biofuels through various pathways. These are broadly classified as biochemical (e.g. cellulosic-ethanol production) or thermochemical (combustion, gasification and pyrolysis) routes. Gasification is the process of partial combustion of biomass to produce a low calorific value gas, syngas, which is a combination of CO, H_2, CH_4 and CO_2 along with tar (condensable organic compounds) and other contaminants (NH_3, H_2S, HCN etc.). Syngas can be further converted into liquid fuel via Fischer-

Tropsch synthesis or fermentation. The syngas composition depends upon several factors such as type of biomass used, type of gasifier selected, type of bed material in the gasifier, gasifying media used and the operating condition (temperature, pressure, and equivalence ratio). These factors affect the primary syngas composition and the amount of tar and contaminants released during the gasification process, which need to be controlled for downstream use of the syngas produced.

On the other hand, recycling carbon dioxide is of prime importance due to the harmful effects mentioned earlier. Carbon sequestration using different avenues has been the focus of various studies. Using CO_2 for gasification serves a dual purpose i.e. reducing pollution and generating syngas and is beneficial both environmentally and economically. Therefore, this research work focuses on exploring the application of carbon dioxide as a gasifying agent in gasification of pine.

Chapter 1 provides an introduction to the importance of this process, motivation behind the study and a sneak peek into the objectives of the research. Chapter 2 is a detailed review of literature around this topic. Chapter 3 comprises of the work done towards the first objective: understanding the effects of temperature variation (700^{o}C, 790^{o}C, 850^{o}C and 934^{o}C) and change in CO_2/C ratios (0.6, 0.8, 1.04 and 1.52 w/w) on the biomass–CO_2 gasification process. An extension of the objective was to analyze the syngas component evolution trends and postulate the reactions dominating the process. The process was carried out in a bench scale atmospheric bubbling fluidized bed gasifier with sand as bed material. The gasifying agent carbon dioxide was fed along with nitrogen which acted as a carrier gas and helps achieve fluidization velocities. The effect of change in process variables was evaluated in terms of (i) yield of product streams [char, liquid and gas], (ii) syngas composition, (iii) carbon balance and, (iv) syngas heating value.

The concentration of both hydrogen (H_2) and carbon monoxide (CO) increase with increase in temperature. The climb in the value of H_2 yield is fairly steep at 850^oC. The yield of methane (CH_4) did not change significantly through the temperature range. Water gas reaction, Boudouard reaction and methane dry reforming reactions were hypothesized to be the main reason leading to these trends of the components. Change in CO_2/C ratio had a significant effect on the yields of the output syngas components. Similarly, the yield of lower hydrocarbons (methane, ethylene and acetylene) showed a statistically significant amount of change. The results obtained from this work were compared in detail to an oxygen gasification study from literature performed on the same experimental setup.

The second objective of the research is outlined in Chapter 4 which focuses on the interpretation of the kinetics of char–CO_2 gasification step. The process was carried out employing a fixed bed reactor setup with gas analyzer. Nitrogen and CO_2 entered the reactor after it has been heated up to gasification temperature. The conversion of char was calculated based on the amount of CO in the output gas. The conversion–time data were fitted using three empirical solid–gas reaction models viz. volume reaction model (VRM); non-reactive core model (NRC) and random pore model (RPM). The kinetic parameters were calculated for all the three models. Regression analysis demonstrated that RPM was the best at predicting experimental data. For confirmation, the measured BET surface area of chars obtained at various conversion points was plotted alongside the surface area change predicted by the RPM. The trend and values of the plot appeared to be in agreement. The values of the kinetic parameters calculated using RPM are: activation energy (Ea) = 219 kJ/mol and natural logarithm of frequency factor (ln A) = 5.13 1/s. The second part of this objective was to understand the effect of alkali and alkaline earth metals (sodium, magnesium, potassium and calcium) on the char-CO_2

gasification step. Chars impregnated with four different metal catalysts were gasified and the random pore model was used to calculate the activation energy for each catalyst. The reactivity of the loaded chars was found to be in the order of: K-char > Ca –char > Na –char ≥ Mg –char.

Chapter 5 deals with the modeling part of the research. An ASPEN plus model was developed to simulate the steady state performance of the fluidized bed gasification unit used in the experiments. Knowledge accrued from the experimental objectives was used to improve the performance of the model. Different reactors were used to simulate various steps in the gasifier and a FORTRAN subroutine was dynamically linked to include the kinetics. Parameters such as output syngas composition, individual gas yields, syngas higher heating value and carbon conversion are compared to evaluate the validity of the model. The results were then compared to experimental data and a preliminary two stage model using Gibbs free energy minimization. The comparison showed that the model including kinetics predicted the experimental data with much better accuracy as compared to the thermodynamic equilibrium model.

Acknowledgements

In the fall of 2011, when I joined Auburn University as a graduate student, I had no idea how the journey over the next few years would pan out. In the pursuit of my PhD, I found many successes and faced some failures over the years. However, the support of all the people who had faith in me was undeterred though thick and thin. This created an environment for me to feel more confident and thrive in my journey to academic success. It is, therefore, really important for me to show my appreciation and gratitude for all the people who have always supported me and believed in me.

To begin with, I would like to express my sincere gratitude to my advisors, Dr. Sushil Adhikari and Dr. Mario Eden for their immense support, patience, advice and encouragement. I cannot imagine how difficult this journey would have been without their unwavering support and guidance during crucial times. Their work ethic coupled with their high standards for teaching and research served as a constant source of inspiration for me throughout the years. The continuous encouragement provided by them motivated me to grow and develop as a researcher. In addition, the financial support to attend various national level conferences helped me expand my professional network and become a good presenter.

I would also like to thank my committee members, Dr. Allan David and Dr. Xinyu Zhang for their insightful comments, discussions and suggestions. I appreciate the support provided by Dr. Christopher Roberts, Dr. Rui Xu and Dr. Michael Miller in completion of specifics projects during the course of my research. Additionally, I thank Dr. Steven Taylor for agreeing to serve

as the University reader on my dissertation committee. Dr. Taylor has been very involved in the biofuel research and a constant source of support in spite of his busy schedule. His constant metaphorical ‘pat on the back’ for me after I won the Three Minute Thesis competition in 2014 will always remain a memory to cherish.

My teammates and colleagues in the lab were a major part of my research work. The everyday technical discussions interspersed with some friendly banter served as a motivation for me. I would specially like to thank Dr. Nourredine Abdoulmoumine and Dr. Avanti Kulkarni for creating an environment of friendship and support during my initial days in the lab. Special thanks to Dr. Zhouhong Wang for serving as a major part of the kinetics project. In addition, I thank Dr. Oladiran Fasina’s research group for all the help with the operation of lab equipment.

I am extremely grateful to the funding agencies NSF-IGERT, USDA-NIFA, IBSS that provided financial support for the various projects during the course of this research. A very special thanks to the GRSP program by AL-EPSCoR for helping me with annual fellowship for three years in a row. Not only was the funding a major help, the opportunity to attend their annual conference to present my research and meet the various professionals from other fields was a valuable experience.

Saving the best for last, I would like to appreciate the love and support of my family and friends who have stood by me in tough times. My parents Sunil and Komal Sadhwani, served as a source of encouragement every single day. I would turn to their comfort in happiness and in pain. They have engrained in me all the values that have made me what I am today. They had the biggest smiles when I succeeded and showed immense support when I didn’t. Words will never be sufficient in describing their contribution in my life. My sisters Pooja Sadhwani and Varsha Parvekar always put a smile on my face every time I spoke to them.

My sincere gratitude to Jasmine and Smita Naik for treating me as a family over the last four years. Your love and support has made me miss my family in India a little less. Thank you for all the gifts and packages all these years that have reminded me how blessed I am to have you people in my life.

A very special thanks to Shraddha Praharaj for the love you showered me with over the last three years. Every moment with you motivated me to become a better person. From your support during the 3MT period to helping me mange my time and finances, your contribution is undeniable. You are the best thing to have happened to me in Auburn.

Last but not the least, immense gratitude to the international student organization family, Tapas, Kinsey, Demi, Shankharupa, Ning, Shamim, Jacob and others. Thank you for making me happy every time I got an opportunity to attend and organize the events. I will forever cherish the memories.

Table of Contents

List of Figures

List of Tables

Chapter 1
Introduction

1.1 Background

Coal and petroleum based fuels are the main source of carbon and energy for the entire world. Most of the world's liquid fuel and electricity demand is quenched through these sources. The energy demand is constantly increasing demand from developing and developed countries alike to satisfy the needs of ever-growing population.[1] Coal has been the most attractive option for electricity producers worldwide as it is cheap and easily available.[2] According to the December 2016 monthly energy review by the U.S. energy information administration,[3] coal was the major contributor (33.2%) to the overall electricity production followed by natural gas (32.7%) in 2015. In addition, fossil fuels constitute a major chunk of the transportation fuels being used today. Nearly 92% of the fuels for transportation purposes come from petroleum and another 3% is contributed by natural gas. Figure 1 shows the sources for overall energy production in the US in 2015. Natural gas and its derivatives contributed more than 30 quadrillion BTU to the total energy production whereas renewable sources of energy (hydroelectric, wind, solar, biomass and others) contributed a total of 9.5 quadrillion BTU. The annual energy outlook 2015 report projects that the country's energy demand will steadily rise and will reach 105 quadrillion BTU by 2040. The consumption of fossil fuels will continue to increase in accordance with this demand. [4]

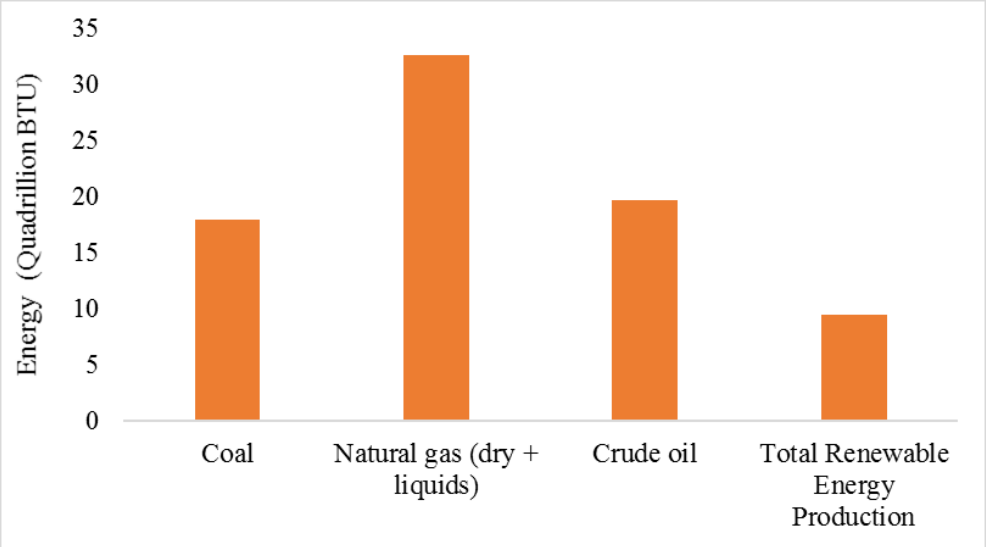

Figure 1- 1 Energy production sources in 2015

The biggest issue with the prolonged and continued dependence on fossil fuels is the environmental concerns that it raises. The combustion of these fuels release NOx, Sox and mainly CO_2 into the atmosphere. Carbon dioxide is the major constituent of the flue gas from many industries. Also, CO_2 is one of the major greenhouse gases that lead to global warming.[5] The level of CO_2 in the atmosphere has been on the rise constantly due to the increased consumption of non-renewable fuels. Figure 1-2 shows the Keeling curve by the Scripps Institution of Oceanography, which depicts the change in the level of carbon dioxide in the atmosphere over the years as measured at Mauna Loa observatory in Hawaii. Over the last 55 years, the concentration of CO_2 has increased from 320 ppm to 400 ppm.[6]

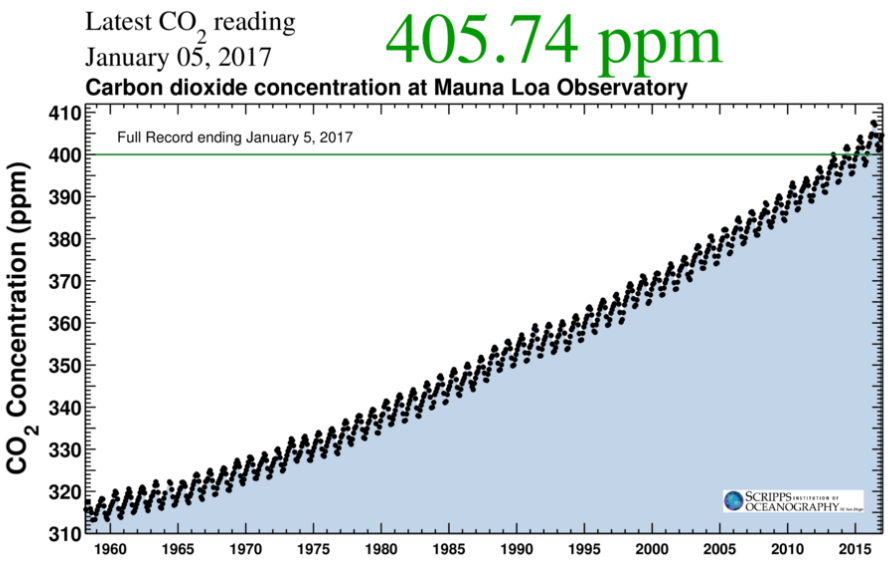

Figure 1- 2 The Keeling curve
[copied for illustration. Source: www.scripps.ucsd.edu]

Coal and petroleum based fuels along with natural gas are the largest sources of carbon dioxide emissions. The combined annual CO_2 emissions from these sources in 2017 is forecasted to be 5,350 million metric tons for the United States. Figure 1-3 shows the annual CO_2 emissions for the past two years and the forecast for 2017.

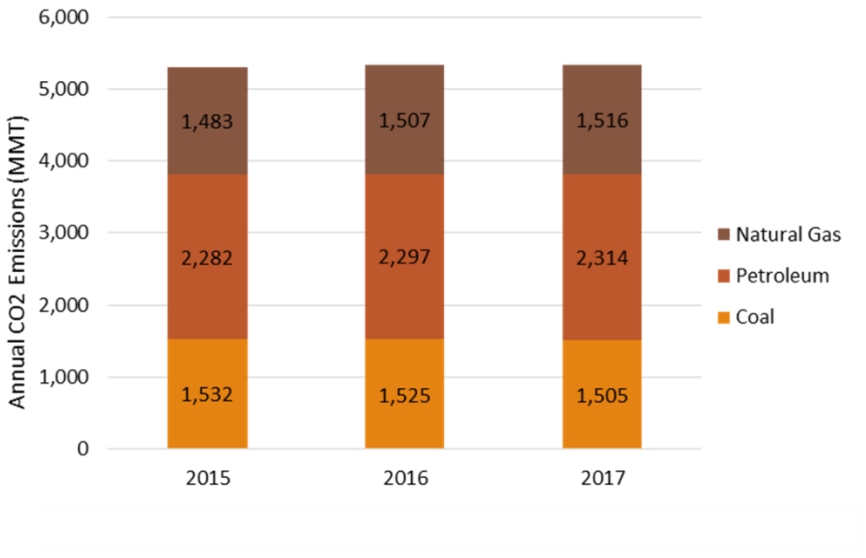

Figure 1- 3 Sources of CO_2 emissions

A continuous economic growth scenario considered by the annual energy outlook report projects that by the year 2040; an additional 550 million metric tons of CO_2 will be added to the atmosphere per year as compared to the emissions today.[4] This continuous increase in CO_2 concentration will lead to a rise in the global average temperature which could go beyond the internationally agreed 2^{o}C threshold. These reasons have led to an increased focus on the research and development of renewable and sustainable energy resources. Various renewable sources of electricity such as solar, wind, hydro and geothermal cannot be used to fulfil liquid fuel demand. However, biomass has the capability to serve as a source of electric power as well as liquid fuels. Due to its biological origin, biomass is considered renewable. The 2011 Billion-Ton update predicts that agricultural and forest lands from across the country can sustainably produce over a billion tons of biomass annually in the U.S., all by developing underutilized land resource while still meeting forecasted demands for food, feed and fiber resources. Also, with continued developments in bio-refinery capacity and technology, the feedstock resources identified in the report could produce about 85 billion gallons of biofuels. That amount is enough to replace approximately 30 percent of the nation's current petroleum consumption by 2030.[7]

1.2 Research motivation

In addition to being renewable, biomass is considered carbon-neutral. The CO_2 produced during the consumption of biofuels can be absorbed by biomass through photosynthesis during its growth. This implies that there is no extra carbon released into the atmosphere. If the biomass is supplied sustainably, the carbon neutral cycle resolves the environmental challenges of CO_2 emissions derived from fossil fuel and their dangerous effects on the global climate. Biomass can be converted to biofuels through various pathways. These are broadly classified as biochemical (e.g. cellulosic-ethanol production) or thermochemical routes (combustion, gasification and

pyrolysis). Direct combustion of biomass feedstock results in the production of energy and fuel-bound nitrogen and sulfur being converted to NO*x* and SO*x*. The combustion hot gas has been used for direct heating and steam production for electricity generation.[8,9,10] Pyrolysis is the heating of biomass in the absence of oxygen producing various organic liquids that can be manipulated or refined to make liquid fuel (bio-oil). This liquid crude oil is storable, transportable, and can potentially be processed in existing petrochemical infrastructures in a fashion much similar to petroleum crude to generate transportation fuels and chemicals. However, its chemical composition has led to difficulties in upgrading and caused technical and economic feasibility issues.[11] Gasification is the process of partial combustion of biomass to produce a low calorific value gas, syngas, which is a combination of CO, H_2, CH_4 and CO_2 along with tar (condensable organic compounds) and other contaminants (NH_3, H_2S, HCN etc.). The solid residue left behind after gasification is called char. Syngas can be used for power generation by combustion in power plants, production of chemicals through Fischer–Tropsch and methanol synthesis[12] and as a fuel like natural gas. Gasification is considered one of the more promising amongst the biofuel pathways due to high conversion and energy efficiency.[13] The concentration of various components in syngas depends on multiple factors like type of biomass fed, type of gasifier, type and flow rate of gasifying agent, process temperature, type of bed material etc.

Carbon dioxide was selected as the gasifying agent for this research because consuming CO_2 for gasification would benefit environmentally as well as financially. The literature for CO_2–biomass gasification is not as extensive as for air, oxygen or steam gasification.[14] An added advantage of the CO_2 gasification process is that the process can be coupled with a power plant or a conventional gasification unit to use up the flue gas CO_2. Additionally, the incentives for

reducing the carbon footprint can make this process an attractive option for energy producers. Lignocellulosic biomass such as agricultural and forest waste are found in abundance in the southeastern U.S. Pine was selected as the feedstock in this research because it is fairly common throughout the region and its cultivation is well established.[15] For this study, pine wood chips were obtained from a local plant in Opelika, Alabama. Pine sawdust and pine char with a particle size range of 150- 600 micron were used for the study.

1.3 Research proposal and objectives

This dissertation is presented as a series of 7 chapters. Chapter 1 presents a brief introduction of biomass gasification and a discussion of the research problems tackled in this project. It also outlines the research objectives as well as the rationale behind the specific objectives. In Chapter 2, a comprehensive literature review is presented that paves the way for the research project. Chapters 3, 4 and 5 deal with the specific objectives outlined in this proposal whereas chapters 6 and 7 outline the overall conclusion and future recommendations for this study. The main objective of this research is to get a profound understanding of the fundamentals of the biomass-CO_2 gasification process. Different experimental setups are used at various stages during the research depending upon the objective under investigation. Preliminary studies using smaller lab scale reactors were carried out to confirm the findings in literature and as a proof of concept. The research objectives specified in this work are outlined to understand the process in its entirety from the fundamental basics to the possibility of practical application. It is proposed in this project to carry out a comprehensive investigation of the impact of crucial gasification control parameters on the characteristics of the biomass–CO_2 gasification process and to explore the effect of certain catalytic elements on the process. Specifically, the following research objectives were targeted:

1.3.1 Objective 1. To understand the effect of temperature and CO_2/C ratio on the output of the process using a fluidized bed reactor setup.

Goal: The goal of this objective was to understand the effects of temperature variation (700^oC, 790^oC, 850^oC and 934^oC) and change in CO_2/C ratios (0.6, 0.8, 1.04 and 1.52) on the biomass–CO_2 gasification process. An extension of the objective was to analyze the syngas component evolution trends and postulate the reactions dominating the process.

Rationale: Over the years, various studies have looked into the gasification of biomass using CO_2 on TGA setup. They have investigated the effects of temperature, CO_2 partial pressure and the combination of CO_2 with other gasifying agents such as steam on the process.[16,17,18] However, certain fundamental heat and mass transfer problems associated with the TGA make it a rather dodgy candidate to study the performance of the process.[19,20,21]. On the other hand, fluidized bed gasifiers are known to ensure great heat and mass transfer due to the high degree of mixing inside the reactor. In addition, the amount of feedstock that can be processed is considerably higher.[22] There is a limited understanding of the effect of gasification conditions, like temperature and CO_2/C ratio, on the components of output syngas in biomass–CO_2 gasification in a fluidized bed. The rationale behind this objective was to carry out an in-depth investigation of gasification gas products at different conditions for pine as a benchmark for similar woody biomass feedstock. The results obtained from this study were compared to an oxygen gasification study performed on the same experimental setup to adjudge the differences between the two gasification media under same conditions.[23]

1.3.2 Objective 2. To understand the kinetics of char–CO_2 gasification step and to investigate the effects of alkali and alkaline earth metals on the process.

Goal: The goal of this objective is to interpret the kinetic performance of the pine char–CO_2 gasification step by fitting three different empirical models to the conversion–time data obtained from the process using a fixed bed reactor setup. The same procedure is to be carried out with catalyst loaded char to understand the effects of metal catalysts on the kinetic parameters of the process.

Rationale: During CO_2 gasification of biomass, the char conversion step is the rate limiting step.[24] Therefore studying the kinetics of the step is of vital importance. Several studies have tried to quantify the kinetic parameters using different methods.[25,26,27] Certain studies have investigated the effect of metal catalysts on gasification reactivity of coal.[28,29] However, none of the studies quantify the effect of metals by showing the corresponding change in kinetic parameters of the process. The rationale behind this objective is to calculate the kinetic parameters of the process and use them to accurately quantify the effect of metals (Na, Mg, K and Ca) on the process.

1.3.3 Objective 3. To develop a model simulating the performance of the biomass–CO_2 gasification process in a fluidized bed gasifier.

Goal: The goal of this objective is to develop a comprehensive model of the biomass–CO_2 gasification process using ASPEN plus that can simulate the steady state performance of the fluidized bed gasifier used for experiments.

Rationale: The performance of the biomass–CO_2 gasification process in a fluidized bed gasifier is studied earlier in this research. Some studies have simulated the process using mathematical

models including the kinetics of the reaction and tried to accurately predict the performance of the process.[30,31,32,33] An ASPEN plus model to predict the steady state performance of the process is to be developed. Various output parameters such as syngas composition, individual gas yields, syngas higher heating value and carbon conversion are to be compared with experimental data to adjudge the validity of the model. In addition, the model is compared to another model based on Gibbs free energy minimization to understand the effects of inclusion of kinetics on the predicted results.

Chapter 2
Literature Review

2.1 Introduction

Due to the constant dependence of human society on fossil fuels, and their negative effects on the environment; there has been a growing interest to find more sustainable alternatives for fulfilment of the energy demand. Various nations have taken steps towards achieving this goal by enacting laws and enforcing regulations on fuel quality and industrial emissions.[34,35] The Energy Independence and Security Act enacted in 2007 has laid out instructions and criteria for development of biofuel research as a measure to tackle the challenge of climate change.[36] Various agencies in the US have outlined the steps to be taken to regulate greenhouse gases, and biomass derived fuels are an important part of the measures suggested. The conversion of biomass to biofuels, bio-based chemicals and bioenergy is particularly attractive as it has the potential to replace petroleum derived liquid fuels while simultaneously producing power, heat and chemicals and promoting rural economies [37,38]. The carbon–neutral nature of biomass and biofuel cycle is a huge boost to the appeal of biomass as a renewable and sustainable alternative to the conventional sources of energy used today.[39] Figure 2-1 depicts the carbon–neutral nature of biomass.

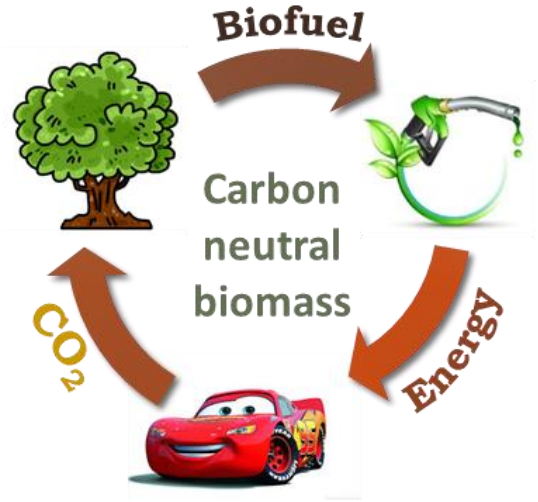

Figure 2-1: Carbon neutral cycle

Biomass is the widely available energy resource around the world, thus reducing the dependency on certain countries for fulfillment of energy demand. Depending on the type of crop chosen, the energy crops can help improve the quality of soil and reduce the amount of fertilizers and pesticides. Biomass cultivation for energy purposes can also help increase employment and benefit the economy[7]. The selection of technology used for conversion of biomass to biofuels is heavily dependent on the biomass type and the desired end product. One aspect of conversion of biomass is the transesterification of animal fats and plant-based oils to produce biodiesel (fatty acid methyl esters) which has the potential to economically replace a fraction of petroleum diesel [40,41,42]. Technologies for the conversion of lignocellulosic biomass to energy or bio-based chemicals and fuels are broadly classified into two categories: thermochemical and biochemical. Figure 2-2 gives a representation of the various conversion pathways, steps involved and the end–product obtained after the series of conversions.[43] The figure shows the variety of bio-products that can be produced from biomass.

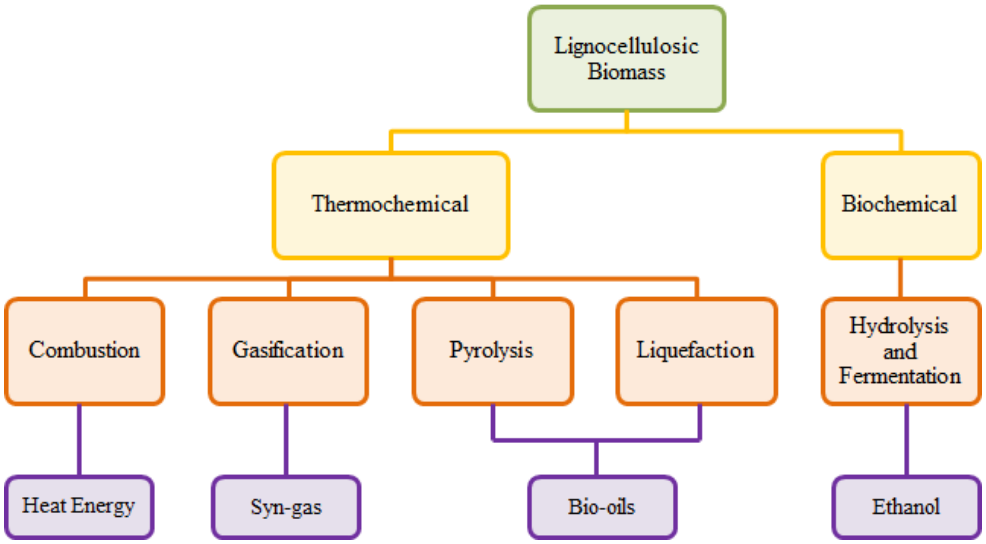

Figure 2- 2: Biomass to biofuel conversion pathways

2.2 Thermochemical conversion techniques

The thermochemical platform focuses on the use of heat as a primary means of converting biomass with or without the use of other agents. The aim here is to convert biomass into power or ready to use fuels and other intermediate products that can be used as feedstocks for other downstream chemical processes[44]. The main thermochemical technologies commonly considered for biomass conversion are pyrolysis, gasification, hydrothermal liquefaction and combustion. Combustion is an exothermic reaction between biomass and oxygen to produce H_2O and CO_2. The heat released during combustion is the source of energy through this pathway. The heat obtained can be converted in to mechanical or electrical power. Co-combustion of coal and biomass to achieve higher conversion has been a topic of interest for various studies[45,46,47]. In contradiction, pyrolysis is the heating of biomass in absence of oxygen producing various condensable and non-condensable gases and char. Condensable gases yield organic liquids that can be manipulated or refined to make liquid fuel (bio-oil). Various studies have investigated the change in the yield of pyrolysis products by changing the vital process parameter like temperature and residence time of biomass[48]. The main aim is produce a product that can be

processed using the existing infrastructure of petroleum refineries [49,50,51]. Hydrothermal liquefaction is a process of obtaining liquid fuels from biomass by directly mixing biomass with water at high temperatures and pressures. This process is well adapted to biomass feedstocks with high moisture content as it avoids the need for drying, like algae. The end–product obtained in this step is also known as bio–oil [52,53].

2.3 Fundamentals of biomass gasification

Gasification lies between pyrolysis and combustion in terms of the amount of oxygen consumed during the process. The energy efficiency in case of gasification is higher than in case of combustion [13]. Gasification is defined as the partial combustion of carbonaceous material to produce a low calorific value gas, syngas along with char, tar (condensable organic compounds) and other contaminants. The typical range of temperature for gasification is 650^{o}C to 1500^{o}C [54]. The major constituents in syngas are carbon monoxide (CO), carbon dioxide (CO_2), hydrogen (H_2), methane (CH_4), non-condensable hydrocarbons (C_1-C_4), and water (H_2O). Syngas can either be directly burned to obtain heat power or can be converted into liquid fuels like gasoline and diesel by various synthetic routes [55,12]. The syngas produced can also be used in a gas turbine to obtain electricity, combusted in the internal combustion engine or can be integrated with the combustion cycle to result in more efficient commercial technology [56]. These various applications give gasification technology an edge over other thermochemical conversion processes. However, there are several challenges associated with development of this technology for large-scale energy production [57].

Various gases can be used as gasifying/oxidizing media for the process of gasification including air, oxygen, steam, carbon dioxide or combinations of these. The amount of oxidizing agent supplied for air and oxygen is measured as equivalence ratio (ER) and for steam and CO_2

is measured as steam to biomass ratio (S/B) and CO_2 to biomass or carbon ratio (CO_2/C). When air is used as gasifying agent, considerable amount of nitrogen could appear in the output syngas thus diluting the concentration of other components. The product distribution as well as the composition of the syngas depends on several parameters including operating conditions, feedstock and gasifier design.

Biomass undergoes three major steps during the process of gasification. These steps are: I) biomass drying, II) devolatilization, and III) char reactions and gas–phase reactions. Figure 2-3 demonstrates the steps that occur during the biomass gasification process.

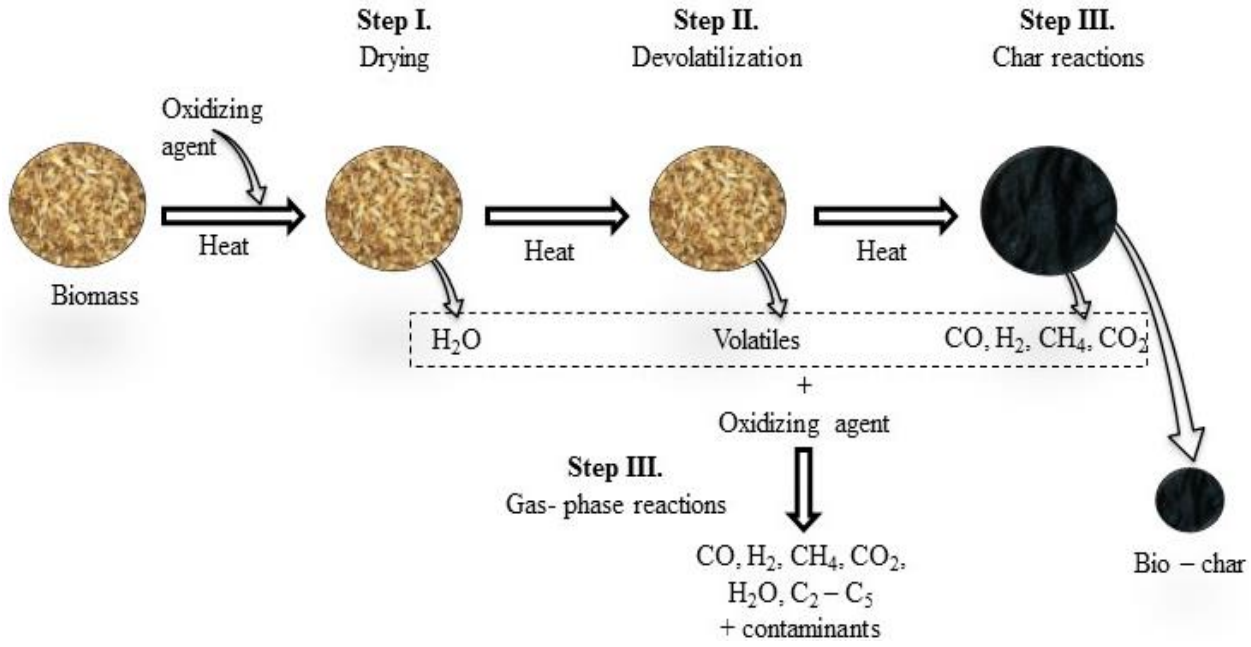

Figure 2- 3. Steps during biomass gasification

Moisture from the biomass is removed during the first step which occurs at or above 100^{o}C. Moisture removal uses up tremendous amounts of energy which is not recoverable and hence a lower moisture content biomass (below 15%) is advised [58]. Devolatilization of biomass occurs between 150^{o}C and 600^{o}C. During this step, thermal breakdown of biomass occurs leading to formation of char, gaseous products and tars. Char and gas phase reactions occur

above 700°C. Char reacts with the oxidizing agent to produce carbon monoxide, steam, carbon dioxide, oxygen and hydrogen in the gasifier. Similarly, the products of step two undergo partial oxidation to produce the gaseous products. Nitrogen in biomass is converted to ammonia (NH_3), hydrogen cyanide (HCN) and oxides of nitrogen (NO, NO_2, N_2O and other NOx) [59]. Sulfur is converted primarily to hydrogen sulfide (H_2S), carbonyl sulfide (COS), carbon disulfide (CS_2) and other minor sulfur containing compounds with H_2S being the most dominant in gasification [60]. Halogens, like chlorine in biomass feedstocks, are released as hydrogen halides such as hydrogen chloride (HCl). Nitrogen, sulfur and halide compounds act as contaminants in syngas because they cause problems downstream. Nitrogen compounds lead to NOx emissions whereas sulfur and halides lead to equipment corrosion.

2.4 Important gasification characteristics

2.4.1 Gasification chemistry

Vital gasification operating conditions like temperature and amount of oxidizing agent are important in determining the composition of the output syngas and other performance indicators like heating value, gas yield, gas efficiency, and carbon conversion. The impact of the operating parameters is influenced by a change in the reactions occurring inside the gasifier. Gasification is governed by a multitude of reactions which occur at different stages during the process. Key gasification reactions that are important for the narrative of this process are [61]:

Combustion reactions	$C + ½\ O_2 \leftrightarrow CO$	ΔH = -111 kJ/mol	[2.1]
	$CO + ½\ O_2 \leftrightarrow CO_2$	ΔH = -283 kJ/mol	[2.2]
	$H_2 + ½\ O_2 \leftrightarrow H_2O$	ΔH = -242 kJ/mol	[2.3]
Boudouard reaction	$C + CO_2 \leftrightarrow 2CO$	ΔH = +172 kJ/mol	[2.4]

Water-gas reaction	$C + H_2O \leftrightarrow CO + H_2$	$\Delta H = +131$ kJ/mol	[2.5]
Water-gas shift reaction	$CO + H_2O \leftrightarrow CO_2 + H_2$	$\Delta H = -41$ kJ/mol	[2.6]
Methanation Reactions	$C + 2H_2 \leftrightarrow CH_4$	$\Delta H = -75$ kJ/mol	[2.7]
	$CO + 3H_2 \leftrightarrow CH_4 + H_2O$	$\Delta H = -205$ kJ/mol	[2.8]
	$2CO + 2H_2 \leftrightarrow CH_4 + CO_2$	$\Delta H = -247$ kJ/mol	[2.9]
Methane steam reforming	$CH_4 + H_2O \leftrightarrow CO + 3H_2$	$\Delta H = +206$ kJ/mol	[2.10]

The combustion reactions occur as a result of free oxygen reaction with carbon or hydrogen to produce CO_2 and H_2O. Heat evolved from these reactions is used to drive the process. Other reactions such as Boudouard reaction and water–gas reaction (also called char reforming reaction) are highly endothermic reactions and occur at higher temperature during the gasification process. The rate of char–oxygen reaction is the highest followed by char–steam reaction and char–CO_2 (Boudouard) reaction [62,63]. A mechanism commonly used to describe the Boudouard reaction is the oxygen exchange reaction proposed by Ergun [64].

$$C_f + CO_2 \leftrightarrow C(O) + CO \qquad [2.11]$$

$$C(O) + C \leftrightarrow C(O) + C_f \qquad [2.12]$$

C_f denotes the free carbon active site and C (O) represents the reactive carbon–oxygen surface complex; it represents an occupied site. Based on this mechanism, CO_2 is first dissociated at a free carbon active site through which a reactive carbon–oxygen surface complex and a molecule of CO are created. In the next step, the carbon–oxygen complex produces a new vacant active site and another molecule of CO. This mechanism signifies the importance of number of active sites in char reactivity during CO_2 gasification. However, there is no universal method to measure the amount of active sites on a particle.

2.5 Feedstock for gasification

Feedstocks used for gasification can be broadly classified into four different categories: woody biomass, herbaceous biomass, agricultural residues and coal. The main difference from a gasification point of view is the composition of the feedstock. Coals are generally higher in carbon content as well as sulfur content and relatively lower oxygen content. Table 2.1 outlines proximate and ultimate analyses of a few biomass samples.

Table 2.1 Properties of gasification feedstocks used in various studies

	Woody biomass [65]	**Agriculture residue [66]**	**Herbaceous biomass [67]**	**Coal [68]**
	Pine	Corn Stover	Switchgrass	Lignite, New Zealand
Proximate analysis (wt% dry basis)				
Volatile matter	83.1	75.2	80.5	51.8
Fixed carbon	16.5	19.2	16.8	42.2
Ash	0.4	5.6	2.7	6
Ultimate analysis (wt% dry basis)				
C	47.1	43.7	50.6	50.6
H	6.5	5.6	5.9	3.7
N	0.5	0.61	1.7	0.5
O	45.5	43.3	38.7	45.2

The table shows variation in properties of feedstock used for gasification studies. As can be expected, these differences will have implications on the gaseous primary products as well as

conversion efficiencies. Various other feedstocks such as municipal and industrial wastes have been used as feedstocks in literature but are not discussed here due to wide variability in their composition and their low potential for usage at a large scale. Other factors including availability and its growth rate (for biomass) are considered while selecting a feedstock for large scale gasification projects.

2.6 Effect of operating conditions on primary gases and gasification performance

2.6.1 Temperature

Temperature of gasification process is a very important in determining the composition of the output syngas, carbon conversion and contaminants [69]. Various gasification reactions are thermodynamically feasible only at or above a certain temperature. Figure 2-4 shows the variation of syngas component concentration and yield with increase in temperature for an oxygen gasification study in a fluidized bed reactor.[23] As temperature increases, the concentration of CO and H_2 increases whereas the concentration of CO_2, CH_4 and other lower hydrocarbons decreases. This is consistent with the increased activity of Boudouard reaction as it is thermodynamically favored at higher temperatures.

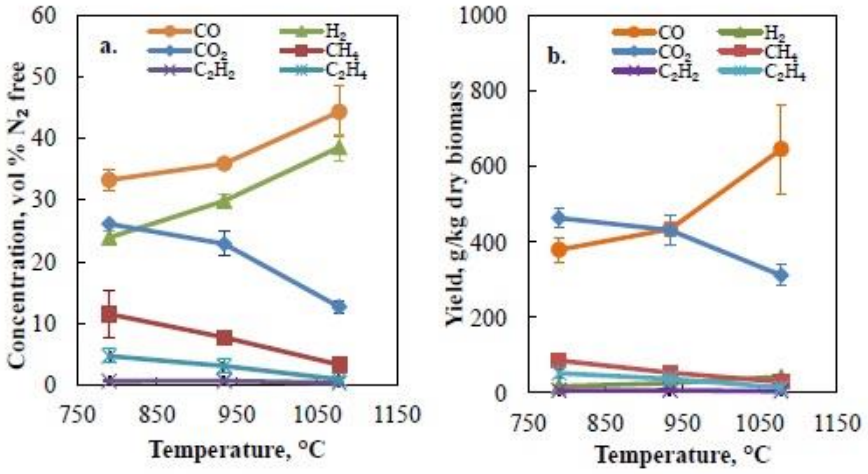

Figure 2- 4 Effect of temperature on primary gases
[copied for illustration. Source: Abdoulmoumine et al.[23]]

Variation in temperature also has an effect on carbon conversion, syngas heating value and gas efficiencies. Other studies with air as gasifying media show a clear trend of increase in CO, and decrease in CO_2. These studies also depict a trend of increase in hydrogen at the cost of methane. These primary syngas components affect the syngas energy as well. It was seen that with an increase in temperature energy content of the syngas increased for gasification with air and it did not affect those with steam as gasifying media. C2 and C3 compounds, though not shown here, were reported to reduce with an increase in temperature due to decomposition to produce CO ad H2. Similar results observed by other studies [70,71] on different reactors and oxidizing agents such as carbon dioxide[18] and steam[72] confirm the significance of the effect of temperature on the process.

2.6.2 Gasifying agent

Various gasifying agents have been studied for biomass gasification including air, oxygen, steam, CO_2 and their combinations[73]. Increasing the equivalence ratio (ER) in air or oxygen gasification implies increasing the amount of oxygen as compared to the amount of biomass. As ER increases, oxidation/ combustion reactions lead to decrease in the amount of CO and H_2 and an increase in the output CO_2 is observed. The heating value of the syngas decreases but both gas yield and carbon conversion increase [70]. The use of steam as a gasifying agent by itself or in combination with oxygen or air leads to an increase in the production of H_2 resulting in a higher syngas heating value [74]. Gil et al.[75] used various steam to biomass and steam to oxygen ratios for gasification and saw a reduction in CO and hydrocarbons accompanied by an increase in the H_2 and CO_2 concentrations. Use of CO_2 as an oxidizing agent in biomass gasification increases the amount of CO and H_2 in the output through the increased activity of Boudouard and water gas

reaction. Corella et al.[76] studied steam gasification of cellulosic wastes in a fluidized bed at various temperatures and reported no effect of temperature on CO, and a slight decrease in CO2.

A study by Pohorely et al.[77] investigated the effect of combination of three gasifying agents: O_2, steam and CO_2 in a fluidized bed reactor at 850°C. Figure 2-5 shows the yield of gases at the output for different gasifying agents. The yields of CO_2, CO, H_2 and H_2O change accordingly to the thermodynamic expectations mainly by means of the water gas shift reaction. The yield of methane and minor organic compounds (C_2–C_7, labelled as 'minorities') was very similar when both H_2O and CO_2 were introduced into the gasifying agent, and it was the lowest when N_2 was used instead. The highest cold gas efficiency and carbon conversion was observed when the mixture of CO_2 and O_2 was used as the gasifying agent.

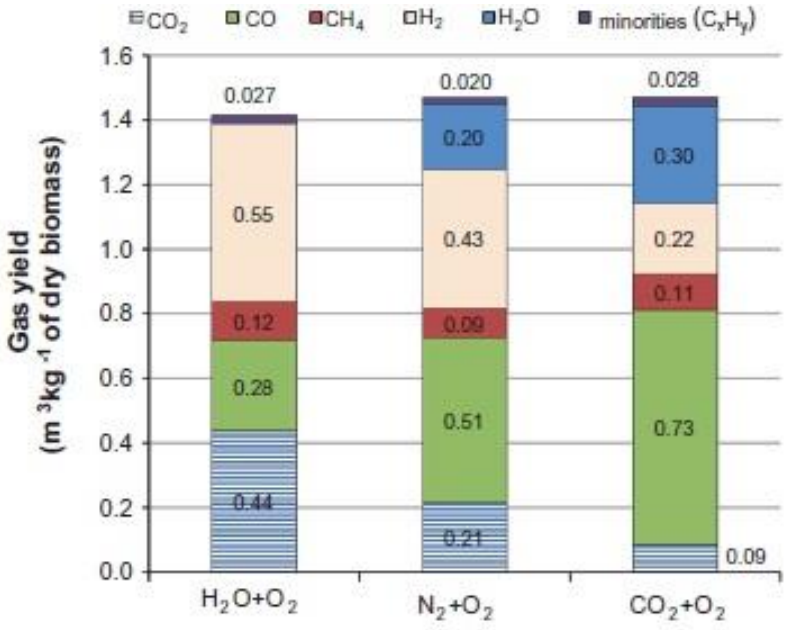

Figure 2- 5 Syngas component yield for different gasifying agents

[copied for illustration. Source: Pohorely et al.[77]]

2.7 Types of experimental setups used for gasification study

2.7.1 Thermogravimetric analyzers (TGA)

Another aspect that affects the output of the gasification process is the choice of gasifier. Different types of gasifiers are used to study gasification on a lab scale. Thermogravimetric analyzers (TGAs) allow a very small quantity (~10 mg) of feedstock sample to be gasified in a single run in an atmosphere of the gasifying agent. TGAs allow for sample mass measurement as the run progresses and allow for control over the heating rate of the sample along with the flow rate of the gasifying agent. This serves a good purpose when the mass loss of the sample is to be studied with respect to time. Various studies have investigated the effect of operating parameters on the gasification process using TGAs. Table 2.1 shows a few studies that have employed TGA setup for gasification analysis.

Table 2.2 Gasification studies using TGA

Study	**Feedstock**	**Oxidizing agent**	**Temp. (°C)**	**Heating rate (°C/min)**
Chen C. et al.[78], 2012	Lignite char	CO_2, steam and mixtures	1000	10
Kumar et al.,[79]., 2007	Corn Stover	Air and N_2	850	10, 30 and 50
Fermoso. et al.[80], 2009	Slash pine heartwood char	N_2, CO_2 and mixtures	750 – 900	40
Senneca O.[81], 2006	Olive husk, pine seed shells and olive woodchips	CO_2, steam and mixtures	800	5, 10 and 100

The majority of gasification research involving CO_2 has been done using TGAs. Yang et al.[16] studied the CO_2 gasification of reed Kraft black liquor and its water-soluble lignin using a TG-FTIR setup. The study analyzed the mass loss as well as the composition of tar formed during the process. The study compared its findings to other studies and discovered that the lignin structure type did not have any effect on the carbon monoxide formation mechanism during gasification. However, the composition of tar was drastically different implying it was strongly dependent on lignin structure type. Butterman et al.[18] used a TGA-GC setup to study steam and CO_2 gasification (with CO_2 concentrations in the range of 0-100%) of different biomass feedstocks as well as pure cellulose and lignin at various heating rates. Enhancement in CO and depression in H_2 and CH_4 concentration was observed as the amount of CO_2 in the input was increased. Additionally, a mechanism was proposed to explain the higher conversion in case of CO_2 gasification. Injection of CO_2 led to formation of microporous char at the end of drying and devolatilization, which makes diffusion and reaction easier during the gasification step.

Chen et al.[82] investigated the pyrolysis and CO_2 gasification characteristics of 8 different combustible solid wastes, representing the most common components of municipal solid waste (MSW) using a thermogravimetric analyzer (TGA). The decomposition trends of all the materials were found to be similar in both N_2 and CO_2 atmospheres for temperatures less than 600^{o}C. However, the degradation for materials subjected to pyrolysis occurred slightly above 600^{o}C and for CO_2 gasification occurred in the range of 700^{o}C to 900^{o}C due to the char–CO_2 reaction.

Another study by Butterman and Castaldi[17] studied the steam and CO_2 gasification of various wood and grass samples at different temperatures in a TGA-GC setup. The mass loss of the sample was quantified along with the composition of the output gas and mechanisms are

proposed to explain the same. Feedstocks with higher lignin fraction produced more char than the one with lower lignin fraction even with the introduction of CO_2. The experimental results were confirmed by comparing it with ASPEN simulation for the process reported in literature.

However, there have been numerous problems reported with studies using TGA. A review article by Antal et al.[19] reports a "jump phenomenon" in the reaction rate in a study about gasification of biomass charcoal with air at elevated temperatures. This phenomenon was attributed to a temperature runaway during which the temperature reported by the TGA device was far lower than the actual temperature of the sample undergoing the reaction. This led to an overestimation of the reactivity of the charcoal. This runaway was reported around the charcoal ignition temperature which leads to the assumption that TGA temperature readings around endothermic or exothermic steps may be incorrect. In another study about the pyrolysis of cellulose using TGA-MS, Lin et al[20] talked about a continuous thermal lag between actual sample temperature and the reported external temperature which leads to incorrect correlations of temperature and conversion. This study uses two different models to estimate the sample temperature. These models are plugged into a known kinetic expression and the entire comprehensive expression is then fit onto the experimental data. This provides a direct correlation between actual sample temperature and conversion. However, it is to be noted that this method requires a known kinetic expression for the process.

A study by Ollero et al.[21] evaluated the heat and mass transfer problems in TGA experiments concentrating specifically on the diffusional limitations. Gasification of wood matter from pressed oil-stone (WPOS) char with CO_2 is undertaken in three different setups mimicking three types of diffusional resistances i.e. no resistance, external resistance and internal resistance. Reactivity of chars quantified using effectiveness factors showed significant

difference between intrinsic reactivity and that measured for a char bed of height 3 mm. Additionally, an inhibition effect was observed because carbon monoxide from product gas was trapped inside the char bed.

2.7.2 Fixed or moving bed gasifiers

Fixed bed or moving bed gasifiers are also common in gasification studies. The bed is kept fixed by constant addition of fresh feed. They are classified as updraft and downdraft gasifiers based on the flow of biomass and oxidizing agent. The flow of oxidant and biomass leads to the formation of particular zones in the reactors. Figure 2-6 depicts the updraft and downdraft gasifiers and the various zones inside.

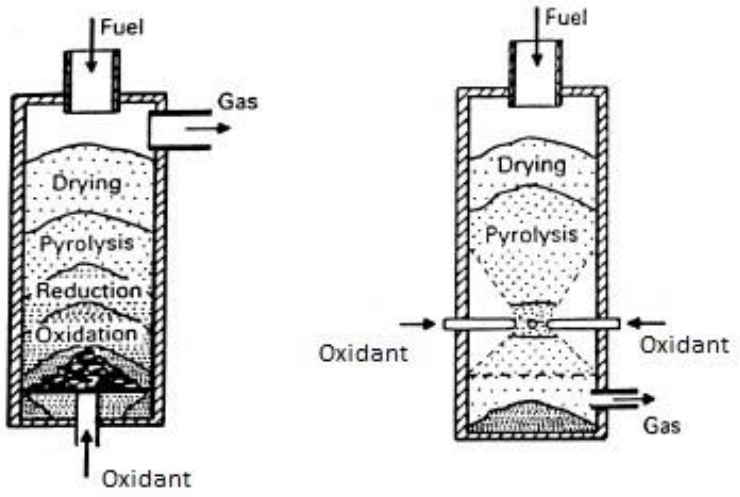

Figure 2- 6 Moving bed gasifiers (a) updraft gasifier and (b) downdraft gasifier

Various studies have used the moving bed gasifiers for different gasifying agents such as air[83,84] and combinations of CO_2 and O_2 with helium[85]. The advantage of using moving bed reactors is their easy and robust construction. The particle size used for these gasifiers can be up to 100 mm saving the energy required to grind the feedstock. Moving bed gasifiers show higher carbon conversion and high thermal efficiency. Syngas produced by an updraft moving-bed

gasifier has high tar content because the tar released from the pyrolysis zone is carried away by the hot gas which is flowing up from reduction (gasification zone). The gas produced is relatively cleaner in case of downdraft gasifier as the gas passes through the oxidation zone before exit. However, low ash fuels are preferred as higher ash content can cause ash agglomeration and clinker formation on grate[86]. Temperature distribution across the reactor is not uniform and leads to formation of hotspots. Due to higher residence time for solid and slow movement of bed, the throughput of the reactors is low and can be used only for small scale power generation[87].

2.7.3 Fluidized bed gasifiers

Fluidized bed gasifiers are more tolerant with respect to the feedstock and have higher throughput when compared with fixed bed gasifiers. Certain studies have used fluidized beds for gasification of large amount of high moisture content biomass[22]. Granular material such as sand is used for the bed, which is fluidized using a fluidizing medium such as air or nitrogen. Other bed materials such as olivine and calcite can be used for in situ cracking of tar to produce better quality syngas. There is an excellent mixing and temperature uniformity in the bed, and the gasification zones cannot be distinguished. The gasifying agent enters the reactor along with the fluidizing medium. Fluidized bed gasifiers are classified as bubbling fluidized bed (BFB) and circulating fluidized bed (CFB) as shown in Figure 2-7.

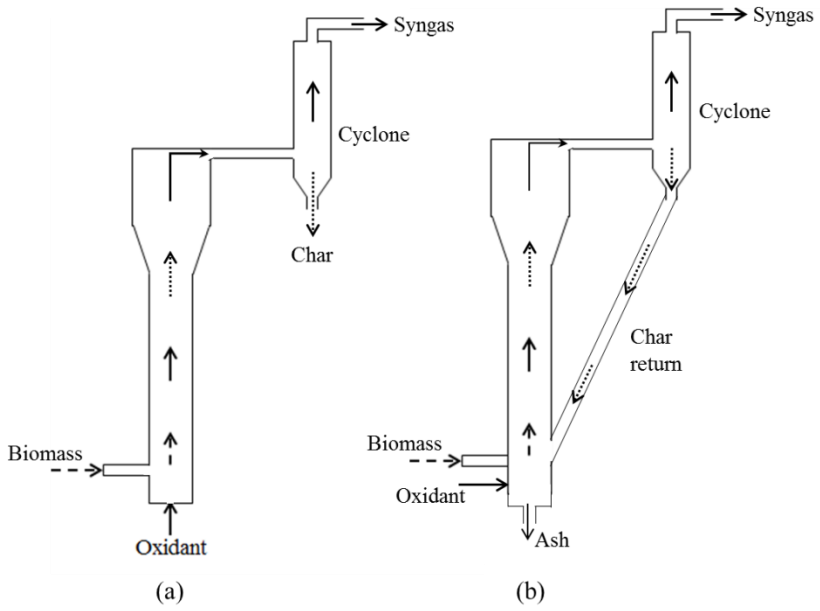

Figure 2- 7 (a) bubbling and (b) circulating fluidized bed gasifier

Both the gasifiers are similar in design except for the fact that in CFB, the particles (biomass and bed material) that get entrained during gas flow through the gasifier can be returned to the reactor. This ensures higher conversion and allows operation at higher fluidization velocities[88]. Bubbling fluidized bed gasifiers are easier to construct and operate due to their simpler designs and are used for smaller scale applications as compared to CFBs [86]. BFBs have been widely used for lab and pilot scale gasification experiments.

Franco et al. [72] studied the steam gasification of three biomass feedstocks in an atmospheric bench scale bubbling fluidized bed gasifier. The effect of temperature, steam-to-biomass ratio and biomass type was studied. An optimum temperature of 830^{o}C and a steam/biomass ratio of 0.6-0.7 w/w were suggested. In addition, reactions influencing the process within the limits of the experiment were determined.

Abdoulmoumine et al.[65] reported the use of a bench scale bubbling fluidized bed reactor for gasification of pine with oxygen to test the effect of three temperature and equivalence ratios on output syngas composition and contaminants. Yield of output syngas increased along with CO

and H_2 as temperature increased. An overall higher yield of tar but in lower concentration in the output syngas was reported. The yield of contaminants NH_3, HCN and HCl reduced as temperature increased.

In another study by Pohořelý et al.[77], CO_2 is used as a moderator during oxygen gasification of biomass with and without steam. The reactor used was a semi-autothermal fluidized bed with catalytically active Italian dolomitic limestone as the bed material. Carbon efficiency and cold gas efficiency increased whereas the amount of tars in the output reduced significantly. Additional studies including a few offering extensive reviews of fluidized bed gasification in O_2, air, steam atmospheres or their mixtures have been reported in literature [89,90,91,76]. Table 2.3 shows a few other studies that have used fluidized beds for gasification.

Table 2.3 Gasification studies using fluidized bed gasifiers

Study	**Feedstock**	**Oxidizing agent**	**Temperature (ºC)**	**Gasifier type; Bed material**
Campoy et al.[92], 2009	Wood pellets	Air, O_2 and steam	750 – 840	BFB; sand
Rapagna et al. [93], 2000	Almond shell	Steam	770	BFB; Olivine, sand
Li X [94] et al., 2004	Sawdust	Air	700 – 850	CFB; Ni/Alumina
Li K [95] et al. 2009	Coal, pine sawdust and rice straw	Air, O_2 and steam	940 – 1020	BFB, sand
Pfeifer [96] et al., 2009	Wood pellet	Steam	650 – 840	CFB, Olivine
Miccio [97]et al., 2009	Pine woodchips	Steam and O_2	780 – 890	BFB, silica sand

An extensive review of biomass gasification studies by Alauddin et al. [98] highlights the number of projects that have investigated the process of gasification using fluidized bed gasifiers and underlines their parameters and key findings. The study also provides a review of various industrial small scale plants employing fluidized bed gasifiers for power or heat generation.

2.8 Gasification kinetics

The process of gasification has a complicated chemistry with a number of reactions occurring at the same time depending on the operating conditions of the gasifier. As mentioned earlier, gasification occurs in three different steps and the products obtained from one step highly influence reactions occurring during other steps. Hence, it is very important to study the kinetics of biomass gasification in order understand the fundamentals of the process. The dominant set of reactions occurring inside the gasifier changes according to the gasifying medium being used which affects the overall kinetics. Especially the char gasification reactions are slower than other steps which makes them the rate limiting or the rate determining steps for the process. Kinetic studies are generally preceded by preparation of biomass char by heating up the biomass in an inert atmosphere (N_2 or Ar) for a few hours at 800^{o}C to 900^{o}C. This ensures that the pyrolysis process has been completed and no products from that step interfere the char–oxidant reaction.

Ahmed and Gupta[24] studied the gasification of food waste char with steam at four different temperatures 750^{o}C, 800^{o}C, 850^{o}C and 900^{o}C. Steam and helium flow rate of 8 g/min and 1.1 g/per minute respectively were used. CO and CO_2 are produced through water-gas and water-gas shift reactions. A mass spectrometer was used to calculate the amount of CO and CO_2 in the product stream by relating their partial pressures to the partial pressure of helium at the exit. Carbon reactivity was defined by equation [2.13] where m= mass at time t and dm/dt = the

carbon mass flow rate measured by mass spec. Figure 2-8 shows the conversion–time data obtained and the calculated reaction rate.

$$r = \frac{1}{m}\frac{dm}{dt} \qquad [2.13]$$

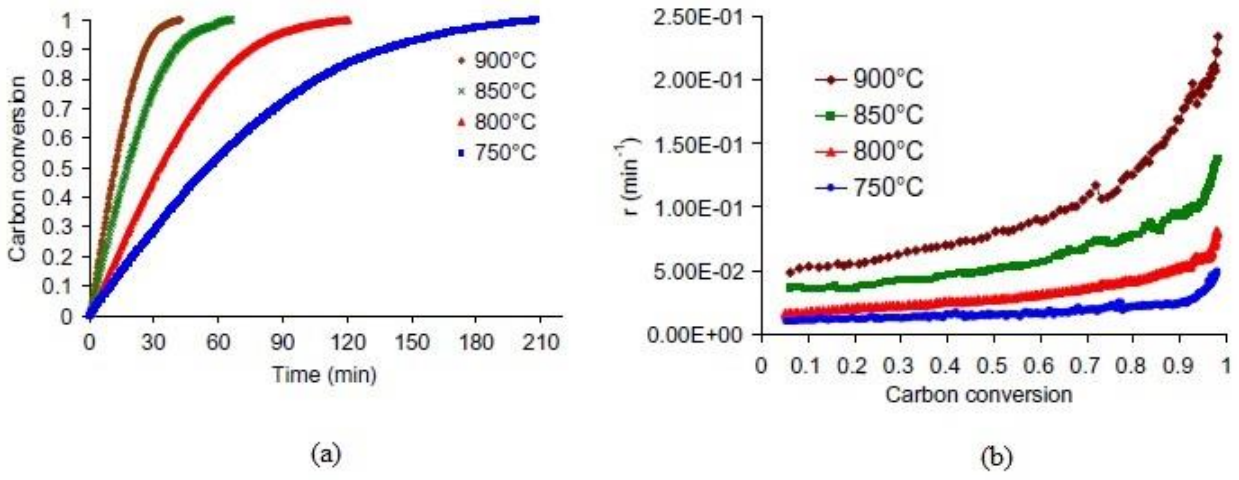

Figure 2- 8 (a) Conversion-time data (b) reaction rate with respect to conversion

[copied for illustration. Source: Ahmed and Gupta[24]]

The values of kinetic parameters were calculated using the Arrhenius equation. The activation energy was calculated as 125.8 kJ/mol and the pre-exponential factor was 67778 (min^{-1}). The increase in reaction rate with carbon conversion was postulated to be due to the ash which may have increased the adsorption rate of steam to the char surface.

Another study by Roberts D.G.[99] analyzed the reaction of coal chars with mixtures of CO_2 and H_2O. The data presented showed that the rate of reaction in a mixture of CO_2 and H_2O is not the sum of the two pure-gas reaction rates but a complex combination of the two. On the basis of Langmuir–Hinshelwood equation, a rate equation for the mixture of steam and CO_2 was developed. The surface areas of chars from the CO_2 – H_2O combination process were found to be

far lesser than the surface areas of the H_2O process chars. The reason for this was postulated to the inhibition or blocking of active sites by CO_2 as the C–CO_2 is a slower reaction.

Ollero et al.[25] performed the CO_2 gasification of wood matter from pressed oil-stone (WPOS) in a TGA at various temperatures in the range of 800ºC to 950ºC. Carbon monoxide was added along with CO_2 to test the inhibition effect it has on the process. To fit the experimental data, a n^{th} order reaction model was used for the cases with absence of CO and Langmuir-Hinshelwood model was used for the CO inhibition cases. The reactivity at 50% char conversion (R_{50}) is taken as representative and reactivity at any conversion is expressed as a function of R_{50}. The values of kinetic parameters for pure CO_2 experiments were found out to be E = 133 kJ/mol, ln k_0 = 9.193 and n = 0.43.

Khalil et al.[26] studied the CO_2 gasification of pine and birch chars using a TGA at pressures of 51 and 101 kPa and proposed a three parameter empirical model to examine the dependence of gasification reactivity on conversion. Mani et al.[27] studied the kinetics of CO_2 gasification of wheat straw char using a TGA. The effects of temperature and particle size were studied using the 50% conversion (R_{50}) technique.

2.8.1 Reaction models and kinetic parameters

Some other methods have been identified in literature for the kinetic analysis of the char–CO_2 gasification step. Most popular of these is the use of empirical models for solid–gas reaction systems to fit conversion–time data obtained experimentally. The Volume Reaction Model (VRM) speculates that the reaction is occurring homogenously throughout the volume of the particle[100]. The conversion of the solid particle with respect to time is described as:

$$X = 1 - \exp(-k\,t) \qquad [2.14]$$

Where ***k*** and ***t*** are rate constant and reaction time respectively. The Non-Reactive Core model (NRC) hypothesizes that the solid- gas reaction initially occurs at the surface and gradually penetrates into the particle. This leaves a constantly shrinking non-reactive core at the center of the particle[100].

$$X = 1 - (1 - \mathrm{k\ t})^{3} \qquad [2.15]$$

The Random Pore Model (RPM), proposed by Bhatia and Perlmutter [101], assumes that the structure of the pores in the solid and hence the surface area available for reaction is constantly changing during the course of the reaction. It considers the effect of enlargement of pores to yield more surface area in the initial stages of conversion, and the coalescence of these enlarged pores leading to the reduction in reactive surface area and thereby decreasing the reactivity of the solid particle in the later stages of conversion.

$$X = 1 - \exp(-k\,t\,[1 + k\,t\,\tfrac{\Psi}{4}]) \qquad [2.16]$$

The pore structure parameter Ψ relates to the initial pore structure of the solid and is an indicator of the amount of change in specific surface area as the reaction progresses. It can be calculated using the initial pore surface area per unit volume S_0, the initial pore length L_0 and the particle porosity ε_0.

$$\Psi = \frac{4\pi L_0\,(1-\varepsilon_0)}{S_0^2} \qquad [2.17]$$

But in this study, Ψ is treated as a fitting parameter obtained by fitting and optimizing the RPM with the experimental data. The other kinetic parameters were determined using the Arrhenius rate law.

$$k = A\exp(-E_a/RT) \qquad [2.18]$$

In addition to these, a study by Zhang et al.[102] looked into the gasification of 14 different biomass chars and proposed a semi-empirical modified RPM to explain the behavior of all the chars. Fei et al.[103] used mathematical modeling by employing a modified quantize mode (MQM) which takes into account the differential mass conservation. Bhat et al.[104] used the volume reaction model (VRM) and shrinking core model (SCM) to study steam and CO_2 gasification kinetics of rice husk char in a TGA at 750^{o}C to 900^{o}C and found the activation energy to be 197 kJ/mol and 180 kJ/mol for the models. Cetin et al.[105] used the VRM with pine char as the feedstock and found the activation energy to be 224 kJ/mol.

Seo et al.[106] investigated the char gasification of the reactivity of biomass char at various temperatures and CO_2 concentrations. The experiments were carried out in a horizontally placed fixed bed reactor and the char for the reaction was prepared in situ. The concentration of CO in the output was measured and conversion was calculated based on the total amount of CO released. Three reactions models, VRM, SCM and RPM, were used to fit the experimental conversion – time data. Reduced chi-square (χ^2) analysis showed that RPM was the best fit for experimental data. Fig 2-9 shows the conversion time data and linearized RPM fit to the data.

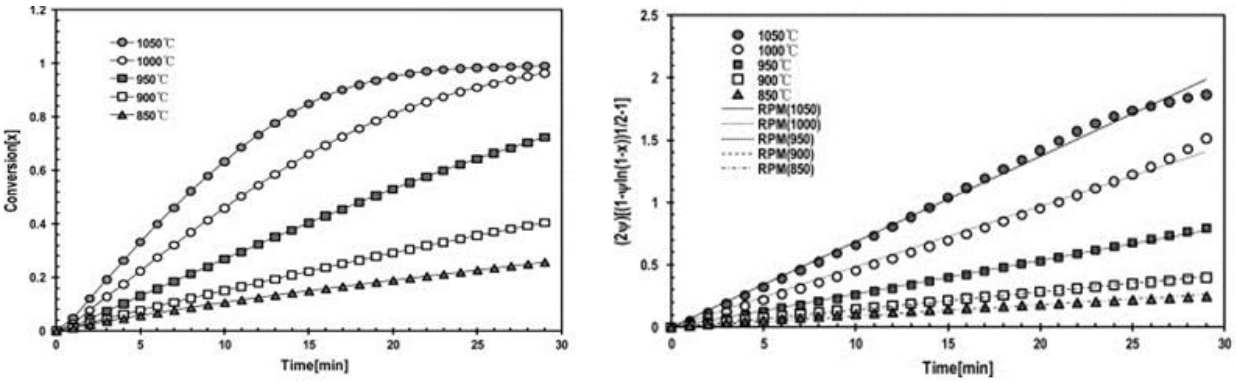

Figure 2- 9 (a) Conversion-time data (b) Linearized RPM fit

[copied for illustration. Source: Seo et al.[106]]

The surface area of the char particles at various conversion levels measured experimentally was compared with the RPM predicted surface area. The pore structure parameter Ψ was calculated to be 4.22 by fitting RPM surface area equation to BET area analysis and 3.16 experimentally.

Some other published works deal with kinetic analysis of char – CO_2 gasification step. Variation in biomass type and calculation method leads to different values of the kinetic parameters. Table 2.4 shows a few of them.

Table 2.4 Kinetic parameters for CO_2 gasification with char

Study	**Model**	**Biomass**	**Ea (kJ/mol)**	**ln A (s^{-1})**	**Ψ (avg.)**	**Temp. (°C)**
Ochoa et al.[107], 2000	RPM	SB char	156	N/R	4.7	900 - 1160
	RCM	SB char	149	N/R	-	900 – 1160
	RPM	HVB char	165	N/R	7.0	900 – 1160
	RCM	HVB char	183	N/R	-	900 - 1160
Sircar et al [108], 2014	VRM	Pine	217	15.4	-	725 - 900
	NRC		186	10.7	-	725 – 900
	RPM		125	5.0	5.5	725 - 900
Yuan et al.[109], 2011	RPM	Pine	248	18.3	50	850 - 1050
Bhat et al. [104], 2006	VRM	Rice husk	197	N/R	-	750 - 900
	NRC		180	N/R	-	750 - 900
N/R = Not reported; RCM = Random capillary model; SB = sub bituminous Argentinian coal, HVB = High volatile bituminous						

2.8.2 Factors affecting char reactivity

2.8.2.1 Effect of metal catalysts

Due to the slow nature of all char gasification reactions they tend to be the rate limiting step for the process. Numerous catalytic options have been investigated in order to inflate the rate of these reactions. The overall gasification reaction may be considered as a combination of non–catalytic process and a catalytic process associated with the mineral content of char [110]. Investigation of the effect of internal metal content on gasification requires acid washing of char to remove or reduce the amount of metal present inherently [111]. Duman et al.[112] investigated many raw and acid–washed chars for gasification reactivity with CO_2. A significance reduction in the amount of K and Ca was observed which was accompanied by considerable reduction in reactivity of the biomass.

The inherent presence of alkali and alkaline earth metals in the char leads to an increase in the reactivity whereas the presence of silicates and alumina has a negative effect. A possible explanation is that the melting of alumina-silicates could cover the available active sites or cover the pores required for oxidant diffusion.[113] Hattingh et al.[114] compared the effect of catalytic species ash constituents on CO_2 gasification activity of three coal chars. The sample with highest amount of ash did not have the highest activity due to large amount of SiO_2. The highest reactivity sample contained the highest amount of Ca and Mg and the lowest amount of SiO_2. Another research work by Aho et al.[115] studied the pyrolysis and gasification of pine chars leached with different concentrations of acids such as sulfuric acid, nitric acid and hydrochloric acid. Certain elements were doped on top of these acid washed chars so as to remove the effect of inherently present elements. Alkali metals had a strong influence on the yield and composition of the pyrolysis products. The higher reactivity of the calcium doped char was consistent with

literature while lower than expected reactivity was observed for K+ and Na+ doped acid washed pine.

In addition to inherent constituents, catalysts doped externally onto biomass char are also known to improve the reactivity of the heterogeneous gas- solid reaction. The externally added catalyst incorporates itself onto the char surface and affects the carbon surface chemistry. Lili et al.[28] experimented with the carbonates of lithium (Li_2CO_3), sodium (Na_2CO_3) and potassium (K_2CO_3), and their combinations in various proportions, for the CO_2 gasification of Pinghshuo (PS) coal by thermogravimetric analysis. The results indicated that the standalone effect of Li was the largest whereas a synergistic effect between Li and K or Na was observed above a temperature of 1300 K. Hurley et al.[116] examined the effect of several impregnated metal ions viz. Fe (III), Co (II), Ni (II), and Ru (IV) and a raw iron ore (natural limonite) on the air/CO_2 gasification of pine sawdust at 700^{o}C and 800^{o}C. The catalysts loading was carried out on the biomass itself using a wet impregnation technique using nitrates of the respective metals. All the metals were successful in decreasing the amount of chars and tars in the output in air + CO_2 and pure CO_2 conditions. Huang et al.[117] investigated the effect of Na, Mg, K, Ca and Fe on the CO_2 gasification reactivity of fir char using a TGA. The degree of carbonization, crystal structure and morphology of char samples was characterized by X-ray diffractometry (XRD) and scanning electron microscopy (SEM). Na and Ca led to an improvement in formation of crystal structure and Mg enhanced the degree of carbon structure ordering. SEM analysis showed that spotted activation centers were distributed on the surface of char samples impregnated with catalysts. Figure 2–10 shows the conversion and differential mass loss curves obtained from the experiment. The carbon conversion ratios of the six char samples increased, in the sequence K–char > Na–char > Ca–char >Fe–char > Mg–char > raw char. The mechanism to explain the

involvement of metals in increasing the char – CO_2 gasification reactivity was put forward by Moulijn et al.[118] which is shown in equations [2.19], [2.20] and [2.21].

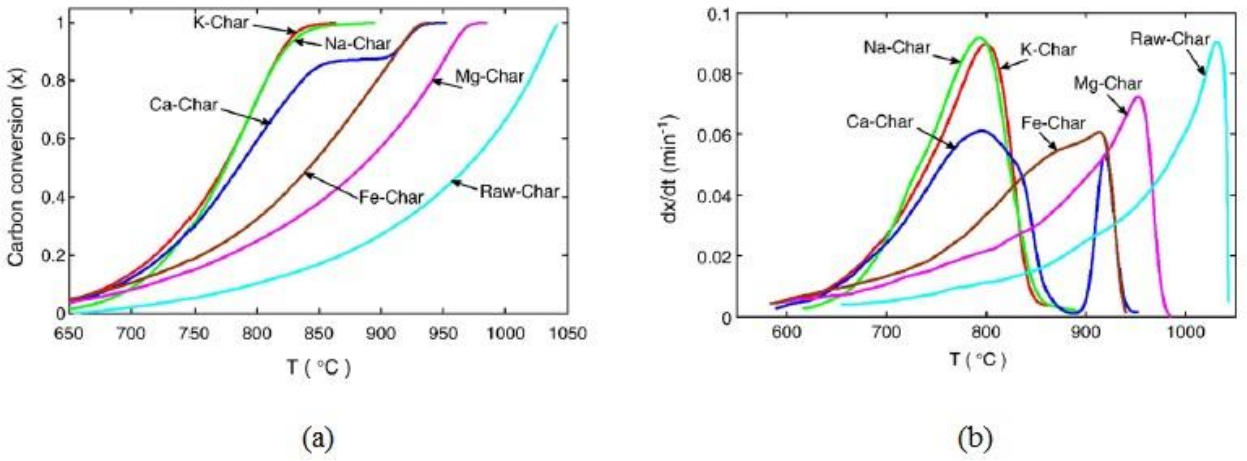

Figure 2- 10: (a) Carbon conversion and (b) differential mass loss curves

[copied for illustration. Source: Huang et al.[117]]

$$MO + CO_2 \leftrightarrow MO\,(O) + CO \qquad [2.19]$$

$$MO\,(O) + C \leftrightarrow MO + C\,(O) \qquad [2.20]$$

$$C\,(O) \leftrightarrow CO \qquad [2.21]$$

where M is the metal ion. Most catalytic studies show that the performance of alkali metals in improving the char – CO_2 gasification reactivity has been higher than alkaline earth and transition metals. However, Lahijani et al.[119] found a different trend while studying the effect of metal nitrate salts on CO_2 gasification of pistachio shell char. The catalytic effect was in the order of Na > Ca > Fe > K > Mg. The lesser catalytic activity of K in this study was attributed to the increased sintering tendency of biomass ash at high temperatures. Na – char was used for kinetic studies and the activation energy of 5 wt% Na loaded char was calculated to be 151.46 kJ/mol. Table 2.5 shows the activation energies from some catalyzed char gasification research works.

Table 2.5: Summary of catalyzed char gasification studies

Study	Feedstock	Char type	Ea (kJ/mol)	Temp. (°C)	Apparatus
Zhou et al [120], 2012	Petroleum coke	Pure char	198	950 - 1100	TGA
		$FeCl_3$-char	168	950 - 1100	
Lahijani et al.[119]., 2013	Pistachio shell	Pure char	204	800 – 875	Tubular reactor
		$NaNO_3$ - char	152	800 – 875	
Lee et al[121]., 1996	Tire	Pure char	239	850 - 1000	Tubular reactor
		3%K_2CO_3 char	193	850 - 1000	
		6%K_2CO_3 char	184	850 - 1000	

2.8.2.2 Pyrolysis condition for char preparation

The preparation of char for studying only the gasification step is done by subjecting it to pyrolysis. The loss of volatiles, the rearrangement of char microstructure to become more graphitic and the reduction in the amount of inherent inorganic compounds occur during pyrolysis. All these parameters are crucial to the reactivity of char and are affected by the pyrolysis conditions (temperature, heating rate, particle size etc.). Xu et al.[122] investigated the char surface active sites and their relationship to gasification reactivity. The study showed that the use of high pyrolysis temperature and slow heating rates enhanced the C/H and C/O ratios in coal char and led to a reduction in the active mineral compounds at the char surface making it less active. Another study[80] reported that the reactivity of wood char decreased with increase in pyrolysis temperature which was attributed to the ordering of carbon matrix and reduction in active sites. Min et al.[123] concluded that higher temperatures led to the creation of highly

microporous chars which cause mass transfer limitations for CO_2. Rapid pyrolysis and high heating rates lead to the formation of larger surface area and higher concentration of active sites on the char surface.

2.8.2.3 Particle size distribution

The gasification reaction of char with CO_2 depends greatly on the surface area available for reaction. As the particle size decreases, the total surface area/volume of the systems increases leading to better heat and mass transfer and higher conversion. Larger particles may give rise to the phenomenon of CO inhibition wherein the concentration of product CO in pores builds up to high levels suppressing the flow of CO_2 into the pores[124]. This inhibition effect worsens as the temperature increases due to higher amount of CO produced. The studies looking into the effect of changing particle size have concluded that the reaction is chemically controlled for particle sizes below 650 micron[113]. Certain studies have looked into the intra-particle diffusional effects in CO_2 gasification of biomass. Mani and Mahinpey[27] studied the gasification kinetics of wheat straw char with CO_2 at various particle sizes from 60 micron to 925 micron. The study reported that the change in particle size did not increase the value of Thiele modulus high enough to consider strong pore diffusion in the char gasification and the process was chemically controlled. Lee and Kim[121] studied waste tire char gasification with CO_2 and determined that gasification rate was independent of particle size for sizes less than 650 micron. A review of biomass-CO_2 gasification by Lahijani et al.[113] mention a few other studies that have concluded that at lower particle sizes (like the ones in this study), the diffusional effects are not prominent and the process is chemically controlled. However, Rapagna and Latif[125] attributed the effect of particle size on the steam gasification of ground almond shells to the extra and/or intraparticle heat transfer limitations. Various endothermic reactions occurring inside the biomass particles during

CO_2 gasification lead to a temperature difference between the particle temperature and the temperature of the fluidizing agent.

2.9 Gasification modeling

Gasification of biomass is a sensitive process in that a slight change in the operating parameters or composition of feedstock causes the composition of the output syngas to change. In addition to these, the type of gasifier used and the design of gasifier play a very important role in defining the output of the process. Therefore, it is important to perform an extensive research on this topic with considerations for a number of feedstocks and gasifying agents over a wide range of operating parameters. However, the sheer number of experiments to be performed for such a study will be both expensive and impractical. Computational model simulating the working of a gasifier solves the problem by allowing the user to tweak the necessary parameters and understand its effect without having to physically perform the experiment. There have been many efforts in order to accurately simulate the functioning of gasifiers and predict the composition of the output. In order to develop a comprehensive model, it is important to select the correct method and adapt the most suitable modeling tools, along with the mathematical knowledge of the parameters to be varied[126]. Gasification modeling focuses on modeling the three individual steps involved in gasification along with considerations for reactions occurring and the properties of the gasifier. Fixed bed gasifiers can be easy to model owing to their simple design whereas fluidized bed gasifiers have various factors that affect their performance. Based on the type of tools employed for simulation, gasification models can fall into various categories.

2.9.1 Thermodynamic equilibrium modeling

Thermodynamic equilibrium models are the simplest models that are used to describe the functioning of the gasification process. Thermodynamic models are independent of gasifier

design and are found to be very useful for preliminary comparison and for process studies on the influence of basic operating parameters. These models consider the chemical equilibrium condition, i.e. where the reacting system is most stable, achieved when the entropy of the system is maximized whereas the Gibbs free energy is minimized. This model does not consider the kinetic or dynamic aspects of the process and instead focuses on the most 'stable' product composition assuming that the reactants react in a fully mixed condition for an infinite period of time. In the stoichiometric modeling, specific chemical reactions are identified and used for the estimation of end gas composition. This results in errors due to consideration of only the important reactions and omission of others. Ravikiran et al.[127] used non-stoichiometric thermodynamic modeling to simulate steam and oxygen gasification of any carbonaceous fuel. Figure 2-11 demonstrates the ASPEN plus model used and the results are presented as contour plots on Van Krevelen coordinates (H/C ratio vs O/C ratio).

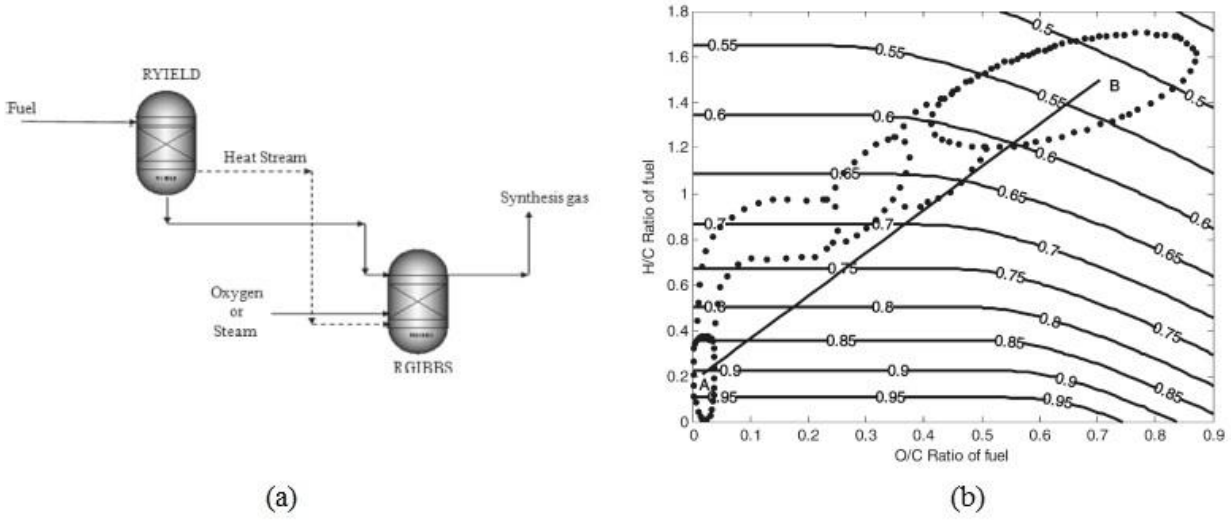

Figure 2- 11 (a) ASPEN plus model and (b) results by Ravikiran et al.

In the model, the feedstock is represented as a non-conventional solid component. The RYIELD reactor is used to split the solid into its constituent elements. The RGIBBS reactor is used to carry out the multiphase reaction equilibrium based on the minimization of Gibbs free

energy. The model also considers heat integration as the heat evolving from the breakdown in the RYIELD reactor is supplied to the RGIBBS reactor. Nguyen et al.[128] considered a three stage steady-state empirical model including pyrolysis, char reactions, and gas phase reactions. Ruggiero and Manfrida [129], Yoshida et al.[130], Li et al. [131] and Jarungthammachote et al.[132] are other studies that used the thermodynamic modeling for gasification.

2.9.2 CFD and ANN models

Computational Fluid Dynamic (CFD) models serve as a tool to study the behavior of a given gasifier design by combining both kinetic and thermodynamic models. CFD models are purely mathematical models that use a set of simultaneous equations for conservation of mass, energy, momentum and species in the gasifier. CFD models can be used to accurately predict the temperature and gas yield around the reactor if the hydrodynamic equations are known. Cheng et al. [14] used the Eulerian–Langrangian approach to simulate the behavior of CO_2 gasification in a fluidized bed. The solid char was considered as the continuum, and the solid fluctuating energy was described with granular temperature from the kinetic theory. The phases were able to interpenetrate into each other, and the sum of all the volume mass fraction was unity. The accumulation of mass in each phase was balanced by the convective mass fluxes. The oxidation reactions were modelled as homogenous reactions and water-gas shift reaction was modelled as a thermodynamic equilibrium reaction. The commercially available software FLUENT 14.0 was used to simulate the biomass gasification. The model was validated against an air gasification study due to the absence of CO_2 gasification studies using fluidized bed in literature (which objective 1 of the current research work is fulfilling). In the Artificial Neural Network (ANN) approach, the neural network learns by itself from the sample experimental data. A work by Aranavat et al.[133] studies the ANN approach for simulating circulating fluidized bed gasifier.

2.9.3 ASPEN plus modeling

CFD modeling yields good results only in presence of all the governing equations for the system. ASPEN plus models are a good way to complexity and develop a model that incorporates the principal gasification reactions and physical characteristics of the reactor. Each stream can be categorized according to the detailed pre-defined ASPEN categories. Complex systems can be modeled separately and tested as separate before being integrated into a single model. ASPEN plus has a large data bank of properties of various streams which aid greatly in the modeling process. Nikoo and Mahinpey[134] developed a comprehensive model for biomass gasification in an atmospheric fluidized bed to predict the steady state performance of the process. The model includes both hydrodynamic and kinetic parameters which were adopted from literature. The model used four ASPEN plus reactors. RGIBBS reactor was used to simulate the decomposition of feed into constituent elements by specifying the yield distribution according to biomass ultimate analysis. The separation column separated the volatiles and solids. The reactions of volatiles were simulated using RGIBBS reactor and assuming thermodynamic equilibrium. The fluidized bed reactor was simulated by separating it into two regions, freeboard and bed. One RCSTR reactor was used for each region and the hydrodynamics were and char gasification kinetics were nested into these as external FORTRAN codes. The model was compared with lab-scale results using different sets of operating conditions. The authors found good qualitative agreement between the model's prediction and experimental data and suggested improvements for further accuracy. Figure 2-12 demonstrates the ASPEN plus model and the comparison of its results with experimental studies. Separate studies have tried to simulate coal gasification using this method[135]. Table 2.6 provides a summary of a few other works that have used the various types of modeling approaches discussed in this section [136].

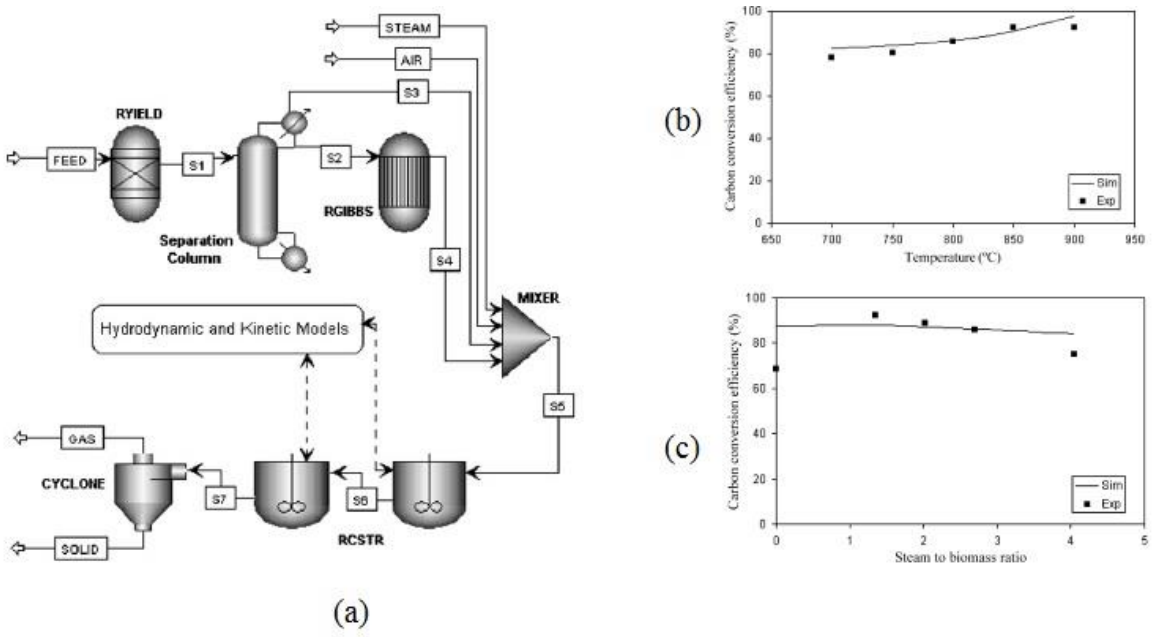

Figure 2- 12 (a) ASPEN plus model and (b) & (c) Experimental validation

[copied for illustration. Source: Nikoo and Mahinpey[134]]

Table 2.6 Summary of gasification modeling studies

Study	Feedstock	Model consideration	Parameters studied
Doherty [137]et al, 2009	Hemlock wood	Gibbs free energy minimization	Equivalence ratio, temperature, steam/biomass (S/B) ratio
Kaushal [138]et al., 2011	Wood chips	One dimensional, two-phase steady state model	Temperature of bed material, Moisture content, S/B ratio
Beheshti [139]et al., 2015	Beech wood	ASPEN plus with dedicated FORTRAN subroutines	Temperature, particle size, CO and H_2 yield
Jakobs [140]et al., 2012	Ethylene glycol	CFD	Spray quality

2.10 Gasification and syngas applications

2.10.1 Large scale applications

Biomass gasification has been subject of lab scale and pilot scale studies for many years and the research has resulted in an abundance of knowledge about this field. However, this vast reserve of technological know–how has not been translated into large scale commercial success due to certain issues pertaining to the process[141]. The design and economics of gasification based power generation units have been studied all over the world[142,127,143]. The major area of concern for investors in this sector is the economic barrier that separates the cost of energy generated from biomass technologies and the cost of power production from conventional sources of energy in use today [144]. The cost of petroleum crude is around $50 a barrel which has fallen nearly 50% in the last two years and the projection for the coming year looks the same[145]. This reduction in pricing tends to take the attention away from the harmful effects of the constant use of these fuels and leading to a reduced consideration of alternative sources. In addition to the reduced attention, the costs for syngas cleanup and constant supply of biomass for gasification are high. To achieve economic feasibility for any biomass process, it is generally accepted that the radius of biomass supply should not be more than 50 km (32 miles). Due to this restriction, even with high yield and short rotation plantation of energy feedstock, it will be difficult to satisfy the need of biomass supply for a large scale power plant [146]. A solution to this would be co-gasification of different types of biomass or combination of biomass with another carbonaceous source such as coal. Certain research works have studied the diverse aspects involved in co-gasification of biomass and coal blends[147,148]. Another technology being tested for practical application of gasification in power generation is called combined heat and power cycle

(CHP) or integrated gasification combined cycle (IGCC) where gas or steam turbines are employed in the power production scheme [149,150].

2.10.2 Conversion to biofuels

Syngas application in power generation and as a feedstock for production of liquid fuels makes biomass gasification an attractive option as a sustainable alternative energy technology. Liquid fuels can be produced using syngas through various pathways, the most important of them being Fischer–Tropsch synthesis [151]. The combination of carbon monoxide and hydrogen that results into higher order hydrocarbons is shown in equation [2.22].

$$n\,CO + 2n\,H_2 \rightarrow (CH_2)_n + n\,H_2O + heat \qquad [2.22]$$

This process can be conducted at 200^{o}C to 350^{o}C and yields a range of products depending on the temperature, pressure and catalyst. The current research in this field explores the use of various catalysts and different reaction mediums e.g. supercritical conditions for the process [152]. Other options for biofuel production from syngas include methanol synthesis through hydrogenation, DME production (conversion from methanol), and ethanol and other bio products via fermentation [153].

$$CO + 2\,H_2 \rightarrow CH_3OH \qquad \Delta H = -91\ kJ/mol \qquad [2.23]$$

Methanol is an important feedstock for production of various fuels and chemicals. The production of gasoline from methanol is an established commercial process[61]. Methanol not only remains the second largest consumer of syngas but there has been remarkable growth as part of the methyl ethers used as octane enhancers in automotive fuels[154].

In addition to applications of syngas, the char produced during gasification can be used for a variety of purposes. Gasification char generally tends to have a high surface area. This leads to the applicability of char as a catalyst for certain processes. Additionally, char has a very high carbon content and may be used for improving the quality of soil for crop growth.

Chapter 3

Effect of temperature and CO_2/C ratio on biomass gasification using carbon dioxide

Abstract

Gasification of pine using carbon dioxide as an oxidizing medium was carried out in a bench-scale atmospheric bubbling fluidized bed gasifier and the results were compared with oxygen gasification study from literature. Evolution of gases CO, CO_2, H_2 and CH_4 was quantified as a function of temperature in the range 700°C – 935°C and CO_2/C ratios in the range of 0.5 – 1.5 (wt./wt.). The main aim of this study was to determine the effect of temperature and CO_2/C ratios on the output syngas and to understand which reactions were influential within the operational limits of the experimental parameters. Additionally, results from CO_2 gasification and oxygen gasification were thoroughly compared to reveal the better process. Statistical analyses were performed to determine the significance of changes in operating parameters on the process. Variation in temperature seemed to have a significant effect on the output, and the effects of CO_2/C ratios were similarly profound. The analyses of the gas evolution trends suggested that the Boudouard reaction, char reforming reaction and free radical combination reactions dominated the chemistry of the process.

3.1 Introduction

Gasification is a complex process with many different reactions occurring at the same time. To understand the basics of the process, it is important to study the effect of change in operating parameters such as temperature and oxidant flow rate. CO_2 gasification studies in

literature have reported the use of TGA to investigate these parameters. However, there have been numerous problems concerning the heat transfer, mass transfer and temperature misrepresentation reported with studies using TGA.[19] Fluidized bed reactors are known to ensure great heat and mass transfer due to the high degree of mixing inside the reactor.[22] Several studies have reported the use of fluidized bed for gasification purposes.[72] Throughout the studies mentioned above and others encountered during the course of our literature review, there has not been a study focusing on carbon dioxide as the sole oxidizing agent (without the compounding effects of other oxidizing agents such as steam or oxygen) in a fluidized bed reactor. The current study was undertaken to address this and study the effects of temperature and CO_2 flow rate on the output syngas and postulate the dominant set of reactions within the operational limits of the parameters[155]. The results from this study have been extensively compared with the oxygen gasification results by Abdoulmoumine et al.[23] which was conducted on the same experimental setup and biomass as this study. This comparison provides us with valuable insights into the differences between gasification using oxygen and CO_2.

3.2 Experimental

3.2.1 Feedstock

For this study, pine wood chips were obtained from a local plant in Opelika, Alabama. The wood chips were dried in open air for a few days before being ground and sieved. Particle size of the final feedstock was in the range of 100-650 microns with mean size 315 micron. Ultimate and proximate analyses were carried out in accordance with ASTM standards. CHNS/O elemental analyzer (Perkin Elmer, Model 2400, Waltham, MA) was used to perform the ultimate analysis. The HHV of the pine sample was determined using a bomb calorimeter (IKA Bomb calorimeter, ModelC-200, Wilmington, NC).

3.2.2 Fixed bed reactor

Before conducting the study on the fluidized bed reactor setup, a preliminary study was conducted on a smaller scale using a fixed bed reactor setup to understand the difference between air gasification and CO_2 gasification. Figure 3-1 depicts the schematic representation of the fixed bed reactor setup. The temperature selected for this preliminary investigation was 800^oC.

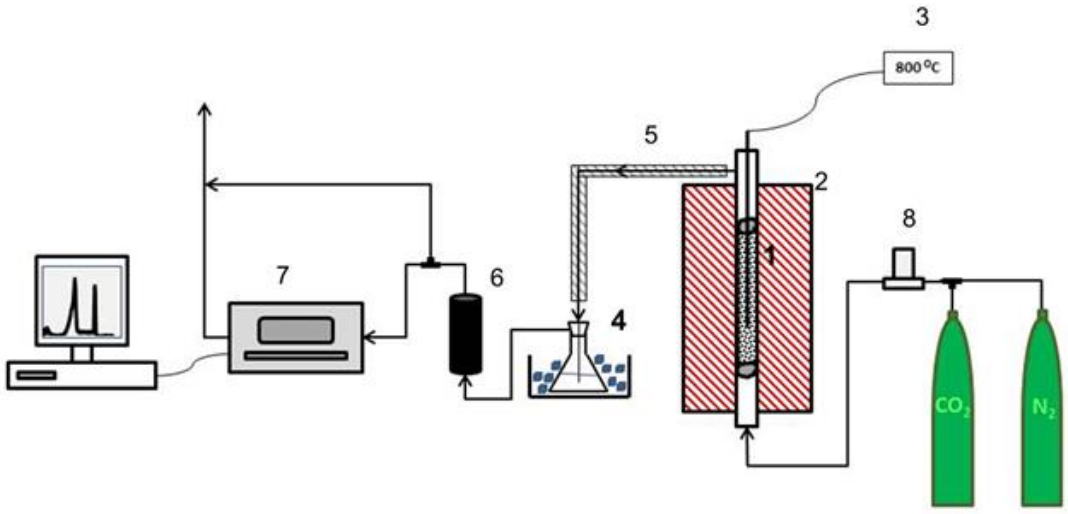

Figure 3- 1 Fixed bed gasifier setup
1. Tubular reactor, 2. Furnace; 3. Temperature indicator; 4. Condenser, 5. Heated line,
6. Activated carbon filter, 7. Gas analyzer; 8. Gas flow meter

Five grams of biomass was held between two quartz wool plugs inside a stainless steel tubular reactor placed in a furnace (Thermo Scientific, Lindberg Blue M). The oxidizing agent (air or CO_2/N_2) entered from the bottom of the reactor. Syngas from the reactor passed through a condenser and activated carbon filter before it was analyzed by gas chromatograph–thermal conductivity detector (GC-TCD) setup for primary gases (CO, H_2, CH_4, CO_2). Each run was conducted for a total of 60 minutes. Oxidizing agent air entered the reactor at a flow rate of 100 ml/ min for an equivalence ratio* of 0.3. On the other hand, for CO_2 gasification, a combination

of CO_2 and N_2 at 50% v/v entered the reactor for a total flow rate of 100 ml/min. Gas sample was analyzed every 10 minutes and char was collected at the end of the run.

* Equivalence Ratio is defined as the ratio of amount of oxygen supplied during gasification to the amount of oxygen required for complete combustion of biomass.

Figure 3-2 represents the gas profiles for H_2, CH_4 and CO from air and CO_2 gasification experiments. The legend on the graph specifies the gas and the oxidizing agent for e.g. "H_2 – CO_2" implies hydrogen plot for CO_2 gasification. All the data represented in the graph and Table 3.1 is on 'N_2 – free' basis.

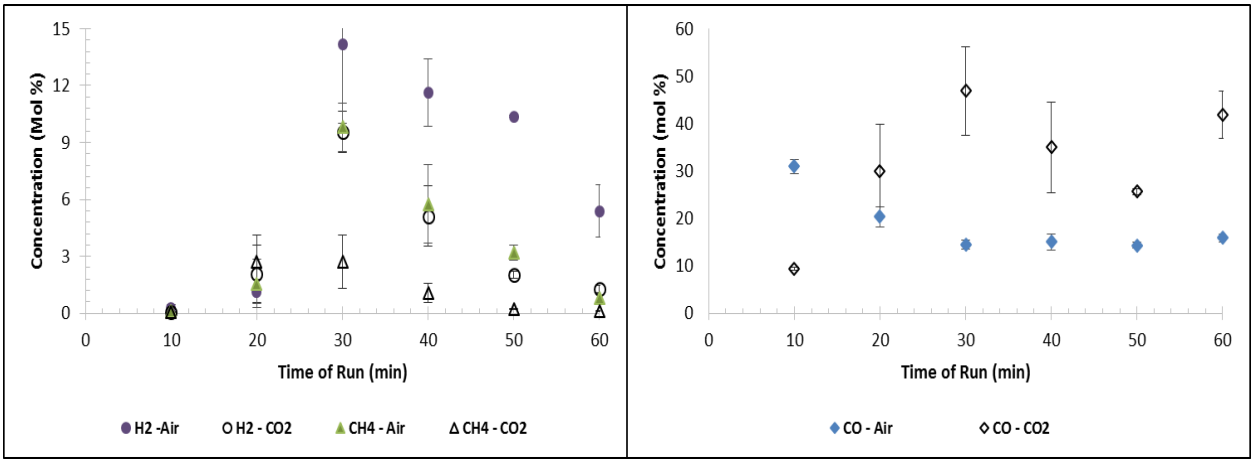

Figure 3- 2 (a) H_2 and CH_4 profile and (b) CO profile for air and CO_2 gasification at 800°C

The trends for H_2 and CH_4 appear to be the same for both oxidizing media throughout the run time but the actual values for air gasification are noticeably higher than CO_2 gasification for both the gases. However, the trend for CO is the opposite. A lot more CO is seen for air gasification initially but it drops as the run progresses. For CO_2 gasification, there is lower CO at the beginning but increases sharply during the run and stays considerably higher throughout till the end of the run. Table 3.1 shows the comparison of HHV (higher heating value) of the syngas obtained and the biomass conversion for both the oxidizing media. The HHV of syngas is

calculated by the sum of the volume fractions multiplied by higher heating values of gas components from literature. One-way ANOVA test performed at 95% confidence interval showed that change in oxidizing medium had a significant effect on both the properties as the values were statistically different [F (0.05, 1, 3) = 10.128].

Table 3. 1 Syngas characteristics for different oxidizing media

Property	**Magnitude**		**P - value**
	Air	**CO_2**	
HHV of syngas (MJ/Nm^3)	5.51 ± 0.55	7.93 ± 0.71	0.023
Biomass conversion (%)	91.8 ± 1.21	83.87 ± 2.14	0.005

The HHV of the output gas was higher for CO_2 gasification and so was the amount of unconverted biomass at the end of the 60-minute run. Interestingly, if the experiment using CO_2 was allowed to run for more time, the amount of CO kept on increasing and biomass reached almost complete conversion. This may be due to the fact that char–CO_2 gasification step is very slow and generally considered to be the rate limiting step[21]. This preliminary work shows that air and CO_2 gasification vary significantly and therefore the effects need to be investigated further.

3.2.3 Fluidized bed reactor

3.2.3.1 Experimental setup and procedure

Figure 3-3 shows the gasification experimental setup used in this study. It consists of a bench scale fluidized bed reactor with a height of 30.8 in. and the inner diameter of 2 in. The length of the reactor is 22.75 in. whereas for the freeboard is 8 in. Pine sawdust from the biomass hopper is fed through a twin screw feeder–auger assembly into the reactor. The reactor is heated to the gasification temperature using a set of electrical heaters. The fluidizing and oxidizing

gases (N_2 and CO_2 respectively) enter the bottom of the gasifier through a distributor plate. The bed material (sand), gases and biomass mix inside the reactor and gasification occurs. The output gas passes through a high temperature filter (350^oC), condensers cooled by ethylene glycol and water mixture (-5^oC), electrostatic precipitator with a negative 20kV supply to the rod, and an activated charcoal filter before it is analyzed using the online gas analyzers. The average feed rate of biomass into the reactor was 300 g/ h.

Pine was gasified at four different temperatures between 700^oC and 950^oC, which is considered as the normal range for gasification. Each run was allowed to continue for nearly 40 minutes after achieving steady state. The average value of the concentration of a species across the entire steady state was considered its concentration for that particular temperature. Two runs were conducted for each temperature and the steady state concentration values obtained from each run were averaged. The flow rate of N_2 into the reactor was 10 liters per minute and the flow rate of CO_2 was varied from 1 liter per minute to 2.24 liters per minute in accordance with the CO_2/C ratio. The overall superficial velocity for the gases was between 0.10 m/s and 0.13 m/s. The minimum fluidization velocity required for the current setup is 0.064 m/s, which for the current gasifier setup equals to 7.74 liters of total gas flow per minute. The calculation for the minimum fluidization velocity is shown in Appendix B.

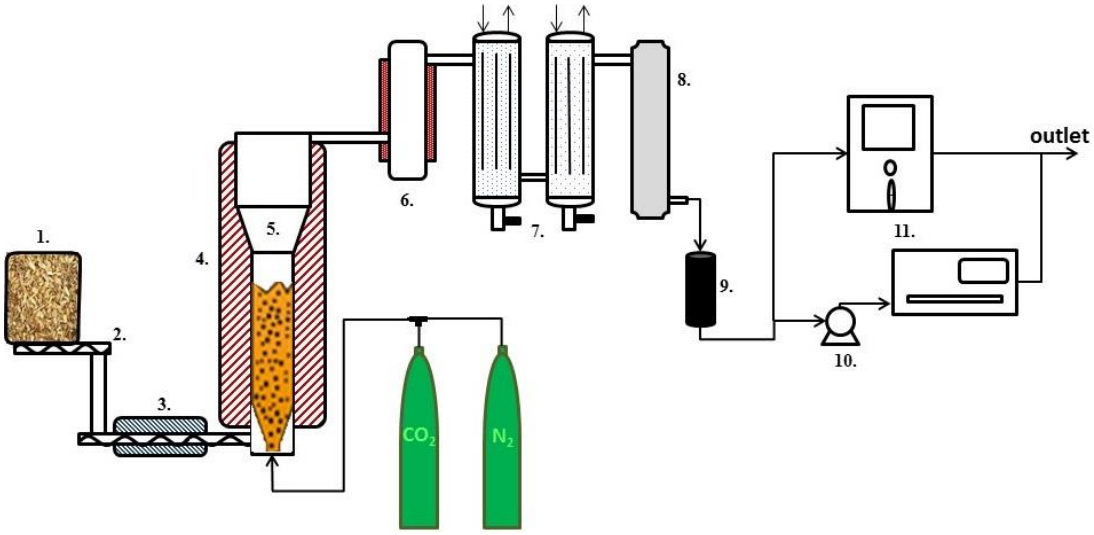

Figure 3- 3 Schematic of Bench-scale fluidized bed gasification setup.
1. Biomass hopper, 2. Screw feeder; 3. Heat exchanger; 4. Gasifier heaters, 5. Gasifier, 6. High temperature filter, 7. Condensers; 8. Electrostatic precipitator; 9. Activated carbon filter; 10. Pump; 11. Inline gas analyzers

3.2.3.2 Product sampling and analysis

The products obtained from the setup are char, liquid condensate and gas. Char was collected from the reactor and the high temperature filter. A mixture of char and sand was retrieved from the reactor and hence the amount of char left was calculated by subtracting the weight of sand from the total. The liquid condensate was collected from the bottom of the condensers. The gaseous product was analyzed for primary gases CO, H_2, CH_4 and CO_2 using an online gas analyzer (NOVA, Niagara Falls, NY) whereas lower hydrocarbons C_2H_2, C_2H_4 and contaminants like NH_3 were analyzed using an online FTIR (Fourier transform Infrared) gas analyzer fitted with a 4 m gas cell and a liquid nitrogen cooled MCT detector.

3.2.3.3 CO_2/C ratio

The CO_2/C ratio is the ratio of the amount of CO_2 injected to the amount of carbon entering the reactor in the biomass. This ratio helps us compare results with different studies

independent of the biomass type. Four different ratios in the range of 0.6 - 1.6 were used in this study. The ratios corresponded to CO_2 flow rates of 1 LPM to 2.24 LPM during the experiments.

3.2.3.4 Results and discussions

The proximate and ultimate analyses for pine are shown in Table 3.2. Values for pine were found to be similar to those reported in literature.[108]

Table 3. 2 Pine proximate and ultimate analysis

Proximate analysis (wt. %)	
Moisture content (wet basis)	8.03 ± 0.16
Ash content	0.72 ± 0.01
Volatile matter	80.79 ± 0.03
Fixed carbon	18.49 ± 0.03
Higher Heating Value (MJ/kg)	20.81 ± 0.6
Elemental Analysis (wt. % dry)	
C	47.49 ± 0.15
H	6.21 ± 0.08
N	0.07 ± 0.03
O (by difference)	46.23± 0.27

As mentioned earlier, to understand the difference between air and CO_2 gasification, the results from this study have been extensively compared to oxygen gasification by Abdoulmoumine et al.[23] performed on the same experimental setup, biomass and biomass feeding rate.

3.2.3.4.1 Gas evolution plots

Figure 3-4 shows the typical gas evolution plots observed during a run with the fluidized bed gasifier. Gas evolution plots for 700°C, 790°C, 850°C and 934°C were observed. The four primary gases (CO, H_2, CH_4 and CO_2) are measured in real time. The figure below shows the composition of syngas in molar percentage against the time of collection for three different temperatures. The plots do not stabilize immediately as it takes time for the process to attain steady state. The time to achieve steady state depends on temperature. As the temperature increases, the steady state time goes from approximately 30 minutes for 700°C to less than 10 minutes for 934°C. This is due to the fact that when biomass enters the reactor at high temperature, it is subjected to high heating rate and devolatilizes and degrades faster. The CO instantaneous yield at 934°C increases from 1.83 g/min at run time 3 min to 4.3 g/min at 15 min where it stabilizes. However, at 700°C, the yield changes from 0.45 g/min at 3 min to 1.01 g/min at 15 min and doesn't stabilize until 25 minutes into the run.

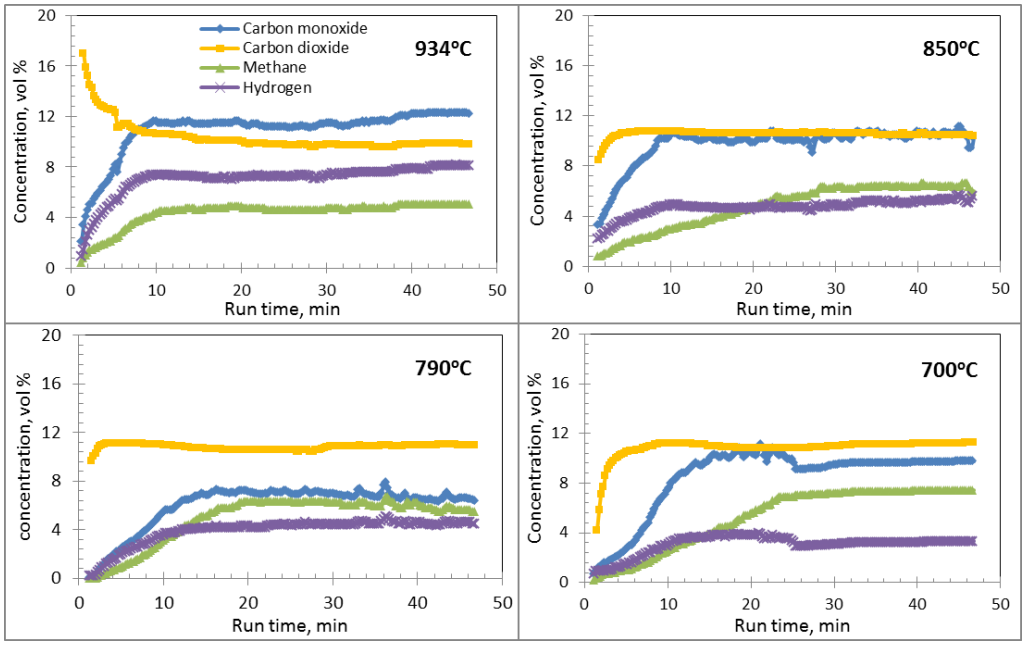

Figure 3- 4 Typical gas evolution plots at different temperatures

Figure 3- 4 (b) shows the total mass balance for biomass-CO_2 gasification process during a typical run at 850^oC for one hour. The input contains biomass and CO_2 streams. The output gas stream contains CO, CO_2, H_2, methane, ethylene and acetylene. The overall mass balance achieved was 96%.

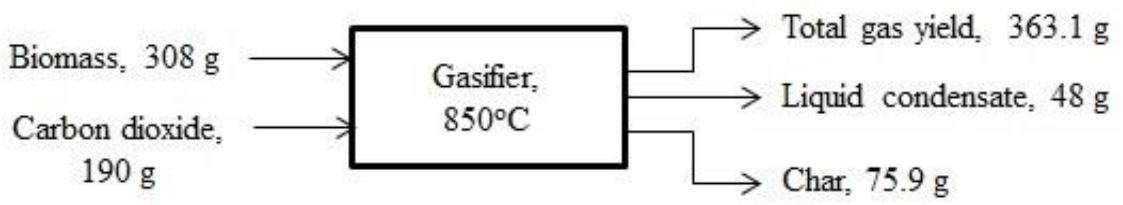

Figure 3- 4 (b): Mass balance for biomass-CO_2 gasification process at 850^OC

The mass transfer limitation caused by the intra-particle diffusion of CO_2 can be adjudged by calculating the value of Thiele modulus (ϕ). The value of ϕ as calculated in Appendix C is found out to be 0.106. This implies that the process is kinetically controlled and the influence of mass transfer can be neglected.

3.2.3.4.2 Effect of temperature

Figure 3-5 illustrates the effect of temperature on the yield of the three product streams (char, liquid and gas) obtained from the process. One-way ANOVA analysis performed on the yields [F (0.05, 3, 4) = 6.6] shows that all the three are significantly affected by temperature. P-values for char, liquid and gas yields are 0.005, 0.002 and 0.0001 respectively. Figure 3-5 shows a significant reduction in the amount of char as temperature increases. Chars obtained at the end of each run were analyzed with a gas sorption analyzer [Quantachrome autosorb – iQ] using nitrogen as the adsorbate gas. Micropore analysis using the Dubinin–Radushkevich method showed that increase in temperature led to an increase in both surface area of micro pores and total pore volume. These properties for chars obtained at different temperatures, 934^oC (surface

area = 350.5 m^2/g; pore volume = 0.1428 cc/g); 850°C (surface area = 237.7 m^2/g; pore volume = 0.06202 cc/g); 790°C (surface area = 52.73 m^2/g; pore volume = 0.01504 cc/g) and 700°C (surface area = 19.71 m^2/g; pore volume = 0.00795 cc/g) are significantly different. Hence, an increase in temperature leads to an increase in microporosity of the char. These micropores facilitate the diffusion of CO_2 into the char particle further enhancing the char-CO_2 reaction and conversion.

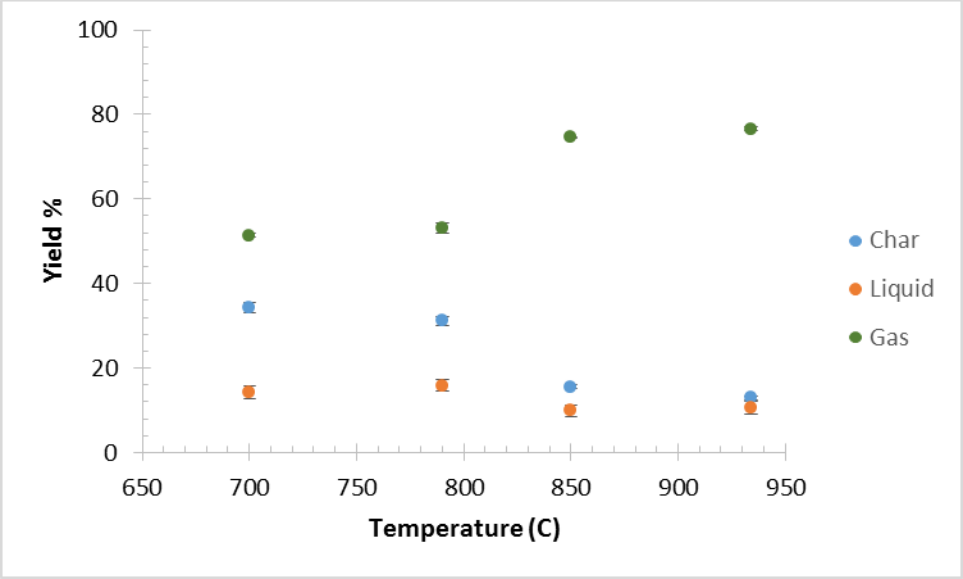

Figure 3- 5 Product stream yields for different temperatures.
[Error bars represent standard error]

Table 3.3 compares the product stream yields from this work to the yields from the oxygen gasification study by Abdoulmoumine et al.[23]. The comparison clearly highlights that oxygen gasification leads to higher gas and liquid condensate yields whereas char yield is higher for CO_2 gasification which implies that a lower amount of biomass gets converted than in oxygen gasification. A possible reason for this could be that oxygen-gasification reactions are exothermic and occur with more ease as compared to the endothermic and slow char–CO_2

gasification steps. Presence of oxygen leads to char oxidation reactions, which significantly increase conversion and reduce the char yield.

Table 3. 3 Comparison of product stream yields in air and CO_2 gasification

	Present study				**Abdoulmoumine et al.**	
Temperature	**700**	**790**	**850**	**934**	**790**	**934**
Char	34.28 ± 2.15^{A1}	31.13 ± 2.3 ^{A1}	15.6 ± 0.94 ^{A2}	12.89 ± 0.8 ^{A2}	6.07	3.65
Liquid	14.29 ± 1.11^{B1}	15.85 ± 0.3 ^{B1}	9.87 ± 0.51 ^{B2}	10.57 ± 0.1 ^{B2}	20.87	16.93
Gas	51.42 ± 1.1 ^{C1}	53.02 ± 2.5 ^{C1}	74.54 ± 0.4 ^{C2}	76.53 ± 0.9 ^{C2}	73.06	79.42

All yields reported in **percentage**. Means not connected with the same superscript are significantly different at the 0.05 level based on the Tukey's comparison test.

Various endothermic reactions occurring inside the biomass particles during CO_2 gasification lead to a temperature difference between the particle temperature and the temperature of the fluidizing agent. The calculation of the heat transfer between bulk gas and reacting particle is shown in Appendix D. The particle temperature correction was calculated as 1.1^{o}C.

The effect of temperature on CO_2 gasification is further analyzed by looking into the variation in the composition of output syngas. Figure 3-6 shows averaged steady state values of all the gases over the entire range of temperature. At 700^{o}C and 790^{o}C, the amount of CO_2 in the output (2.74 g/min and 2.85 g/min respectively) is almost the same as the amount of CO_2 being fed into the reactor (2.95 g/min). This implies that any CO_2 that may be consumed through the gasification reactions is restored by the CO_2 evolution during the devolatilization step. Hence, devolatilization is the dominant step at these temperatures.

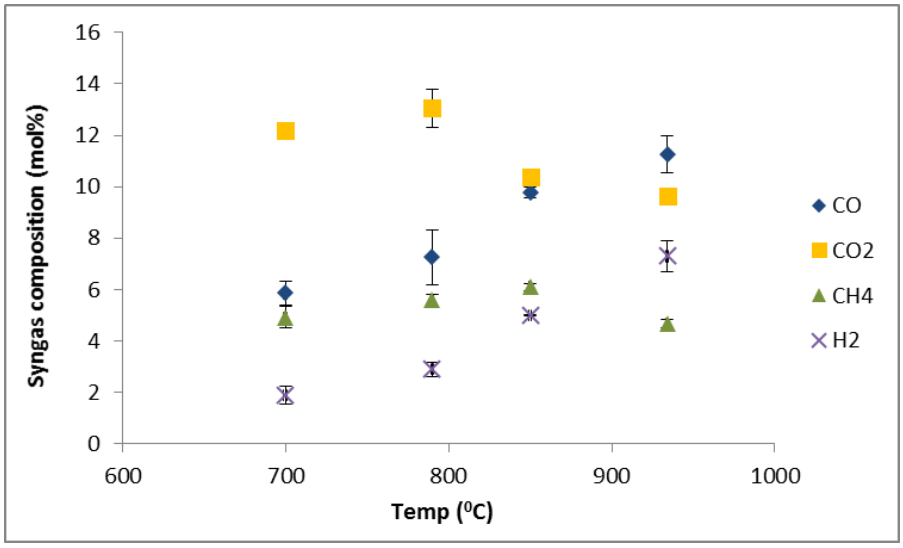

Figure 3- 6 Steady State Syngas composition profiles at different temperatures

The composition profile with temperature depicts that temperature has a noticeable effect on almost all the primary gases. This change can be due to various reasons, such as i) effect on the production in devolatilization step whose rate is faster at elevated temperatures[156] or ii) the change in gases through the endothermal char gasification reactions which are favorable at high temperatures. The concentration trend of each component is examined to postulate the reactions that can possibly lead to it.

3.2.3.4.3 Gasification chemistry

Gasification is a complex process wherein many reactions are taking place at the same time and often competing with each other. Table 3.4 contains the most common gasification reactions for the process.[61] The values on the right of the reactions indicate the heat of reaction at a temperature of 298 K. As per convention, negative value implies the reaction gives out heat or is exothermic and the reaction with positive value implies it absorbs heat or is endothermic. This heat of reaction can give us an idea about the ease of reaction at various temperatures. It is important to note that the devolatilization step that occurs during the process also contributes to

the CO_2, CO, CH_4 and lower amounts of H_2 and C_2 hydrocarbons. These result from the primary decomposition of the solid fuel and secondary reactions of the volatiles

Table 3. 4 Important biomass gasification reactions

Reaction no.	**Reaction Name**	**Reaction Chemistry**	**ΔH (MJ/kmol)**
R1.	Combustion	$C + ½ O_2 \leftrightarrow CO$	-111
R2.	Combustion	$CO + ½ O_2 \leftrightarrow CO_2$	-283
R3.	Boudouard	$C + CO_2 \leftrightarrow 2CO$	+172
R4.	Water-gas	$C + H_2O \leftrightarrow CO + H_2$	+131
R5.	Water-gas shift	$CO + H_2O \leftrightarrow CO_2 + H_2$	-41
R6.	Methanation Reactions	$C + 2H_2 \leftrightarrow CH_4$	-75
R7.		$CO + 3H_2 \leftrightarrow CH_4 + H_2O$	-205
R8		$2CO + 2H_2 \leftrightarrow CH_4 + CO_2$	-247
R9.	Methane steam reforming	$CH_4 + H_2O \leftrightarrow CO + 3H_2$	+206

The CO concentration in the gas composition plot increases continuously throughout the temperature range. Its value changes from 5.8% at 700^{o}C to 11.3% at 934^{o}C. The CO yield increased from 216 g/kg to 423 g/kg dry biomass. Even though the rise occurs to be significant, the main change occurs at 850^{o}C where the yield shoots up from 220 g/kg to 408 g/kg dry biomass. Therefore, it is inferred that the activity of the reactions producing CO increases with temperature and is highest around 850^{o}C. These descriptions fit perfectly for the reactions R3 and R4 (Boudouard and water-gas reactions). Franco et al. [72] reported these reactions to be very dominant specifically for pine around 830^{o}C. This phenomenon occurs because of a rapid

devolatilization step when biomass first enters the reactor. During this step any available oxygen from H_2O, CO_2 or CO evolving from the biomass structure itself is adsorbed by the highly porous char[17]. These trapped oxygen entities can later react with char and CO can be released around 800^oC contributing to the rise in its concentration. Additionally, biomass decomposition results in some O_2 release from oxygenated materials bringing oxidation reaction R1 into play.

Similar to the trend for CO, the hydrogen trends show a smaller increase initially but a steeper climb after that. This trend is also reflected in the gas yield values where there is a significant climb at 850^oC where it changes from 7.5 g/dry kg to 15.0 g/ dry kg biomass. This further cements the thought that the water gas reaction R4 is a very dominant reaction as hydrogen is one of its products. However, it leads to the addition of only one molecule per molecule H_2O consumed and cannot explain the enormous increase in H_2 yield. Water gas shift (WGS) reaction R5 is less likely to occur because of unavailability of free H_2O in the system.

The char surface after depolymerization and condensation reactions is coated with free radicals. A study[157] postulates the formation of hydrogen free radical during the devolatilization step. These are generally extracted by other free radicals. However, the hydrogen free radical has greater tendency to form molecular hydrogen in the range of 700^oC to 1100^oC. This combination of hydrogen free radicals leads to the steep increase in the hydrogen concentration.

Since CO_2 is injected into the reactor as a reactive gas, it is difficult to classify CO_2 at the output as being generated during the process by reactions like devolatilization or water gas shift; or just as the unreacted portion from the input stream. Hence, CO_2 concentration plot cannot be used to point out the reactions dominating the process.

Statistical analysis performed on methane concentration and yield show that it does not change significantly throughout the temperature range which implies that all the methane is

produced during the devolatilization step and no gasification reactions affect its output. However, Guizani et al.[158] reported a slight increase in methane concentration during biomass pyrolysis at 850ºC when 20% CO_2 was added to nitrogen atmosphere. This little 'extra' methane however is consumed through methane dry reforming (MDR) reaction which is the reverse of reaction R8. This reaction is thermodynamically possible only above 640ºC and is active during our experimental conditions. The MDR reaction produces 2 molecules each of CO and H_2 and can be a contributing reaction to the significant increase in the yields of CO and H_2 beyond 790ºC (as shown in Table 3.5).

Table 3.5 shows various gas yields with respect to temperature. One-way ANOVA was performed with Tukey's HSD test to judge the significance of the effect of temperature on the gas yields and compare them with the values obtained during the oxygen gasification study.

Table 3. 5 Comparison of gas yields for CO_2 and air gasification

	Present study				**Abdoulmoumine et al.**	
Temperature	**700**	**790**	**850**	**934**	**790**	**934**
CO	216.0 ± 14.1 **A1**	213.6 ± 9.0 **A1**	408.8 ± 29.8 **A2**	423.8 ± 35.2 **A2**	379.63 ± 32.4	434.72 ± 19.9
CH_4	104.2 ± 17.1 **B1**	120.4 ± 13.6 **B1**	145.7 ± 10.7 **B1**	100.7 ± 3.9 **B1**	85.80 ± 16.6	53.69 ± 3.12
H_2	4.98 ± 1.1 **C1**	8.06 ± 2.5 **C1, C2**	14.9 ± 0.7 **C2 C3**	19.64 ± 2.1 **C3**	17.45 ± 3.4	25.73 ± 1.5
C_2H_2	1.17 ± 0.1 **D1**	1.88 ± 1.2 **D1**	2.89 ± 0.2 **D1**	0.57 ± 0.1 **D1**	6.09 ± 1.36	7.03 ± 0.4
C_2H_4	80.93 ± 5.5 **E1**	96.14 ± 37.2 **E1**	98.96 ± 12.5 **E1**	59.30 ± 3.9 **E1**	51.97 ± 12.39	37.32 ± 15.74

All yields reported in **g/kg dry biomass**. Means not connected with the same superscript are significantly different at the 0.05 level based on the Tukey comparison test.

The yields of CO and H_2 for CO_2 gasification are seen to be considerably lower than oxygen gasification. During oxygen gasification, presence of oxygen leads to higher CO production (R1) which also leads to an increase in H_2 production through water gas shift reaction (R5). These two reactions are almost absent during CO_2 gasification. Also, the amount of lower hydrocarbons produced in CO_2 gasification is much higher than oxygen gasification at both comparison temperatures.

One-way ANOVA was performed at 95% confidence interval on the yields (g/ kg dry biomass) C_2H_2 and C_2H_4. The highest value for C_2H_2 yield was 2.89 g/kg dry biomass at 850^oC whereas for C_2H_4 it was 98.9 g/ kg dry biomass at the same temperature. The statistical analysis showed that temperature did not have a significant effect on the concentrations of these two compounds (p-values 0.061 and 0.311 respectively).

Variations of important process characteristics for CO_2 gasification are shown in Table 3.6. None of the characteristics are a significant function of temperature and are not statistically different in the temperature range. A major difference spotted in the two gasification media was the conversion of carbon from biomass to gaseous products. Abdoulmoumine et al. reported values of 82.98 % and 82.1 % for 790^oC and 934^oC respectively whereas the current study using CO_2 gasification[##] had values of 73.19% and 81.9 % for the same temperatures. The overall carbon conversion for this study (char and gas products combined) was around 95% for all temperatures.

[##]Carbon conversion in CO_2 gasification considers total carbon in from both biomass and CO_2; and total carbon out includes unconverted CO_2.

Table 3. 6 Gasification characteristics with temperature variation

Temp (^oC)	**Syngas yield (Nm^3/kg dry biomass)**	**Carbon Conversion to gases (%)**	**HHV of Syngas 'N_2-free'(MJ/Nm^3)**
700	0.87 ± 0.04^{A1}	61.37 ± 3.2^{C1}	11.68 ± 0.38^{D1}
790	0.77 ± 0.03^{A1}	73.19 ± 23.3^{C1}	12.39 ± 0.99^{D1}
850	0.9 ± 0.04^{A1}	78.44 ± 4.3^{C1}	13.75 ± 0.31^{D1}
934	0.77 ± 0.03^{A1}	81.9 ± 2.9^{C2}	12.09 ± 0.45^{D1}

Means not connected with the same superscript are significantly different at the 0.05 level based on the Tukey comparison test.

The higher heating value (HHV) calculated on an N_2- free basis for both the media do not show much difference. For oxygen gasification it is highest at 790^{o}C (12.7 MJ/m^3) and decreases after that whereas for CO_2 gasification it peaks at 850^{o}C (13.75 MJ/m^3) which correlates with the higher hydrocarbon yields at that temperature.

The comparison between the two oxidizing media above shows that conventional gasification (using air/ oxygen) has more advantages as compared to CO_2 gasification. However, this process can still be financially viable since it consumes CO_2 which is a pollutant from almost every major industry. This process can be coupled with a power plant or a conventional gasification unit to use up the flue gas CO_2. Additionally, the incentives for reducing the carbon footprint can make this process an attractive option for energy producers.

3.2.3.4.4 Effect of CO_2/C ratio

Four CO_2 ratios in the range of 0.6 – 1.6 were used to study the effect of change in CO_2 flow rate on the process. The temperature chosen for this step was 850^oC. Table 3.7 shows the flow rates and velocities for CO_2 in correspondence with the CO_2/C ratios.

Table 3. 7 CO_2 flow rates and velocities

CO_2/ C ratio (w/w)	**CO_2 Flow rate (LPM)**	**Linear Superficial Velocity (m/s)**
0.6	1	0.0082
0.8	1.3	0.0107
1.04	1.6	0.013
1.52	2.24	0.01842

Figure 3-7 shows the variation of syngas component yields for various CO_2/C ratios. The yield of CO and H_2 under these conditions is in agreement with the findings reported in a review by Di Blasi.[63] One way analysis of variance test performed at 95% confidence on the component yields shows that CO and H_2 are significantly affected by the change in CO_2/C ratio (p-values 0.016 and 0.011 respectively). Tukey's comparison test shows that the change occurs between ratios 0.8 and 1.04. There is no significant change between CO_2/C ratios 1.04 and 1.52. The reason for this could be due to the slow nature of the char-CO_2 gasification step which allows only a certain amount of CO_2 to react in that low residence time. Table 3.8 shows that change in CO_2 flow rate has a significant effect on the yield of hydrocarbons.

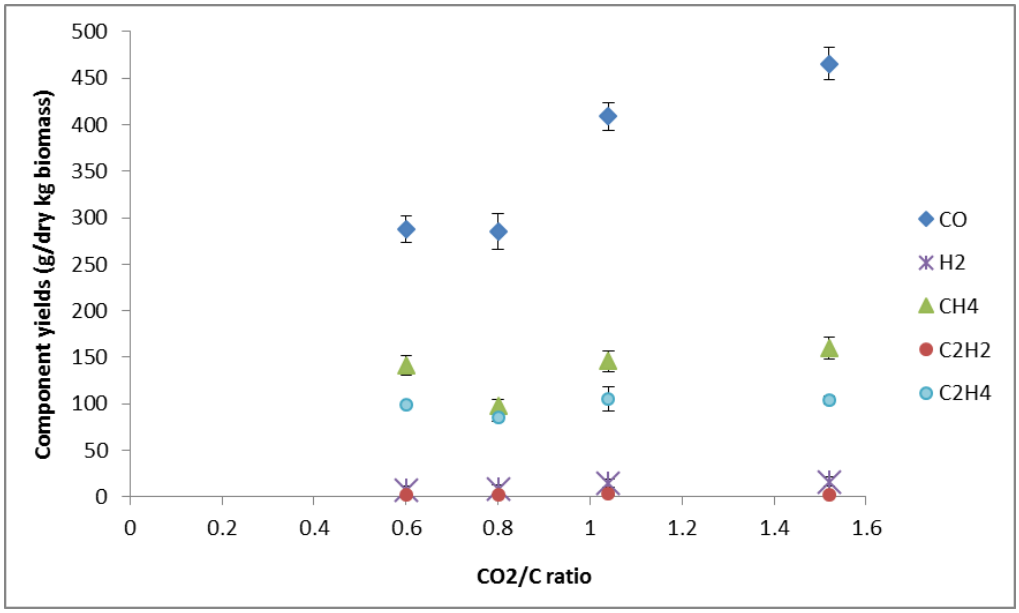

Figure 3- 7 Variation of syngas composition with CO_2/C ratio

Table 3. 8 Hydrocarbon yields for various CO_2/C ratios

CO_2/C ratio	**0.6**	**0.8**	**1.04**	**1.52**
CH_4	141.1 ± 10.4^{B1}	97.63 ± 7.2^{B2}	145.7 ± 10.7^{B1}	159.6 ± 11.7^{B1}
C_2H_2	2.49 ± 0.1^{D1}	2.31 ± 0.1^{D1}	3.1 ± 0.2^{D2}	2.5 ± 0.2^{D1}
C_2H_4	98.6 ± 0.9^{E1}	85.9 ± 1.7^{E2}	104.7 ± 4.3^{E1}	104.1 ± 1.4^{E1}

All yields reported in **g/kg dry biomass**. Means not connected with the same superscript are significantly different at the 0.05 level based on the Tukey comparison test.

There is a significant change in the quantity of CH_4 (p value 0.0129). This could be due to the change in activity of methane dry reforming (MDR) reaction which has been postulated earlier to be responsible for the consumption of methane during the process. Along with CH_4, both C_2H_4 and C_2H_2 yields change significantly with change in CO_2/C ratio. Table 3.9 shows the variation of important gasification characteristics with CO_2/C ratio. The table shows that there is significant variation in the yield of syngas at higher CO_2/C ratios which may be due to an

increase in the amount of methane as mentioned above. However, the conversion of biomass to gaseous product and the HHV of the output syngas do not change significantly.

Table 3. 9 Gasification characteristics with CO_2/C ratio variation

CO_2/C ratio (w/w)	**Syngas yield (Nm3/kg dry biomass)**	**Carbon Conversion to gases (%)**	**HHV of Syngas 'N$_2$-free'(MJ/Nm3)**
0.6	0.84 ± 0.06 **A1**	75.41 ± 2.6 **C1**	15.79 ± 1.06 **D1**
0.8	0.71 ± 0.05 **A1**	74.21 ± 2.6 **C1**	12.85 ± 0.86 **D1**
1.04	0.91 ± 0.04 **A1, A2**	78.44 ± 4.3 **C1**	14.67 ± 0.99 **D1**
1.52	1.1 ± 0.07 **A2**	85.36 ± 2.9 **C1**	13.12 ± 0.88 **D1**

Means not connected with the same superscript are significantly different at the 0.05 level based on the Tukey comparison test.

3.3 Conclusions

In a bench scale fluidized bed gasifier, the effect of temperature and CO_2/C ratio on biomass gasification using CO_2 was studied and the results compared to oxygen gasification study reported in literature. Lower char yield and consequently higher carbon conversion were observed in oxygen gasification than CO_2 gasification due to the presence of free oxygen available for combustion reactions. At lower temperatures, devolatilization seemed to be dominating the process. Effect of temperature on the process was significant, affecting the two main components of syngas – CO and H_2 which showed an increase with temperature. However, their yield was still lower as compared to oxygen gasification. Char oxidation reaction and subsequent water gas shift reaction during oxygen gasification were postulated to be the main reason. The peak HHV value for CO_2 gasification was slightly higher than air gasification due to the presence of more hydrocarbons.

It was also concluded that with increasing temperature, CO_2 gasification produces highly microporous char that greatly enhances CO_2 diffusion during the gasification step leading to higher conversion. The main reactions that come into play during the gasification step are char–CO_2 reaction (Boudouard), water gas reaction (char reforming) and free radical reactions leading to molecular hydrogen formation. There is some increase in methane as the temperature is increased but it reacts with CO_2 through the methane dry reforming (MDR) reaction which is thermodynamically possible only above 640^oC. This reaction may be the reason for significant increase in CO and H_2 concentrations beyond 790^oC. The change in CO_2/C ratio affects the yields of CO, H_2 and lower hydrocarbons. However, there was no significant change observed between CO_2 /C ratios of 1.04 and 1.52.

Chapter 4

Kinetics of southern pine char-CO_2 gasification and effect of metals on the process

Abstract

Carbon dioxide gasification of southern pine char was carried out in a fixed bed reactor at temperatures in the range of 800^{o}C – 975^{o}C. Evolution of carbon monoxide was used as the basis for conversion. The conversion vs. time data was fitted to three different solid- gas reaction models: volume reaction model (VRM); non-reactive core model (NRC) and random pore model (RPM). Regression analysis showed that RPM was the best at predicting experimental data. The measured change in char surface area was in agreement with the change in surface area predicted by the RPM. Furthermore, the RPM was used to predict the kinetic parameters of gasification of chars that were loaded with alkali and alkaline earth metals such as Na, Mg, K and Ca. The reduction in activation energy and hence increase in gasification reactivity was highest for potassium followed by calcium, sodium and magnesium. The pore structure parameter was highest for sodium implying a significant change in surface area of the char with initial conversion.

4.1 Introduction

Gasification of char is one of the steps in the biomass gasification process. Char reactions tend to be slow and endothermic. Conversion of char is the rate-limiting step when CO_2 is used as a gasifying agent.[24] Therefore, it is of vital importance to study the kinetics of the reaction of char with CO_2. Different methods have been employed by various studies to interpret the kinetic

parameters of the char-CO_2 gasification step. The reaction of char with CO_2 leads to a change in the pore structure and surface area of the solid during conversion. Three different reaction models based on different solid-gas reaction mechanisms are used in this study. The Random Pore Model (RPM) contains a pore structure parameter (Ψ) that represents the change in surface area of the char particle during conversion. Since the reaction of carbon and CO_2 is the slowest step, various catalysts have been used in literature to increase the reaction rate. Alkali, alkaline earth and transition metals have shown promising results. The current study focuses on identifying a kinetic model for the southern pine char-CO_2 gasification from the models mentioned above and using the model to quantify the effect of alkali and alkaline earth catalysts on the process.[159]

4.2 Methodology

4.2.1 Feedstock preparation

Pine wood chips were obtained from a local plant in Opelika, Alabama. The wood chips were dried in open air for a few days and ground using a hammer mill 1-inch screen size and sieved. 100 grams of ground pine was placed in a large tubular reactor which was heated at 10^{o}C/min up to 800^{o}C and held there for 60 minutes. Nitrogen was flowing continuously through the reactor at 7 l/min. Each run yielded around 25 grams of char. After a few runs, all the char was mixed and subjected to the same treatment again to achieve uniformity. Ultimate and proximate analyses were carried out in accordance with ASTM standards. CHNS/O elemental analyzer (Perkin Elmer, Model 2400, Waltham, MA) was used to perform the ultimate analysis. The HHV of the char sample was determined using a bomb calorimeter (IKA Bomb calorimeter, ModelC-200, Wilmington, NC). Particle density was calculated from volume measurements using a gas pycnometer (Micromeritics AccuPyc 1340, Norcross, GA). A camsizer was used to

determine the particle size distribution of the char sample. Surface area measurements were done using Brunauer–Emmett–Teller (BET) surface area and porosity analyzer (Micromeritics, TriStar II, Norcross, GA). The char samples were degassed at 300^{o}C with a continuous flow of helium for 16 hours. The samples were then placed in the analyzer and Nitrogen was used as the adsorbate gas to measure the surface area. Char for experiments was kept in an air-tight container and stored in a controlled environment until it was used for carbon dioxide gasification.

4.2.2 Loading of metal catalysts

Four different metal catalysts (Na, Mg, K and Ca) were impregnated onto the pine char. The maximum amount of loading targeted was 0.1-gram metal per gram carbon in the char. In accordance with this target, a calculated amount of metal acetate was dissolved in ultrapure water and stirred using a magnetic stirrer until complete miscibility was achieved. 30 grams of char was added to this aqueous solution and placed on a temperature controlled shaker (New Brunswick scientific, Excella E24, Edison, NJ) at 25^{o}C for 48 hours. This mixture was allowed to stand for another 24 hours. The wet loaded char was filtered and spread out in an aluminum tray and placed in an oven to dry at 105^{o}C for 24 hours. The initial and final weights of char were noted and approximate amount of loading was determined. An ICP MS with an octopole reaction/ collision cell (Agilent 7900 ICP MS, Santa Clara, CA) was used to measure the exact amount of catalyst loading on the char. The loaded char samples were analyzed under a scanning electron microscope (ZEISS EVO50 SEM, Jena, Germany) to study the distribution of the metals on the char surface.

4.2.3 Fixed bed experimental setup

Figure 4-1 depicts the experimental setup used for the CO_2 gasification of pine char. The setup consists of a stainless steel tubular reactor (i.d. =0.5 in.) mounted vertically inside a

furnace (Thermo scientific, Lindberg Blue M). A known amount (2.5 ± 0.2 g) of char was placed between two quartz wool plugs inside the reactor to make a fixed bed. A thermocouple passes through the bed indicating the temperature of the bed throughout the process. Nitrogen was flown through the reactor at 0.3 ± 0.05 l/min when the reactor is being heated. Once the gasification temperature was reached, CO_2 flow was switched on at 1.3 l/min. The gases escaping the reactor were passed through ice-cooled iso - dodecane and a bed of activated carbon to prevent any unwanted compounds from entering the gas analyzer. The gas mixture (N_2, CO and CO_2) is analyzed using a micro GC (Agilent 3000A, Santa Clara, CA) which analyzes a sample every 3 minutes.

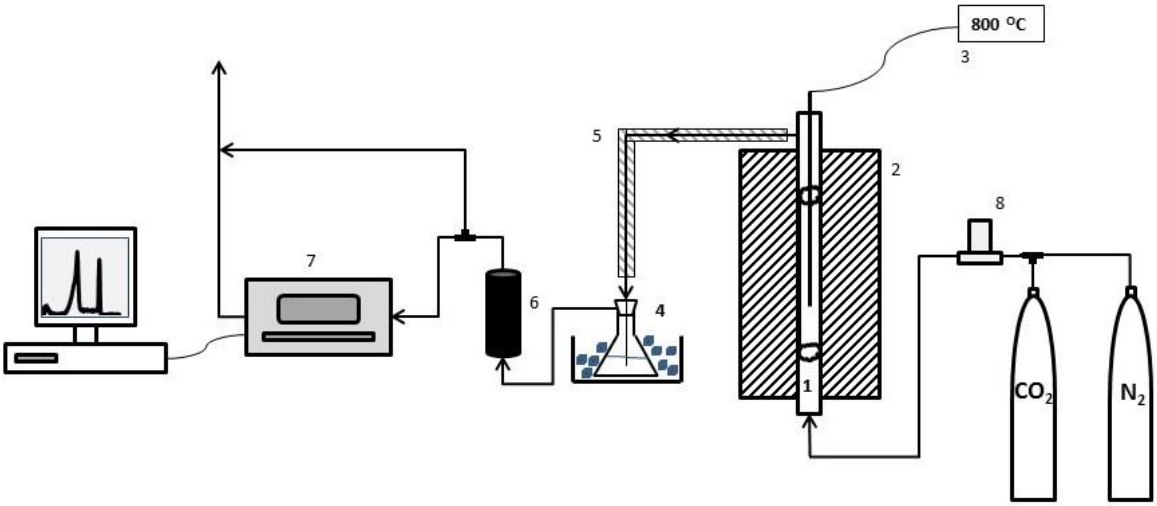

Figure 4- 1 Schematic of fixed bed char gasification setup
1. Tubular reactor; 2. Furnace; 3. Temperature indicator; 4. Condenser; 5. Heated line; 6. Activated carbon; 7. Gas Analyzer; 8. Flow meter

The Boudouard reaction or char - CO_2 reaction is a highly endothermic reaction which takes place at high temperatures[61] (Equation 4.1). Since the Boudouard reaction is the only reaction taking place, the conversion of char can be easily estimated using the evolution of CO as basis. The yield of CO (g/min) at any time is calculated by comparing nitrogen input flow rate and its

concentration in the output. Conversion can thus be measured as the ratio of amount of CO evolved up to time *t* to the total amount of CO released as shown in Equation 4.2.

$$C\ (char) + CO_2 \longrightarrow 2\ CO;\ \Delta H = +172.67\ kJ/mol \quad [4.1]$$

$$\text{Conversion [X] at time t} = \frac{cumulative\ amount\ of\ CO\ produced\ until\ time\ t}{Total\ amount\ of\ CO\ produced} \quad [4.2]$$

All the samples were gasified until complete conversion. This was adjudged by the diminishing concentration and finally absence of CO in the output gas. The time taken for complete conversion varied from 220 minutes at 800^{o}C to 50 minutes at 975^{o}C. Alternatively, for the purpose of surface area measurements at various conversion levels, the flow of CO_2 was turned off and the furnace is shut down at a predetermined point to achieve the desired conversion. After the run was completed, the reactor was allowed to cool down with N_2 still flowing.

4.2.4 Reaction models and kinetic parameters

Three different solid-gas reaction models viz. volume reaction model (VRM), non-reactive core model (NRC) and random pore model (RPM) are used to interpret the conversion profiles obtained at each temperature. These models were chosen because they assume different mechanisms for the solid-gas reactions. The VRM speculates that the reaction is occurring homogenously throughout the volume of the particle. The conversion of the solid particle with respect to time is described as:

$$X = 1 - \exp(-k\,t) \quad [4.3]$$

where k and t are rate constant and reaction time respectively. The NRC hypothesizes that the solid- gas reaction initially occurs at the surface and gradually penetrates into the particle. This leaves a constantly shrinking non-reactive core at the center of the particle.

$$X = 1 - (1 - \mathrm{k\ t})^{3} \qquad [4.4]$$

The RPM proposed by Bhatia and Perlmutter [101], assumes that the structure of the pores in the solid and hence the surface area available for reaction is constantly changing during the course of the reaction. It considers the effect of enlargement of pores to yield more surface area in the initial stages of conversion, and the coalescence of these enlarged pores leading to a reduction in reactive surface area and thereby decreasing the reactivity of the solid particle in the later stages of conversion.

$$X = 1 - \exp(-k\,t\,[1 + k\,t\,\tfrac{\Psi}{4}]) \qquad [4.5]$$

The pore structure parameter Ψ relates to the initial pore structure of the solid and is an indicator of the amount of change in specific surface area as the reaction progresses. It can be calculated using the initial pore surface area per unit volume S_0, the initial pore length L_0 and the particle porosity ε_0.

$$\Psi = \frac{4\pi L_0\,(1-\varepsilon_0)}{S_0^2} \qquad [4.6]$$

In this study, Ψ is treated as a parameter obtained by fitting and optimizing the RPM with the experimental data. The other kinetic parameters were determined using the Arrhenius rate law.

$$k = A\exp(-E_a/RT) \qquad [4.7]$$

4.3 Results and discussions

4.3.1 Char properties

The physical properties and ultimate analysis of char are shown in Table 4.1. The higher heating value (HHV) of the char appears to be much higher than that of raw pine (HHV = 20.81 MJ/kg). This is due to the higher amount of carbon and consequently lower amount of oxygen in the char. The BET surface area for char appears to be in agreement with the study by Sircar et al.[108] (BET area = 218 m^2/g)

Table 4. 1 Physical properties and ultimate analysis of unloaded char

Physical properties	
Ash content (wt %, d. b.)	2.8 ± 0.31
Bulk Density, (g/cm^3)	2.18 ± 0.6
Particle density, (g/cm^3)	2.32 ± 0.35
Particle size range, (microns)	150 - 600
BET surface area, (m^2/g)	197.6 ± 7.3
Higher Heating Value (MJ/kg)	32.65 ± 0.35
Elemental Analysis (wt. % d. b.)	
C	84.67 ± 0.95
H	2.56 ± 0.08
N	0.04 ± 0
O (by difference)	9.96 ± 0.73

d. b. = dry basis

4.3.2 CO yield and char conversion

The instantaneous CO yield (g/min) was calculated by quantifying the amount of nitrogen entering and leaving the reactor. The conversion of char during the process is calculated based on the evolution of CO using Equation 2. Figures 4-2(a) and 4-2(b) show the CO yield and char conversion with time. The initial CO yields for 900°C, 850°C and 800°C are considerably lower than 975°C and 945°C. Also, the plots for 975°C, 850°C and 800°C show constant declining yields whereas profiles for 900°C and 945°C show an increase in the yield in the middle and initial phases of conversion respectively. This shows the importance of the kinetics of the process which leads to many variations in such a narrow range of temperature. Char conversion profiles show the variation in times taken to achieve complete conversion; which are in the range of 50-90 minutes for the four higher temperatures and 220 minutes for 800°C.

Boudouard reaction is a highly endothermic reaction occurring inside the char particles during char-CO_2 gasification. This may lead to a temperature difference between the particle temperature and the temperature of the gasifying agent. The calculation of the heat transfer between bulk gas and reacting particle is shown in Appendix F. The particle temperature correction was calculated between 0.85°C to 7°C at different reaction temperatures.

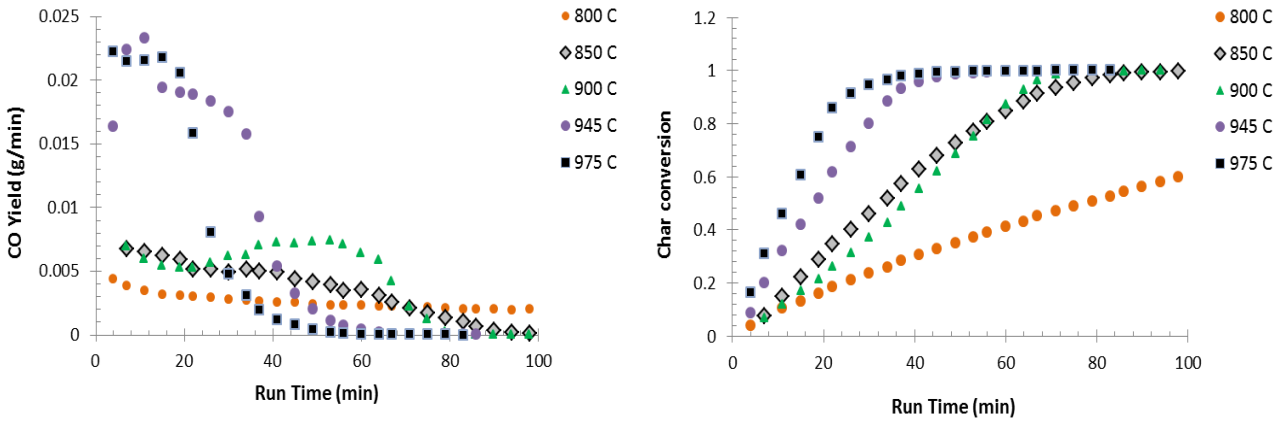

Figure 4- 2 Variation of (a) instantaneous CO yield with time (b) char conversion with time

4.3.3 Model fitting

The conversion time plot was used to fit all three reaction models described above. The models are fitted using statistical software (SAS) which uses a non-linear Gauss Newton method to find the parameter values. The software also performs a lack-of-fit test to judge if the model fits the data. The fits for each model are shown in Figures 4-3 (a), (b), and (c).

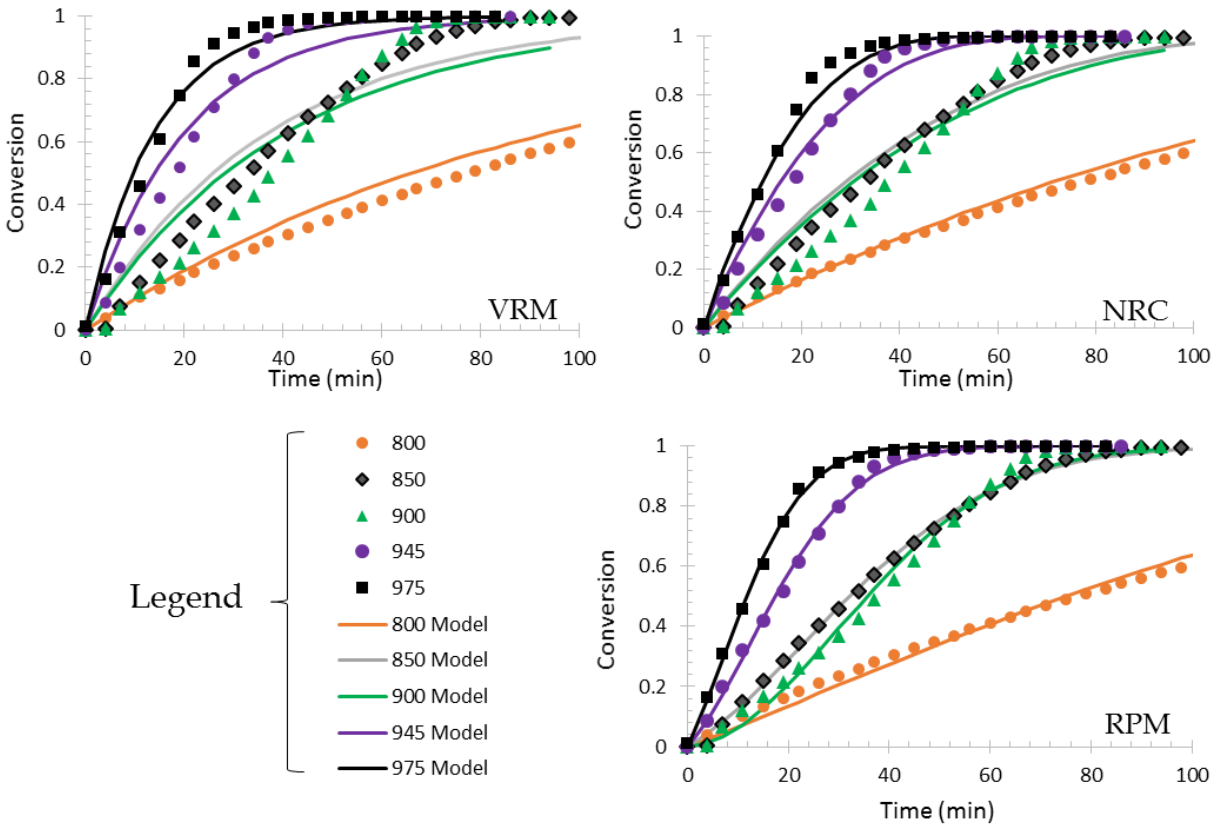

Figure 4- 3 Experimental data fitted with (a) VRM, (b) NRC and (c) RPM

A visual evaluation of the fits reveals that VRM and NRC show better agreement for profiles at lower temperatures but are off when predicting the data at 900^{o}C and 945^{o}C. However, the fits for RPM appear to be efficiently predicting the conversion profiles at all temperatures. For better judgment, the experimental and predicted conversion profiles for each temperature and model were subjected to general regression in Minitab software. The R^2 values obtained from the

regression confirm that of the three models, RPM was best at predicting the experimental data. The R^2 values averaged over temperature for each model are shown in Table 4.2.

Table 4. 2 R^2 values for various models averaged over temperature

Model	**Adjusted R^2 value (%)**
VRM	94.69
NRC	96.89
RPM	99.15

Also, kinetic rate constants obtained for each temperature in all three models were used in Equation 7. The natural log of the rate constant (ln K) was plotted against the inverse of temperature (1/T) to determine the values of the kinetic parameters. These values were then compared to values from similar studies in literature and Table 4.3 shows the comparison.

The value of Ψ obtained from RPM fits increased with increase in temperature. This correlates well with reports in literature.[108,119] RPM predicts that the surface area of the particle increases during the initial conversion phase due to the expansion of pores. The surface area of the particle can be correlated to conversion using Equation 4.8.

$$S = S_0(1 - X)\sqrt{1 - \Psi \ln(1 - X)} \qquad [4.8]$$

S is the volumetric surface area (m^2/cm^3) of the particle and S_0 is its initial value. *S* can be converted into specific surface area (SSA, m^2/g) by dividing it with the density of the particle. The measured values of specific surface area through BET measurements are then compared to the calculated values by plotting against conversion. Table 4.4 shows the measured values of BET surface area at different conversion values for 850°C.

Table 4. 3 Comparison of kinetic parameters from current study with literature

Study	Model	E_a (kJ/mol)	ln A	Ψ (avg.)	Temp. (°C)
Current study	VRM	280 ± 32	7.94 ± 0.4	-	800 - 945
	NRC	248 ± 14	6.03 ± 1	-	800 - 945
	RPM	219 ± 16	5.13 ± 1	9.88	800 - 945
Sircar et al.[108] (2014)	VRM	217	15.4	-	725 - 900
	NRC	186	10.7	-	725 – 900
	RPM	125	5.0	5.5	725 - 900
Yuan et al.[109] (2011)	RPM	248.5	6.75	50.01	850 - 1050
Fermoso et al.[80] (2009)	VRM	184	14.36	-	750 - 900
	NRC	185	14.2	-	750 - 900
	RPM	184	14.22	0.7	750 - 900

Table 4. 4 Variation of measured surface area with conversion at 850°C

Conversion [X]	SSA (m^2/g)
0.1	290.41
0.2	393.88
0.45	533.74
0.85	562.24
0.93	705.24

To account for the reduction in amount of char due to conversion, the value of SSA is multiplied with (1-X). Figure 4.4 shows the comparison between measured and calculated surface area plotted against conversion.

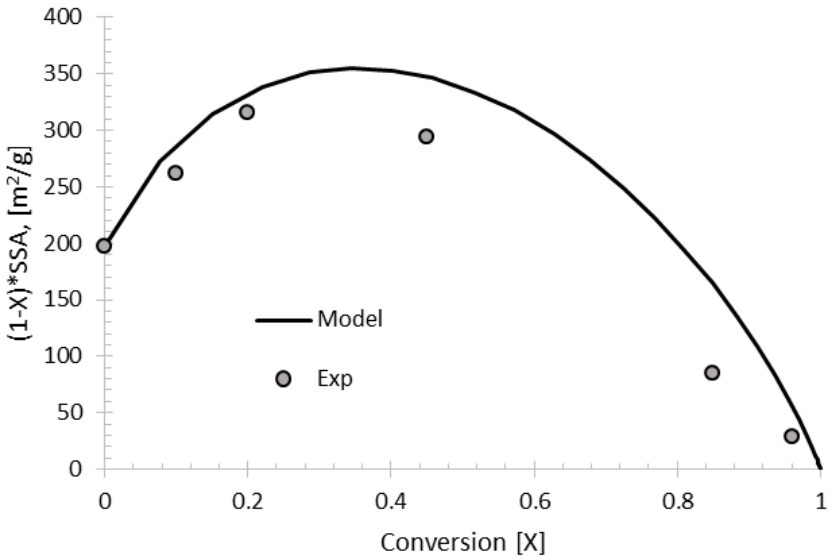

Figure 4- 4 Comparison of change in measured and calculated surface area plotted against conversion.

The trend of the measured points and their proximity to the predicted values validate the use of RPM to predict experimental data. On the other hand, some studies[106] do it the other way, i.e. use the measured BET area data to calculate the value of Ψ.

4.3 Effect of metal catalysts

The exact amount of catalyst loading onto the char is shown in Table 4.5. The bold values are the concentration values of metal being loaded. The amount of catalyst impregnated on char is measured in wt %. The loaded char samples were investigated by SEM-EDX which showed the distribution of metals over the char surface. The SEM images are shown in Figure 4-5.

The loaded char was subjected to the same CO_2 gasification procedure as discussed above at four temperatures: 800ºC, 850ºC, 900ºC and 945ºC. RPM was used to predict the conversion vs time behavior for each catalyst. Figure 4-6 shows the RPM plots for each catalyst. Visual evaluation of the plots suggests that the fits for calcium, potassium and magnesium appear to be better than the fits for sodium which was confirmed by general regression performed on the predicted and experimental data.

Table 4. 5: Metal catalyst loading on char

Sample	**Actual loading (wt %)**			
	Na	**Mg**	**K**	**Ca**
Unloaded char	0.52	0.02	1.02	1.05
Na –char	**1.24**	0.11	0.80	0.42
Mg – char	0.31	**1.00**	0.71	0.35
K – char	0.75	0.16	**1.95**	0.80
Ca - char	0.16	0.06	0.66	**1.85**

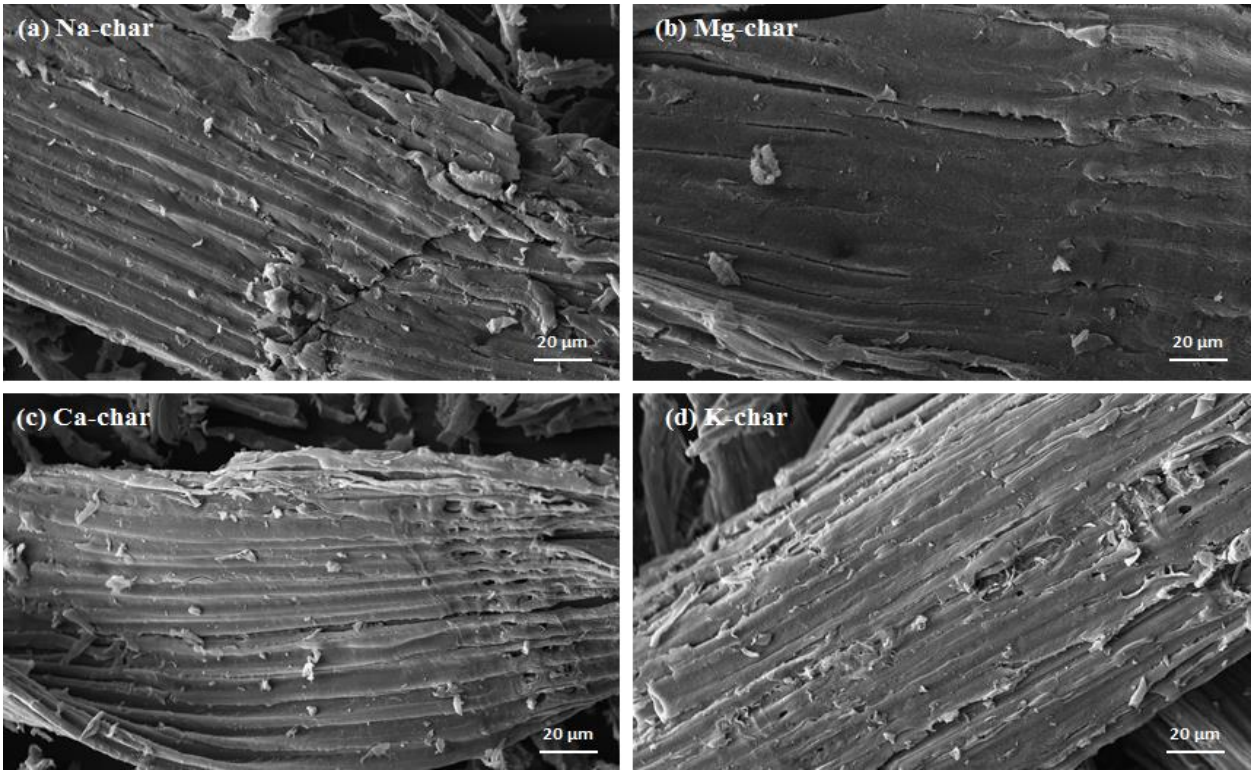

Figure 4- 5: SEM images: (a) Na- char, (b) Mg – char, (c) Ca – char, (d) K – char

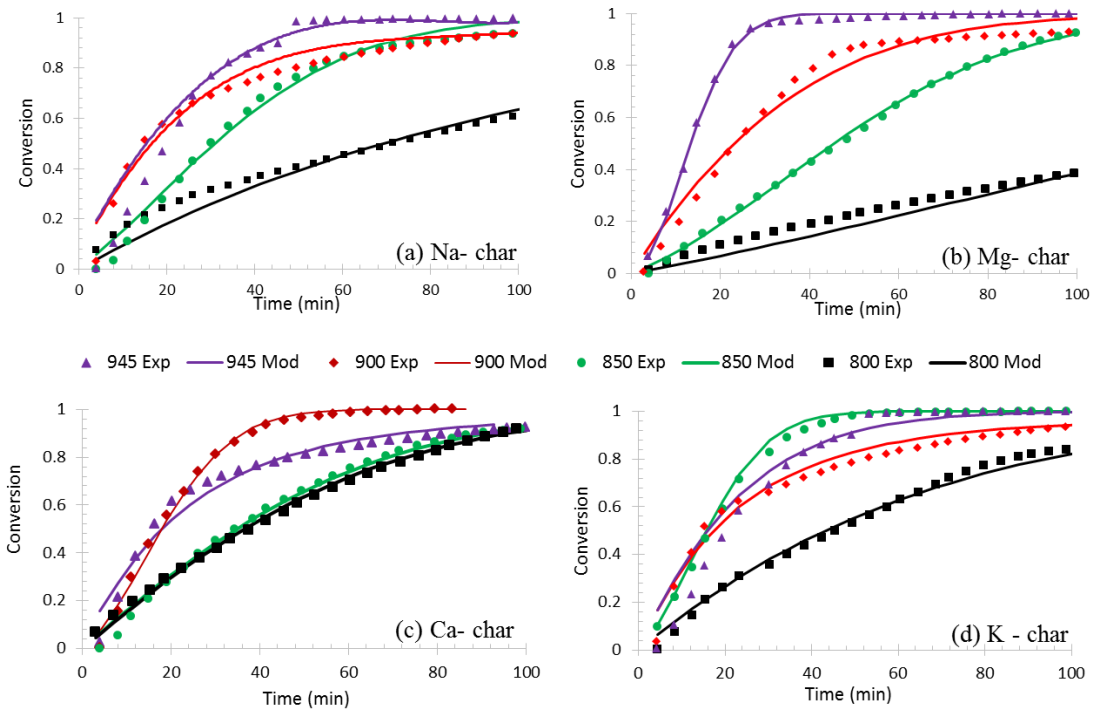

Figure 4- 6: RPM fits for (a) Na- char, (b) Mg – char, (c) Ca – char, (d) K – char

Values of pore structure parameter Ψ and kinetic parameters E_a and ln A are shown in Table 4.6. As compared to the unloaded char, the time required for complete conversion reduced with the addition of metal catalysts. The mechanism used to describe the CO_2 gasification is a widely accepted oxygen-exchange mechanism proposed by Ergun[113] as shown in equations [9] and [10]:

$$C_f + CO_2 \longrightarrow C(O) + CO \qquad [9]$$

$$C(O) + C \longrightarrow C(O) + C_f \qquad [10]$$

Where C_f denotes the free carbon active site and C(O) represents the carbon-oxygen surface complex. The presence of metal aids in the extraction of oxygen from CO_2; the formation of an intermediate metal-carbon-oxygen complex and its decomposition. This leads to a faster utilization of surface active sites and conversion from CO_2 to CO. All four metal catalysts were successful in lowering the activation energy of the process. However, the catalytic effect was highest for potassium as it managed to lower the activation energy by 114 kJ/mol followed by calcium (102 kJ/mol), sodium (75 kJ/mol) and magnesium (74 kJ/mol). The data obtained in this study is in agreement with the data by Lahijani et al.[119] where the activation energy for CO_2 gasification of pistachio nut shell char with 5% Na loaded was 151.46 kJ/mol.

Table 4. 6 RPM kinetic parameters for all catalysts

Catalyst	**E_a (kJ/mol)**	**ln A**	**Ψ(avg)**
Na	142.4 ± 17	11.4 ± 3	21.2 ± 8
Mg	143.4 ± 37	14.4 ± 3	4.9 ± 2
K	104.2 ± 24	8.3 ± 1	11.7 ± 9
Ca	115.8 ± 58	8.3 ± 5	8.7 ± 2

4.4 Conclusion

Three solid-gas reaction models were used to interpret the kinetics of pine char gasification with CO_2 in a fixed bed reactor. Regression analysis and char surface area measurements suggested that the random pore model (RPM) was best suited to predict the experimental data. Values of pore structure parameter, activation energy and frequency factor were calculated and compared with literature.

Chars impregnated with four different metal catalysts were gasified and the random pore model was used to calculate the activation energy for each catalyst. The reactivity of the loaded chars was found to be in the order of: K-char > Ca –char > Na –char >= Mg –char. The pore structure parameter was the highest for sodium implying that change in surface area with conversion is highest for sodium.

Chapter 5

Process modeling of fluidized bed biomass-CO_2 gasification using ASPEN plus

Abstract

Gasification of pine sawdust and pine char with carbon dioxide was earlier carried out to understand the effect of process parameters such as temperature and CO_2 flow rate, along with determining the kinetics of the process while using different catalysts. In this work, a comprehensive model using ASPEN plus simulator was developed to simulate the output performance of the fluidized bed gasifier. Different reactor models are used to simulate the various stages in a biomass-CO_2 gasification process. A dynamically linked FORTRAN subroutine is used to include the kinetic model for the Boudouard reaction into the simulation. Results from sensitivity analysis performed on the model are compared with the experimental results for changing operating conditions such as gasification temperature and CO_2 flow rate. Parameters such as output syngas composition, individual gas yields, syngas higher heating value and carbon conversion are compared to evaluate the validity of the model.

5.1 Introduction

Due to the number and complexity of parameters involved in gasification, it is essential to carry out an in depth study of the factors affecting the process. Variation in type of feedstock, ash content, temperature, oxidant type can all significantly affect the output of the process. A study incorporating all these characteristics can be cumbersome and financially not feasible. Modeling of a process can provide instant access to results of variation in conditions without the

need for physical experiments. CFD modeling involves the method of simultaneously solving multiple equations that deal with the conservation of mass, energy, momentum and species in the process. These purely mathematical models are able to predict the behavior of the process accurately but need a set of very precise equations governing all the affecting parameters [136]. ASPEN plus modeling is a tradeoff between the complexity of the process and the need to have the knowledge of all the equations. This method allows the use of pre-defined processes and reactors which can be customized using codes that can be incorporated into the model. Multiple stages of a process can be separately modeled and then combined into one single simulation [160]. Inherent sensitivity analysis tools and the option of allowing financial assessment using add-ons such as FORTRAN subroutines makes this approach very attractive for practical modeling purposes.

As mentioned earlier, the overall concept of this research is to capture the CO_2 from industries or power plants, and use it as a feed for biomass-CO_2 gasification. The resultant syngas can be used for manufacturing chemicals through methanol synthesis or Fischer-Tropsch synthesis, and for fuel and power generation purposes. The block diagram in Figure 5-1 outlines the idea of this research followed by the details of the current objective.

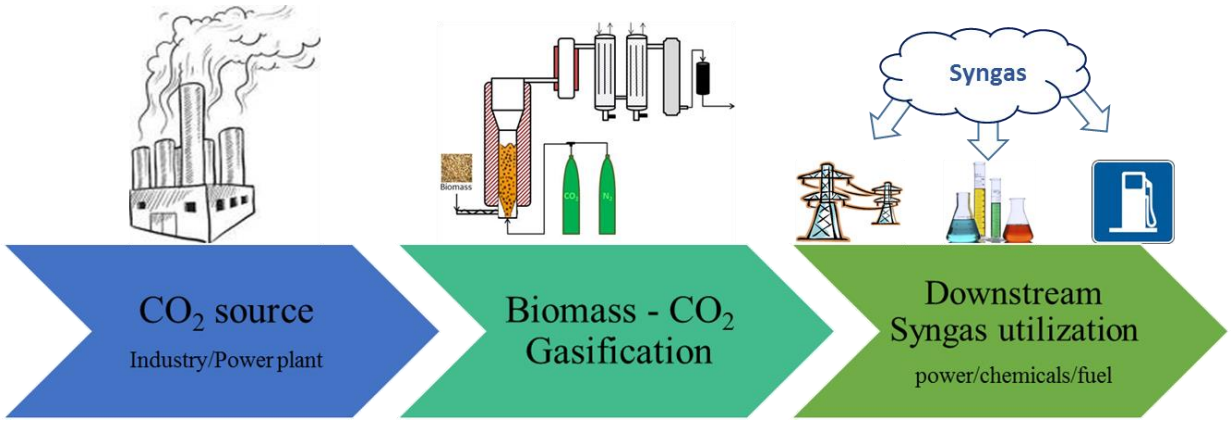

Figure 5- 1 Outline of the current research concept

The idea behind this objective is to simulate the gasification process from the point of receiving CO_2 from the source, to the point of delivery for downstream syngas utilization. This model is designed to mimic the performance of the bench-scale fluidized bed gasifier from Objective 1 [155]. The main purpose of this model is to provide energy-producers with a viable CO_2- gasification model which they can combine with models for upstream CO_2 source and downstream syngas processing, and perform life cycle analysis of the overall concept of this research.

At initial stages of this research, a preliminary ASPEN Plus model was developed that utilized Gibbs free energy minimization to predict the effect of operating parameters such as temperature, pressure, and oxidizing media on biomass conversion and syngas composition [161]. This preliminary model did not consider the chemistry or the kinetic aspects of the process. The process of gasification was simulated using a single reactor which yielded the most 'stable' product composition assuming that the reactants react in a fully mixed condition for an infinite period of time. The details of this model are described in Appendix H.

The main aim of this current study was to develop a model that is able simulate the steady-state output of the bench scale atmospheric fluidized bed gasifier studied in Objective 1. This was achieved by incorporating the findings about the chemistry and kinetics of the process from Objectives 1 and 2. The output from the sensitivity analysis of the model is compared to the actual experimental data for temperature and CO_2/C ratio variation.

5.2 ASPEN Plus simulation

The current simulation was modeled using ASPEN Plus version 8.6 and uses different reactors to simulate various stages of the gasification process. The overall stream classification

was specified as MCINCPSD to enable the inclusion of gases, conventional inert solids, and/or non-conventional materials. The various chemical components taking part in or produced during the process are specified in the component list at the beginning during the setup of the simulation (Appendix I). The components 'BIOMASS' and 'ASH' are defined as non-conventional solids with an option of specifying the particle size distribution whereas carbon is defined as a conventional solid. All other components are specified as conventional components as defined in the ASPEN Plus library. The proximate and ultimate analyses along with the particle size distribution for the biomass are specified from experimental data.

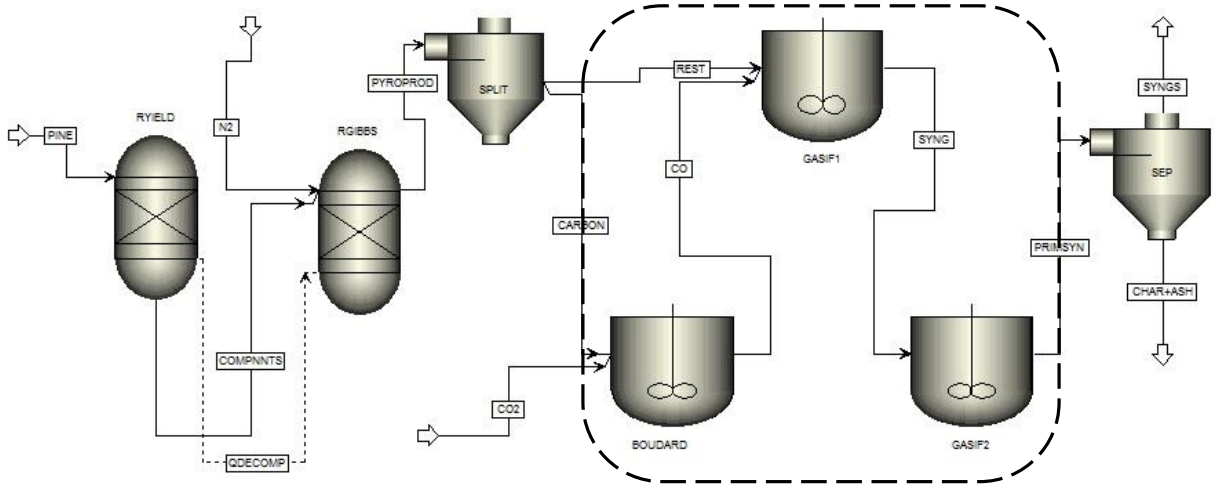

Figure 5- 2 ASPEN Plus simulation for biomass-CO_2 gasification

The stream PINE containing biomass enters process block RYIELD. The feed decomposes into its constituting components carbon, hydrogen, oxygen, nitrogen, ash and moisture based on the proximate and ultimate analyses. The output from the RYIELD block is then conditioned to the temperature and pressure for the gasification process. This stream along with nitrogen, enters the RGIBBS reactor. This step simulates the devolatilization stage of the process. The underlying assumption here is that this step occurs in accordance to the minimization of Gibbs free energy. This assumption is supplemented by some studies in the

literature[134,162,163]. The reactor identifies all possible products from the list of components specified earlier and reaches a stable product configuration, and the product stream from this step 'PYROPROD' enters the separator block 'SPLIT' which splits the stream into carbon and the rest.

The gasification reactions have been distributed into different steps based on the importance of the reactions as deducted in the results from Objective 1 [155]. All the steps are simulated using the RCSTR reactor model in the ASPEN library which ensures complete mixing of all the components throughout the entire volume of the reactor as is the case with the experimental fluidized-bed gasifier. The results from the experimental studies identified Boudouard reaction (R3), Water-gas reaction (R4), and Methane dry reforming reaction (reverse R8) as the dominant reactions. Additionally, Boudouard reaction is also the rate-limiting step of the process, for which random pore model was identified as the kinetic model in Objective 2 [159]. This kinetic model is included in the simulation using a FORTRAN subroutine (Appendix J), written separately and then dynamically linked using the 'aspcomp' procedure in ASPEN Plus. The subroutine is written in the version Fortran-90, using MS Visual Studio 2010 along with Intel Compiler XE 13 as the compiler combination.

The entire gasification step is simulated by the three reactors inside the hyphenated box shown in Figure 5-2. The model is structured such that the dominant reactions occur first and are allowed to reach equilibrium; followed by the non-dominant reactions in the process. The reactor blocks 'BOUDARD' and 'GASIF1' simulate the dominant set of reactions as mentioned earlier, whereas the rest of the gasification reactions occur in reactor block 'GASIF2'. The FORTRAN subroutine for the kinetic model is executed across the 'BOUDARD' reactor block wherein carbon and CO_2 streams enter and the Boudouard reaction is specified as the only reaction

occurring. Since, this reaction can occur only in the sand bed during the experiment, the volume of the reactor block is specified as the volume of the bed, ignoring the volume of the freeboard. The product stream from this block contains carbon monoxide, unconverted CO_2 and carbon based on the kinetics.

Table 5. 1 Important gasification reactions

Reaction no.	Reaction Name	Reaction Chemistry
R1.	Combustion	$C + ½ O_2 \leftrightarrow CO$
R2.	Combustion	$CO + ½ O_2 \leftrightarrow CO_2$
R3.	Boudouard	$C + CO_2 \leftrightarrow 2CO$
R4.	Water-gas	$C + H_2O \leftrightarrow CO + H_2$
R5.	Water-gas shift	$CO + H_2O \leftrightarrow CO_2 + H_2$
R6.	Methanation Reactions	$C + 2H_2 \leftrightarrow CH_4$
R7.		$CO + 3H_2 \leftrightarrow CH_4 + H_2O$
R8		$2CO + 2H_2 \leftrightarrow CH_4 + CO_2$
R9.	Methane steam reforming	$CH_4 + H_2O \leftrightarrow CO + 3H_2$

All the products including the ‘REST’ stream after the split enters the ‘GASIF1’ block where Water-gas reaction (R4) and Methane dry reforming reaction (reverse R8) are specified, and proceed to achieve the chemical equilibrium of the reactions. This is followed by reactor block ‘GASIF2’ which contains the rest of the gasification reactions (R1, R2, R5, R9 and

methanation reactions). All these reactions can take place in either the bed or the freeboard and hence the volume of the entire gasifier is specified as the volume of the reactor block. The end product then enters a separator or cyclone block 'SEP' which separates the stream and delivers the char and ash at the bottom and the syngas at the top.

5.2.1 Results and analysis

5.2.1.1 Effect of temperature on product gas composition

The initial temperature for all the reactors in the model was set at 800^{O}C. The sensitivity analysis tool in ASPEN Plus allows the variation of a defined parameter and tabulates the results in accordance with the variation. Using this tool, the temperature for the process model was varied in the range of 700^{O}C to 935^{O}C, at intervals of 25^{O}C; to emulate the process temperature range studied in the experiments. The results from the sensitivity analysis were compared to the data from the steady-state performance of the gasifier. The concentrations and yields of the syngas components such as CO, H_2, CH_4 were compared along with process characteristics like char, liquid and gas yields; carbon conversion to gases, overall syngas yield and higher heating value.

Figure 5-3 illustrates the effect of temperature on the yield of the three product streams (char, liquid and gas) and its comparison to the experimental data. The solid lines on the plot indicate the variation of the yields with temperature as predicted by the model whereas the dots indicate the experimental data points. The char yield for the model is defined as the amount of carbon and ash obtained in solid form at the end of the process; whereas the water vapor in the product stream is classified as liquid yield. The trends for the char and gas yields predicted by the model seem to follow a similar trend as the experimental data. The trend for liquid yield from

the model shows a gradual but steady decline as opposed to a fluctuating trend from experimental data.

The magnitude of the values predicted by the model for all the three product streams are very close to the data points at higher temperatures but show deviation from them at the lower temperatures of $790^{O}C$ and $700^{O}C$ as shown in Table 5.2. The possible reason for this could be the extent of the devolatilization step that occurs in the initial stages. As was postulated in Objective 1, devolatilization is the overpowering step at lower temperatures. Hence, the 'activity' of this step determines the stream yields at those temperatures. The model assumes complete devolatilization of the feed even at $700^{O}C$ and $790^{O}C$ which may not be the case experimentally due to insufficient residence time for the reacting feedstock in the gasifier. Additionally, the model identifies all products that are thermodynamically possible during this step leading to higher extent of devolatilization.

However, at higher temperatures, $850^{O}C$ and $934^{O}C$, the activity of devolatilization during the experiments increases to match the extent predicted by the model. In addition, the activities of the gasification reactions increase leading to a higher gas yield and lower char yield. The magnitude of the values predicted by the model for all the three product streams are very close to the experimental data points.

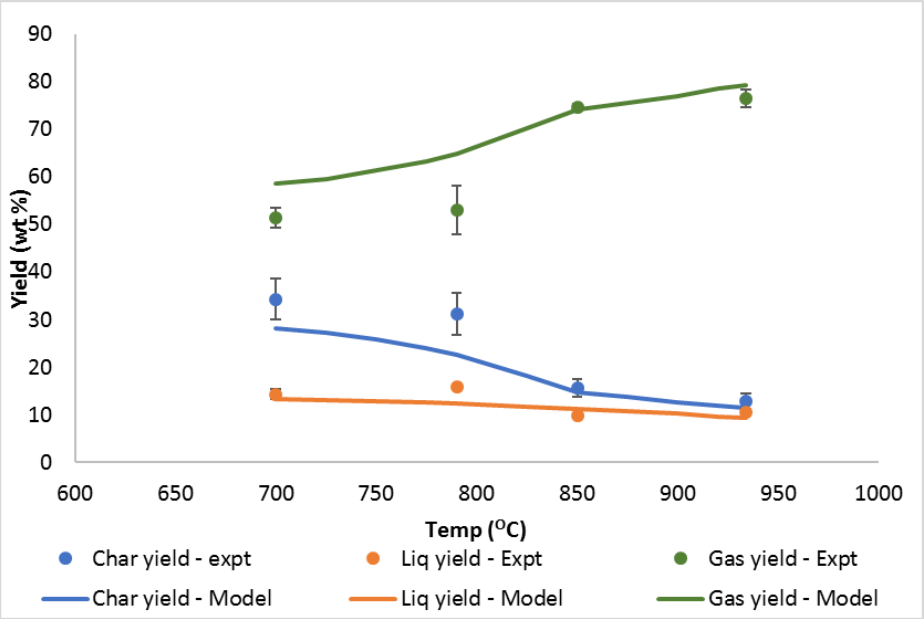

Figure 5- 3 Comparison of stream yields for different temperature

Table 5. 2 Comparison of product stream yields

	Experimental			Model		
	Char yield	**Liquid yield**	**Gas yield**	**Char yield**	**Liquid yield**	**Gas yield**
Temp(°C)						
700	34.29 ± 2.15	14.29 ± 1.11	51.42 ± 1.1	28.26	13.26	58.48
790	31.13 ± 2.3	15.85 ± 0.3	53.02 ± 2.5	22.59	12.45	64.96
850	15.60 ± 0.94	9.87 ± 0.51	74.54 ± 0.4	14.77	11.18	74.05
934	12.89 ± 0.8	10.57 ± 0.1	76.53 ± 0.9	11.48	9.37	79.15

All yields reported in **percentage**. The experimental yields are means of results from duplicate runs.

For better judgement, the experimental data points and the model predictions for all three streams were subjected to general regression using statistical software Minitab. The adjusted and

predicted R-squared values from the analysis are shown in Table 5.3. The adjusted R^2 values represent the fitting of the current experimental and model data points whereas the predicted R^2 represents the potential of the model to predict the next data point. Additionally, the root mean square error (RMSE) values for all the streams have been mentioned. RMSE is the measure of the average variation between the model and experimental data points at a particular parameter level.

Root Mean Square Error (RMSE) =

$$\sqrt{\frac{\sum_{i=1}^{N}(X_{mod,i} - X_{exp,i})^2}{N}}$$

Where $X_{mod,i}$ is the model predicted data point for the i^{th} level of the parameter; and $X_{exp,i}$ is the experimental data point. N is the total number of levels of the changing parameter.

Table 5. 3 R-squared and RMSE values for product stream yields

Stream	Adjusted R^2 value (%)	Predicted R^2 value (%)	RMSE
Char	93.6	82.1	5.3
Liquid	78.7	68.1	1.9
Gas	87.0	69.3	7.1

The effect of temperature is further studied using steady-state syngas composition profile for both model prediction and experimental data points. Figure 5-4 shows the averaged steady state values of the output syngas composition from the experiments as compared to the simulation. The model predicted trends for carbon dioxide and hydrogen appear to be close to the experimental values. The trend for carbon monoxide appears similar to the trend for char yield discussed earlier wherein there is a noticeable difference between the predicted and experimental points at lower temperatures but the difference diminishes as the temperature increases. This can

again be attributed to the activities of the devolatilization and gasification steps in the model and practical conditions. The most noticeable difference is the trend for methane which keeps decreasing throughout the temperature range for the model but increased initially before decreasing during the experiments.

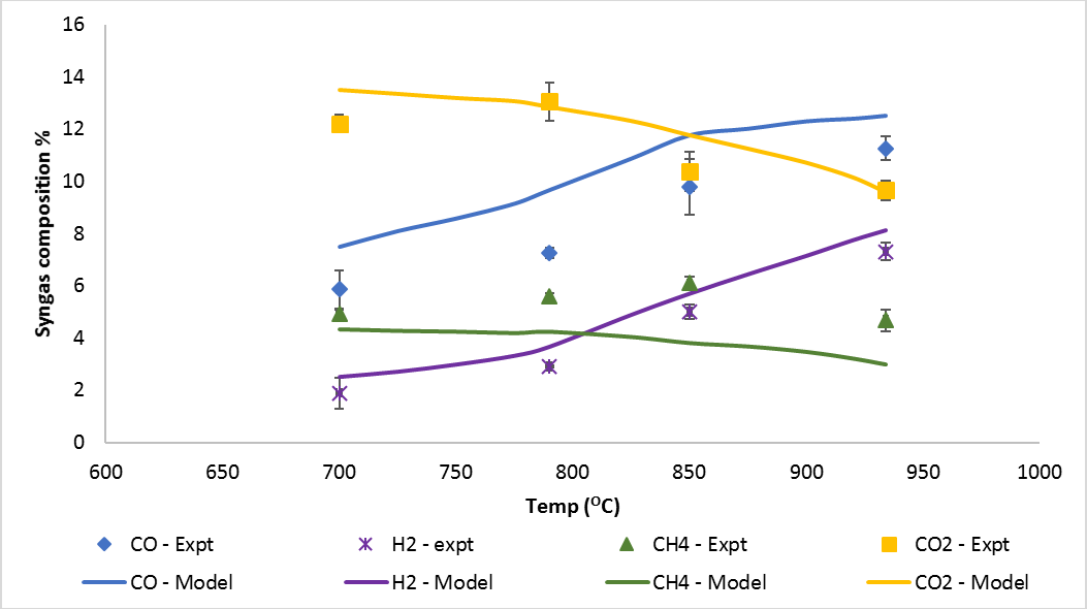

Figure 5- 4 Comparison of syngas composition at different temperatures

The individual gas yields measured as g/kg dry biomass show a similar trend for all the syngas components. Model predicted yields for carbon monoxide and hydrogen agree with experimental findings and increase throughout the entire temperature range. However, there is a difference in the yields for all three lower hydrocarbons viz. methane, ethylene and acetylene. Model predicted trends for all three keep decreasing as temperature increases, whereas there was initial increase in the yields followed by a reduction at the end of the trend observed in the experimental results. Table 5.4 provides the yields of all the syngas components as well as their adjusted and predicted R-squared values along with the root mean square errors. The high R-

squared values for CO and H_2 indicate a better model prediction whereas the lower values for the hydrocarbons supplement the explanation of the trends.

Table 5. 4 Comparison of individual gas yields (g/kg dry biomass)

Temp(^{O}C)		**700**	**790**	**850**	**934**	**Adj R^2 value (%)**	**Pred R^2 value (%)**	**RMSE**
CO	Exp	216 ± 14.1	213.6 ± 9.0	408.8 ± 29.8	423.8 ± 35.2	84.38	76.57	63.2
	Model	257.9	332.3	409.3	435.3			
H_2	Exp	4.98 ± 1.1	8.06 ± 2.5	14.9 ± 0.7	19.64 ± 2.1	98.72	98.09	1.9
	Model	6.8	9.9	15.6	22.3			
CH_4	Exp	104.2 ± 17.1	120.4 ± 13.6	145.7 ± 10.7	100.7 ± 3.9	14.05	5.79	45.2
	Model	85.6	83.7	76.2	59.6			
C_2H_2	Exp	1.17 ± 0.1	1.88 ± 1.2	2.89 ± 0.2	0.57 ± 0.1	16.85	5.14	1.5
	Model	1.8	0.8	0.2	0.2			
C_2H_4	Exp	80.93 ± 5.5	96.14 ± 37.2	98.96 ± 12.5	59.3 ± 3.9	19.51	8.43	34.4
	Model	73.1	59.3	47.2	33.7			

Variations in other important gasification process characteristics such as syngas yield, carbon conversion to gases and higher heating value of the syngas are shown in the Table 5-5. The trend for model predicted overall syngas yield increases slightly with temperature and the values are close to the experimentally measured ones. A similar trend is seen for the amount of carbon converted to gases, which, with temperature, increases steeply at the beginning and then gradually after 850^{O}C. The values predicted by the model follow the measured ones. This trend also seems to closely mimic the trend for the yield of carbon monoxide. The model predicted

higher heating value of syngas increases with temperature as the yields of CO and H_2 in the output increase. However, since the amount of methane in the output is lower than the experimental values, the value of the model predicted HHV remains lower than the measured HHV throughout the range.

Table 5. 5 Comparison of important gasification process characteristics

	Syngas yield		**Syngas HHV (N_2 free)**		**Carbon conversion to gases**	
Temp (^OC)	Nm^3/kg dry biomass		MJ/Nm^3		%	
	Exp	**Model**	**Exp**	**Model**	**Exp**	**Model**
700	0.87 ± 0.04	0.84	11.68 ± 0.38	10.75	61.37 ± 3.2	62.26
790	0.77 ± 0.03	0.91	12.39 ± 0.99	11.11	73.19 ± 2.3	70.96
850	0.91 ± 0.04	1.01	13.75 ± 0.31	11.35	78.44 ± 4.3	77.15
934	0.77 ± 0.03	1.01	12.09 ± 0.45	11.52	81.9 ± 2.9	79.93

The fuel bound nitrogen evolves from the gasification process as nitrogenous contaminants, of which ammonia is the most noticeable one. Ammonia is released during the devolatilization step and its concentration in the output may change depending on temperature. Table 5.6 shows the comparison between the experimentally measured values and the model predicted values for the concentration of ammonia in the output. Both the trends follow a downward direction implying a decrease in ammonia concentration as temperature increases. This is possibly due to the decomposition of ammonia into nitrogen and hydrogen gases. The change in N_2 and H_2 concentrations is not noticeable as the amount evolved is miniscule as

compared to their initial amounts. The model predicted values for ammonia concentrations seem to be a little higher than the experimental ones which may be due to the greater extent of devolatilization in the model as pointed out earlier.

Table 5. 6 Comparison of ammonia concentrations

	NH_3 concentration (PPM)	
Temp (^OC)	**Exp**	**Model**
700	773	759
790	640	556
850	475	301
934	369	215

5.2.1.2 Effect of CO_2/ C ratio

The CO_2/C ratio was initially kept at 1.04 for all the temperature variation studies. The CO_2/C ratio was varied according to the experimental variations using sensitivity analysis tool in ASPEN Plus. The CO_2/C ratio values were varied in intervals of 0.05 in the range of 0.6-1.52 to emulate the CO_2/C ratio range studied in the experiments. However, for the model, nearly 15 ratio points were studied to obtain a smooth plot throughout the ratio range, as opposed to 4 ratio points studied during the experiments. The input flow rates for CO_2 ranged from 1 liter per minute for ratio of 0.6, to 2.24 liters per minute for ratio of 1.52.

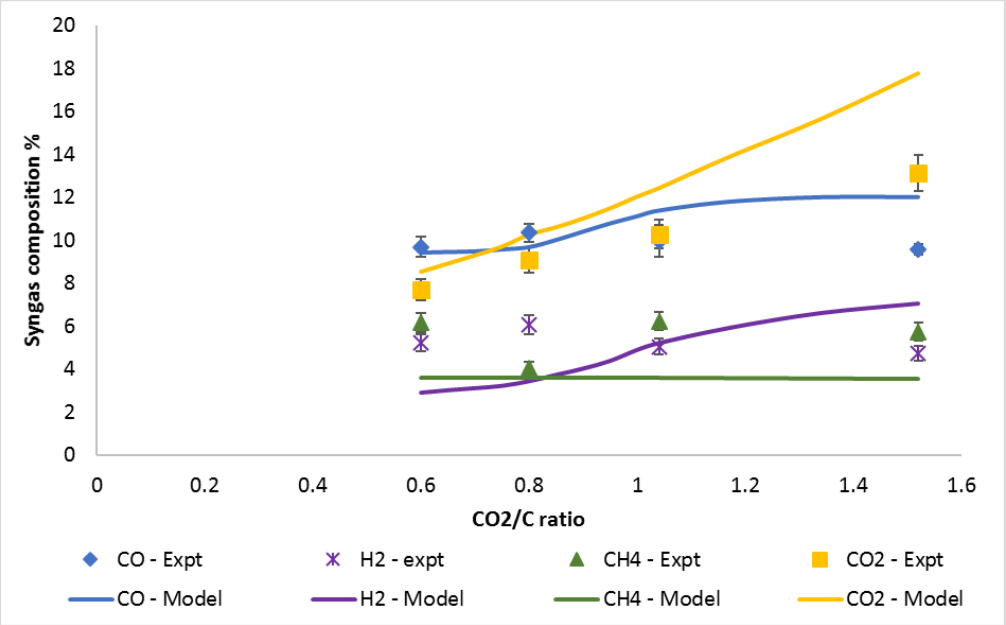

Figure 5- 5 Comparison of syngas compositions

The temperature, in accordance with the experiments was set at 850^{O}C. The results from the sensitivity analysis were compared to the data from the steady-state performance of the gasifier. The concentrations and yields of the syngas components such as CO, H_2, CH_4 were compared along with process characteristics.

The comparison of change in output syngas concentration with changing CO_2/C ratio is shown in Figure 5-5. The model predicted CO_2 concentration increases throughout the range and stays above the experimental values. The CO and H_2 concentrations appear to increase slightly whereas the methane concentration stays constant. The concentrations may not provide a clear comparison between the model and experimental values due to the high CO_2 concentration in the output. The output yields for individual gases are compared in the Figure 5-6.

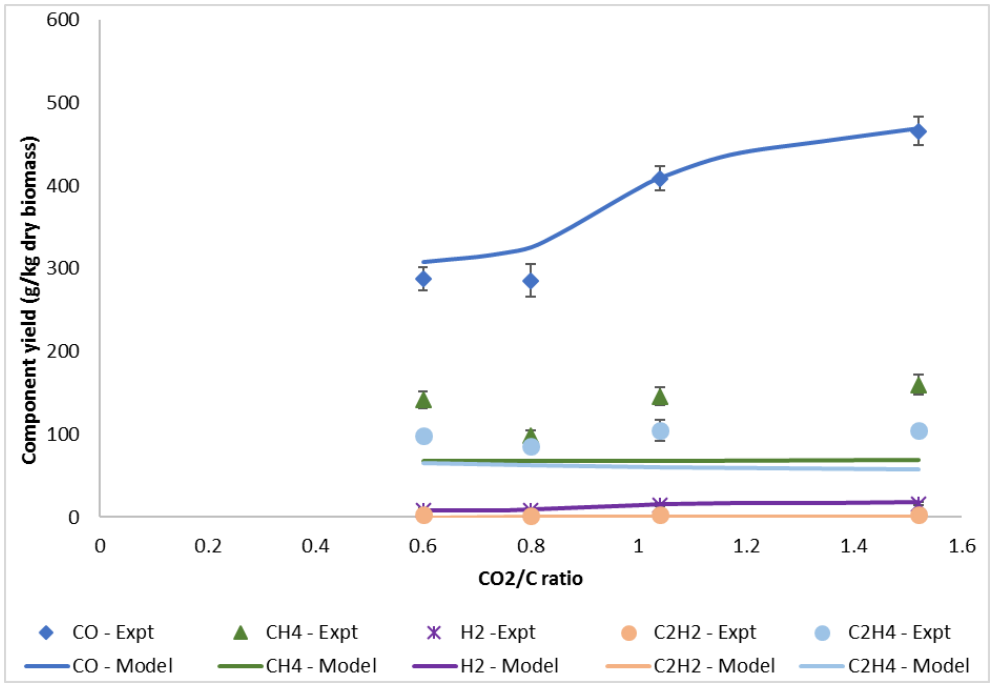

Figure 5- 6 Comparison of syngas yields

The trend for the predicted CO yield increases with temperature in unison with the experimentally measured values as shown in Table 5.7. The trend is similar to the temperature trend of CO, where the first two values for the model appear distant and the next two lie close to the experimental ones. The model predicted values (307.99 to 468.87 g/dry kg biomass) and the experimental values (288.01 to 465.59 g/kg dry biomass) lie in the similar range throughout the changing CO_2/C ratios. A similar trend is observed for hydrogen where the model predicted values (7.51 to 18.13 g/kg dry biomass) are close to the experimental ones (7.76 to 16.18 g/kg dry biomass). As was the case with the temperature variation, the model predicted trends for the hydrocarbons do not comply with the experimentally measured values. The model predicts a slight increase in the methane yield throughout the CO_2/C ratio range (67.43 to 84.64 g/kg dry biomass) whereas the experimental values showed an initial dip followed by a rapid rise in the methane yield (141.13 to 97.63 to 159.64 g/kg dry biomass). A similar trend was observed during the experiments for the yield of ethylene (98.63 to 85.98 to 104.13). However, the model

predicted trend and values are way off which show a decreasing yield (65.69 to 45.86 g/kg dry biomass) with increasing CO_2/ C ratio. The model and experimental values for acetylene yield have different magnitudes but show a similar trend of initial increase, with decrease beyond CO_2/C ratio of 1.04.

Table 5. 7 Comparison of individual gas yields

CO_2/C ratio		**0.6**	**0.8**	**1.04**	**1.52**	**Adj R^2 value (%)**	**Pred R^2 value (%)**	**RMSE**
CO	Exp	288.0 ± 28.28	285.5 ± 38.89	408.7 ± 29.85	465.6 ± 33.99	98.35	97.53	22.5
	Model	307.9	325.6	409.3	468.8			
H_2	Exp	7.76 ± 0.75	7.9 ± 0.92	14.96 ± 0.75	16.19 ± 0.81	98.52	97.79	1.2
	Model	7.5	8.8	15.6	18.1			
CH_4	Exp	141.1 ± 10.4	97.6 ± 7.2	145.7 ± 10.7	159.6 ± 11.7	45.51	17.73	64.6
	Model	67.4	69.2	76.2	84.6			
C_2H_2	Exp	2.49 ± 0.1	2.31 ± 0.1	3.13 ± 0.2	2.5 ± 0.2	14.63	11.94	2.0
	Model	0.7	0.9	0.3	0.8			
C_2H_4	Exp	98.63 ± 0.9	85.98 ± 1.7	104.76 ± 4.3	104.13 ± 1.4	20.45	19.32	46.7
	Model	65.7	55.7	47.2	45.8			

The lower adjusted and predicted R-squared values for methane and ethylene show that the model predicted values and trends are not close to the experimental ones. However, the model successfully predicts the output yields for CO and H_2 as showcased by the higher R-squared values. Variations in the vital gasification process characteristics are shown in Table 5.8.

Table 5. 8 Comparison of important gasification process characteristics

CO_2/C ratio	Syngas yield		Syngas HHV (N_2 free)		Carbon conversion to gases	
	Nm^3/kg dry biomass		MJ/Nm^3		%	
	Exp	**Model**	**Exp**	**Model**	**Exp**	**Model**
0.6	0.84 ± 0.06	0.7	15.79 ± 1.06	10.71	75.41 ± 2.6	62.34
0.8	0.71 ± 0.05	0.78	12.85 ± 0.86	10.34	74.21 ± 2.6	68.61
1.04	0.91 ± 0.04	1.01	14.67 ± 0.99	11.35	78.44 ± 4.3	77.15
1.52	1.1 ± 0.07	1.25	13.12 ± 0.88	11.89	85.36 ± 2.9	86.12

The higher heating value of syngas as predicted by the model does not follow the same trend as the experimental data. The model values are significantly lower than the experimental ones, and increase as the CO_2/C ratio increases. This can be attributed to a lower amount of methane as predicted by the model, which increases throughout the CO_2/C ratio range. However, the experimentally measured HHVs show no particular trend. The overall syngas yields as predicted by the model keeps increasing as the CO_2/C ratio increases, with values pretty close to the experimental values. The predicted carbon conversion to gases is lower than the measured data initially, but increases with the CO_2/C ratio and catches up with the experimental conversion at the higher ratios. This is due to the higher CO and CH_4 yields at CO_2/C ratios 1.04 and 1.52.

5.3 Comparison with thermodynamic equilibrium model

To adjudge the credibility of using ASPEN model with kinetics, the results from the current model are compared to results from an already published thermodynamic equilibrium modeling study[161]. The thermodynamic model, as shown in Appendix C, identifies the products

of the gasification process based solely on the minimization of Gibbs free energy. The gasification step is modeled using only the RGIBBS reactor, which lets all the reactions in the process reach chemical equilibrium and identifies all possible products. The change in the output syngas composition with temperature for the thermodynamic equilibrium model as compared to the current model and experimental data is shown in the Table 5.9. The composition in volume percentage for both models and the experiment are compared on an N_2 -free basis.

Table 5. 9 Syngas composition: comparison of experimental data with two different models

Temp(^{O}C)		**700**	**790**	**850**	**934**
CO	Experiment	23.57	25.22	31.26	34.21
	Current model	26.92	31.75	35.73	37.78
	Thermodynamic Model	44.10	50.23	54.55	56.30
H_2	Experiment	7.62	10.10	16.02	22.20
	Current model	9.07	12.10	17.37	24.58
	Thermodynamic Model	20.30	19.44	18.85	17.67
CH_4	Experiment	19.74	19.39	19.50	14.23
	Current model	15.53	13.91	11.56	9.00
	Thermodynamic Model	9.82	7.87	6.42	6.14
CO_2	Experiment	49.07	45.30	33.23	29.36
	Current model	48.48	42.24	35.34	28.64
	Thermodynamic Model	25.78	22.46	20.18	19.89

All compositions are reported in **percentage and N_2-free basis.**

The syngas composition volume fraction for CO predicted by the thermodynamic equilibrium model is considerably higher throughout the temperature range as compared to both

the current model and the experimental data. This is accompanied by consistently lower values for CO_2. This implies that the Gibbs free minimization in the thermodynamic modeling considers the Boudouard reaction to reach equilibrium and achieve much higher conversion than the model that includes kinetics. Additionally, we do see a difference between the composition values for hydrogen and methane which may be due to prioritization of different reactions in thermodynamic modeling than the reactions that were identified as dominant during experiments. Similar observations about thermodynamic equilibrium models reaching higher conversion levels have been reported in literature[164,127]. The values predicted by the current model appear to be in better agreement with the experimental data than the predictions by the thermodynamic equilibrium model.

5.4 Conclusions

A model was developed using ASPEN Plus to simulate the performance of a fluidized-bed gasifier used in experimental studies. Different reactors were used to simulate the various steps in CO_2 gasification. Knowledge about the chemistry and kinetics accrued from the earlier studies was used for the model to achieve better performance. Results for sensitivity analysis using temperature and CO_2/C ratio variation from the model were compared to the experimental data.

The model predicted values for the concentrations and yields of carbon monoxide and hydrogen with changing temperature were close to the experimental ones as shown by the adjusted R-squared value of 84.38% and 98.72%, respectively. However, the trends for the yields of lower hydrocarbons were incorrectly predicted by the model. The R-squared values of 14.05%, 16.85% and 19.51% proved the disagreement between the model and experimental values. This was attributed to the difference in the extent of devolatilization step in the model and the

experiments. The predicted and measured values for syngas yield, HHV and carbon conversion were in close proximity with a slight variation in the trends. Similar results were observed with CO_2/C ratio variation where the model was ineffective for CH_4 and C_2H_4 yields but proved very effective in predicting CO and H_2 yields. A comparison between the current model and a thermodynamic equilibrium model revealed that the latter predicted much higher conversion for the Boudouard reaction resulting in considerably higher CO concentrations and consistently lower CO_2 values.

Energy producers can use this model as a tool to predict the syngas compositions, and combine it with upstream and downstream models to conduct life cycle analysis of the overall concept. The viability of the process can be increased by the fact that it uses up upstream CO_2 and can be provided subsidies and tax breaks for being a “green process”.

Chapter 6
Conclusion

In a bench scale fluidized bed gasifier, the effect of temperature and CO_2/C ratio on biomass gasification using CO_2 was studied and the results compared to oxygen gasification study reported in literature. Lower char yield and consequently higher carbon conversion were observed in oxygen gasification than CO_2 gasification due to the presence of free oxygen available for combustion reactions. It was also concluded that with increasing temperature, CO_2 gasification produces highly microporous char that greatly enhances CO_2 diffusion during the gasification step leading to higher conversion. The main reactions that come into play during the gasification step are char–CO_2 reaction (Boudouard), water gas reaction (char reforming) and free radical reactions leading to molecular hydrogen formation.

Three solid-gas reaction models were used to interpret the kinetics of pine char gasification with CO_2 in a fixed bed reactor. Regression analysis and char surface area measurements suggested that the random pore model (RPM) was best suited to predict the experimental data. Values of pore structure parameter, activation energy and frequency factor were calculated to be 219 kJ/mol, 5.13 (s^{-1}) and 9.88, respectively. To test the effect of four different alkali and alkaline earth metal catalysts, chars are impregnated with acetate salts of Na, Mg, K and Ca. The actual catalyst loading is quantified using SEM-EDS analysis and ICP-MS analysis. Loaded chars are gasified using the same procedure and the random pore model is used to calculate the activation energy for each metal loaded char. The reactivity of the loaded chars

was found to be in the order of: K-char > Ca –char > Na –char ≥ Mg –char. The pore structure parameter was the highest for sodium implying that change in surface area with conversion is highest for sodium.

An ASPEN plus model was developed to simulate the steady state performance of the fluidized bed gasification unit used in the experiments. Knowledge accrued from the experimental objectives was used to improve the performance of the model. Different reactors were used to simulate various steps in the gasifier and a FORTRAN subroutine was dynamically linked to include the kinetics. Parameters such as output syngas composition, individual gas yields, syngas higher heating value and carbon conversion are compared to evaluate the validity of the model. The model was able to predict the behavior of the gasifier for certain syngas components and characteristics. However, the predicted and experimental values for lower hydrocarbons showed significant disagreement. The difference in activity of devolatilization step that was assumed by the model and the actual experimental activity, was postulated as the reason for the deviation. In addition, results from a thermodynamic equilibrium model employing Gibbs free energy minimization were compared to the current model. The current model was found to be better at predicting experimental results as the Thermodynamic equilibrium model predicted much higher conversions.

Chapter 7
Recommendations for future work

The experiments conducted during the course of this research were performed on different setups based on the objective under investigation. The fluidized bed reactor and the fixed bed reactor setups were used to study different aspects of the gasification process. The results obtained after the completion of the experiments were specific to the scope of the project. However, the recommendations suggested in this chapter may be helpful in efficient operation of the existing experimental setups and may assist in broadening the scope of the research overall.

7.1 Operating conditions

The study employing the bench scale bubbling fluidized bed gasifier involved the variation of operating conditions such as temperature and CO_2/C ratio (CO_2 flow rate). However, the flow rate of nitrogen as a fluidizing gas was an important parameter. Initial trials on the experimental setup suggested that loss of fluidization occurred if the flow rate of nitrogen was less than 8.5 liters per minute (lpm). On the other hand, if the flow rate was too high (>17 lpm), sand particles from the bed were carried over into the filter. Therefore, operation around 10 lpm was found as the ‘sweet spot’ which was within the range and did not result in much dilution of the output syngas. In addition, some biomass feeding issues were observed due to the back-pressure caused by the flow of nitrogen into the gasifier. A small amount of nitrogen was added along with the biomass feed to tackle this issue.

7.2 CO_2 Recycle

Carbon dioxide was the oxidizing agent in this research. However, significant amount of CO_2 was observed in the output syngas. Since, CO_2 does not have any calorific value, it acts as a diluent in syngas and reduces the overall heating value of the final product. This CO_2 can thus be reused in the system as a reactant for gasification. Recycling CO_2 will not only improve the efficiency of the system, but also lead to improved quality of syngas. A possibility of such a recycle system has been explored in literature. [165,166]

7.3 Char recycle and applications

Due to high flow rates and low residence time in the fluidized bed, carbon from biomass is not completely converted. The char collected at the end of the runs is nearly 90% carbon. Recycling the char will be important to improve the utilization of raw materials and increase the efficiency of the process. A circulating fluidized bed gasifier setup may be used for this purpose[167]. In addition, char produced during CO_2 gasification is highly microporous. This can be used in applications that require high surface area such as soil amendment[168] and catalyst for certain processes[169].

7.4 Co-feeding

To make biomass gasification using CO_2 commercially viable, use of different varieties of biomass as feedstock is essential. Co-feeding one biomass type with another or coal may also be beneficial[170,171]. For example, certain biomass with higher alkali and alkaline earth metal content may be co-fed with other feedstock in order to catalyze the gasification process[172]. Additionally, char obtained at the end of gasification process, with higher ash content, may also be used to catalyze the system.

7.5 Model improvements

The ASPEN plus model developed to simulate the steady state performance of the fluidized bed gasifier shows deviation from experimental results specially for the hydrocarbon yields. This is due to the difference in activity of the devolatilization step between the model and experiments. This may be corrected by experimentally determining the product distribution and yields after the devolatilization step and incorporating it into the model. However, such an inclusion will restrict the model to that particular biomass and will not be applicable in general.

Models for upstream CO_2 evolution and downstream syngas utilization can be added to the current model for gasification to determine the viability of the overall process. By treating the current model as one process block, the system will allow for overall heat integration. In addition, such an integration will help in determining the financial feasibility of the overall concept.

References

(1) Wolfram, C., How Will Energy Demand Develop in the Developing World? *Journal of Economic Perspectives* **2012,** *26*, 19.

(2) IEA, *World Energy Outlook 2013*. IEA.

(3) Administration, U. S. E. I. *Monthly energy review November 2015*; 2015.

(4) Administration, U. S. E. i. *Annual energy Outlook 2015 with projections to 2040*; 2015.

(5) Radhi, H., Evaluating the potential impact of global warming on the UAE residential buildings – A contribution to reduce the CO2 emissions. *Build. Sci.* **2009,** *44*, 2451-2462.

(6) Oceanography, S. I. o., The Keeling Curve. 2015.

(7) Downing, M.; Eaton, L. M.; Graham, R. L.; Langholtz, M. H.; Perlack, R. D.; Turhollow Jr, A. F.; Stokes, B.; Brandt, C. C. *U.S. Billion-Ton Update: Biomass Supply for a Bioenergy and Bioproducts Industry*; ORNL/TM-2011/224; Other: BM0102030; CEBM007; TRN: US201118%%1083 United States10.2172/1023318Other: BM0102030; CEBM007; TRN: US201118%%1083Thu Jun 06 09:43:04 EDT 2013ORNLEnglish; 2011; p Medium: ED.

(8) Sjaak van Loo, J. K., *The Handbook of Biomass Combustion and Co-firing*. earthscan 2008.

(9) van den Broek, R.; Faaij, A.; van Wijk, A., Biomass combustion for power generation. *Biomass Bioenergy* **1996,** *11*, 271-281.

(10) Sondreal, E. A.; Benson, S. A.; Hurley, J. P.; Mann, M. D.; Pavlish, J. H.; Swanson, M. L.; Weber, G. F.; Zygarlicke, C. J., Review of advances in combustion technology and biomass cofiring. *Fuel Process. Technol.* **2001,** *71*, 7-38.

(11) Gomez, L. D.; Steele-King, C. G.; McQueen-Mason, S. J., Sustainable liquid biofuels from biomass: the writing's on the walls. *New Phytol.* **2008,** *178*, 473-485.

(12) Huber, G. W.; Iborra, S.; Corma, A., Synthesis of Transportation Fuels from Biomass: Chemistry, Catalysts, and Engineering. *Chem. Rev. (Washington, DC, U. S.)* **2006,** *106*, 4044-4098.

(13) Devi, L.; Ptasinski, K. J.; Janssen, F. J. J. G., A review of the primary measures for tar elimination in biomass gasification processes. *Biomass Bioenergy* **2003,** *24*, 125-140.

(14) Cheng, Y.; Thow, Z.; Wang, C.-H., Biomass gasification with CO2 in a fluidized bed. *Powder Technol.*

(15) Gaby, L. I., The Southern pines. services, F., Ed. united States department of Agriculture: Vol. FS-256.

(16) Yang, Q.; Yin, X.; Wu, C.; Wu, S.; Guo, D., Thermogravimetric-Fourier transform infrared spectrometric analysis of CO2 gasification of reed (Phragmites australis) kraft black liquor. *Bioresour. Technol.* **2012,** *107*, 512-516.

(17) Butterman, H. C.; Castaldi, M. J., CO2 as a Carbon Neutral Fuel Source via Enhanced Biomass Gasification. *Environ. Sci. Technol.* **2009,** *43*, 9030-9037.

(18) Butterman, H. C.; Castaldi, M. J., Influence of CO2 Injection on Biomass Gasification. *Ind. Eng. Chem. Res.* **2007,** *46*, 8875-8886.

(19) Antal, M. J.; Grønli, M., The Art, Science, and Technology of Charcoal Production†. *Ind. Eng. Chem. Res.* **2003,** *42*, 1619-1640.

(20) Lin, Y.-C.; Cho, J.; Tompsett, G. A.; Westmoreland, P. R.; Huber, G. W., Kinetics and Mechanism of Cellulose Pyrolysis. *The Journal of Physical Chemistry C* **2009,** *113*, 20097-20107.

(21) Ollero, P.; Serrera, A.; Arjona, R.; Alcantarilla, S., Diffusional effects in TGA gasification experiments for kinetic determination. *Fuel* **2002,** *81*, 1989-2000.

(22) Kaewluan, S.; Pipatmanomai, S., Gasification of high moisture rubber woodchip with rubber waste in a bubbling fluidized bed. *Fuel Process. Technol.* **2011,** *92*, 671-677.

(23) Abdoulmoumine, N.; Kulkarni, A.; Adhikari, S., Effects of Temperature and Equivalence Ratio on Pine Syngas Primary Gases and Contaminants in a Bench-Scale Fluidized Bed Gasifier. *Ind. Eng. Chem. Res.* **2014,** *53*, 5767-5777.

(24) Ahmed, I. I.; Gupta, A. K., Pyrolysis and gasification of food waste: Syngas characteristics and char gasification kinetics. *Appl. Energy* **2010,** *87*, 101-108.

(25) Ollero, P.; Serrera, A.; Arjona, R.; Alcantarilla, S., The CO2 gasification kinetics of olive residue. *Biomass Bioenergy* **2003,** *24*, 151-161.

(26) Khalil, R.; Várhegyi, G.; Jäschke, S.; Grønli, M. G.; Hustad, J., CO2 Gasification of Biomass Chars: A Kinetic Study. *Energy Fuels* **2009,** *23*, 94-100.

(27) Mani, T.; Mahinpey, N.; Murugan, P., Reaction kinetics and mass transfer studies of biomass char gasification with CO2. *Chem. Eng. Sci.* **2011,** *66*, 36-41.

(28) Meng, L.; Wang, M.; Yang, H.; Ying, H.; Chang, L., Catalytic effect of alkali carbonates on CO2 gasification of Pingshuo coal. *Mining Science and Technology (China)* **2011,** *21*, 587-590.

(29) Irfan, M. F.; Usman, M. R.; Kusakabe, K., Coal gasification in CO2 atmosphere and its kinetics since 1948: A brief review. *Energy* **2011,** *36*, 12-40.

(30) Hu, G.; Li, G.; Zheng, Y.; Zhang, Z.; Xu, Y., Euler–Lagrange modeling of wood chip gasification in a small-scale gasifier. *J. Energy Inst.* **2015,** *88*, 314-322.

(31) Miao, Q.; Zhu, J.; Barghi, S.; Wu, C.; Yin, X.; Zhou, Z., Modeling biomass gasification in circulating fluidized beds. *Renewable Energy* **2013,** *50*, 655-661.

(32) Loha, C.; Gu, S.; De Wilde, J.; Mahanta, P.; Chatterjee, P. K., Advances in mathematical modeling of fluidized bed gasification. *Renewable Sustainable Energy Rev.* **2014,** *40*, 688-715.

(33) Guizani, C.; Louisnard, O.; Sanz, F. J. E.; Salvador, S., Gasification of woody biomass under high heating rate conditions in pure CO2: Experiments and modelling. *Biomass Bioenergy* **2015,** *83*, 169-182.

(34) PARLIAMENT, T. E., DIRECTIVE 2010/75/EU on industrial emissions (integrated pollution prevention and control). UNION, T. E. P. A. T. C. O. T. E., Ed. 2010.

(35) PARLIAMENT, T. E., REGULATION (EU) No 525/2013 on a mechanism for monitoring and reporting greenhouse gas emissions and for reporting other information at national and Union level relevant to climate change and repealing Decision No 280/2004/EC. UNION, T. E. P. A. T. C. O. T. E., Ed. 2013.

(36) Energy Independence and Security Act. Congress, U., Ed. 2007; Vol. Public law 110(140):19.

(37) Hurley, S.; Xu, C.; Preto, F.; Shao, Y.; Li, H.; Wang, J.; Tourigny, G., Catalytic gasification of woody biomass in an air-blown fluidized-bed reactor using Canadian limonite iron ore as the bed material. *Fuel* **2012,** *91*, 170-176.

(38) Vasudevan, P., Liquid fuel from biomass: An overview. *J. Sci. Ind. Res.* **2005,** *64*.

(39) Abdoulmoumine, N.; Kulkarni, A.; Adhikari, S.; Taylor, S.; Loewenstein, E., Economic analysis of municipal power generation from gasification of urban green wastes: case study of Fultondale, Alabama, USA. *Biofuels, Bioprod. Biorefin.* **2012,** *6*, 521-533.

(40) Meher, L. C.; Vidya Sagar, D.; Naik, S. N., Technical aspects of biodiesel production by transesterification—a review. *Renewable Sustainable Energy Rev.* **2006,** *10*, 248-268.

(41) McNeff, C. V.; McNeff, L. C.; Yan, B.; Nowlan, D. T.; Rasmussen, M.; Gyberg, A. E.; Krohn, B. J.; Fedie, R. L.; Hoye, T. R., A continuous catalytic system for biodiesel production. *Appl. Catal., A* **2008,** *343*, 39-48.

(42) Boz, N.; Degirmenbasi, N.; Kalyon, D. M., Conversion of biomass to fuel: Transesterification of vegetable oil to biodiesel using KF loaded nano-γ-Al2O3 as catalyst. *Appl. Catal., B* **2009,** *89*, 590-596.

(43) Alonso, D. M.; Bond, J. Q.; Dumesic, J. A., Catalytic conversion of biomass to biofuels. *Green Chem.* **2010,** *12*, 1493-1513.

(44) Moens, L., Chapter 9 Renewable feedstocks. In *Sustainability Science and Engineering*, Abraham, M. A., Ed. Elsevier: 2006; Vol. Volume 1, pp 177-199.

(45) Liu, X.; Chen, M.; Wei, Y., Kinetics based on two-stage scheme for co-combustion of herbaceous biomass and bituminous coal. *Fuel* **2015,** *143*, 577-585.

(46) Sahu, S. G.; Chakraborty, N.; Sarkar, P., Coal–biomass co-combustion: An overview. *Renewable Sustainable Energy Rev.* **2014,** *39*, 575-586.

(47) Wang, G.; Zhang, J.; Shao, J.; Ren, S., Characterisation and model fitting kinetic analysis of coal/biomass co-combustion. *Thermochim. Acta* **2014,** *591*, 68-74.

(48) (a) Trubetskaya, A.; Jensen, P. A.; Jensen, A. D.; Garcia Llamas, A. D.; Umeki, K.; Glarborg, P., Effect of fast pyrolysis conditions on biomass solid residues at high temperatures. *Fuel Process. Technol.* **2016,** *143*, 118-129; (b) Trubetskaya, A.; Jensen, P. A.; Jensen, A. D.; Steibel, M.; Spliethoff, H.; Glarborg, P.; Larsen, F. H., Comparison of high temperature chars of wheat straw and rice husk with respect to chemistry, morphology and reactivity. *Biomass Bioenergy* **2016,** *86*, 76-87.

(49) Papari, S.; Hawboldt, K., A review on the pyrolysis of woody biomass to bio-oil: Focus on kinetic models. *Renewable Sustainable Energy Rev.* **2015,** *52*, 1580-1595.

(50) Kim, S. W., Pyrolysis conditions of biomass in fluidized beds for production of bio-oil compatible with petroleum refinery. *J. Anal. Appl. Pyrolysis*.

(51) Gable, P.; Brown, R. C., Effect of biomass heating time on bio-oil yields in a free fall fast pyrolysis reactor. *Fuel* **2016,** *166*, 361-366.

(52) Raikova, S.; Smith-Baedorf, H.; Bransgrove, R.; Barlow, O.; Santomauro, F.; Wagner, J. L.; Allen, M. J.; Bryan, C. G.; Sapsford, D.; Chuck, C. J., Assessing hydrothermal liquefaction for the production of bio-oil and enhanced metal recovery from microalgae cultivated on acid mine drainage. *Fuel Process. Technol.* **2016,** *142*, 219-227.

(53) López Barreiro, D.; Riede, S.; Hornung, U.; Kruse, A.; Prins, W., Hydrothermal liquefaction of microalgae: Effect on the product yields of the addition of an organic solvent to separate the aqueous phase and the biocrude oil. *Algal Res.* **2015,** *12*, 206-212.

(54) Bridgwater, A. V., The technical and economic feasibility of biomass gasification for power generation. *Fuel* **1995,** *74*, 631-653.

(55) Choudhury, H. A.; Chakma, S.; Moholkar, V. S., Chapter 14 - Biomass Gasification Integrated Fischer-Tropsch Synthesis: Perspectives, Opportunities and Challenges. In *Recent Advances in Thermo-Chemical Conversion of Biomass*, Sukumaran, A. P. B. S. K., Ed. Elsevier: Boston, 2015; pp 383-435.

(56) Kuo, P.-C.; Wu, W., Design of Co-gasification from Coal and Biomass Combined heat and Power Generation System. *Energy Procedia* **2015,** *75*, 1120-1125.

(57) Zhou, Z.; Yin, X.; Xu, J.; Ma, L., The development situation of biomass gasification power generation in China. *Energy Policy* **2012,** *51*, 52-57.

(58) McKendry, P., Energy production from biomass (part 1): overview of biomass. *Bioresour. Technol.* **2002,** *83*, 37-46.

(59) Zhou, J.; Masutani, S. M.; Ishimura, D. M.; Turn, S. Q.; Kinoshita, C. M., Release of Fuel-Bound Nitrogen during Biomass Gasification. *Ind. Eng. Chem. Res.* **2000,** *39*, 626-634.

(60) Kaufman Rechulski, M. D.; Schildhauer, T. J.; Biollaz, S. M. A.; Ludwig, C., Sulfur containing organic compounds in the raw producer gas of wood and grass gasification. *Fuel* **2014,** *128*, 330-339.

(61) Basu, P., Biomass gasification and pyrolysis: Practical design and theory. Academic Press: Burlington, MA, 2010; p 121.

(62) L Douglas Smoot, P. J. S., *Coal combustion and gasification*. Pringer US: 1985.

(63) Di Blasi, C., Combustion and gasification rates of lignocellulosic chars. *Prog. Energy Combust. Sci.* **2009,** *35*, 121-140.

(64) Ergun, S., Kinetics of the Reaction of Carbon with Carbon Dioxide. *The Journal of Physical Chemistry* **1956,** *60*, 480-485.

(65) Abdoulmoumine, N. Fate and Remediation of Biomass Gasification Gas Contaminants. Auburn University, 2014.

(66) Kitani, O., *Biomass handbook*. Gordon and Breach Science Publishers: 1989.

(67) Kulkarni, A. Biomass Gasification for Power and Fuel Applications using a Bench-Scale Bubbling Fluidized Bed Gasifier. Auburn university, 2015.

(68) Xu, Q.; Pang, S.; Levi, T., Reaction kinetics and producer gas compositions of steam gasification of coal and biomass blend chars, part 1: Experimental investigation. *Chem. Eng. Sci.* **2011,** *66*, 2141-2148.

(69) Emami Taba, L.; Irfan, M. F.; Wan Daud, W. A. M.; Chakrabarti, M. H., The effect of temperature on various parameters in coal, biomass and CO-gasification: A review. *Renewable Sustainable Energy Rev.* **2012,** *16*, 5584-5596.

(70) Narváez, I.; Orío, A.; Aznar, M. P.; Corella, J., Biomass Gasification with Air in an Atmospheric Bubbling Fluidized Bed. Effect of Six Operational Variables on the Quality of the Produced Raw Gas. *Ind. Eng. Chem. Res.* **1996,** *35*, 2110-2120.

(71) Couto, N.; Rouboa, A.; Silva, V.; Monteiro, E.; Bouziane, K., Influence of the Biomass Gasification Processes on the Final Composition of Syngas. *Energy Procedia* **2013,** *36*, 596-606.

(72) Franco, C.; Pinto, F.; Gulyurtlu, I.; Cabrita, I., The study of reactions influencing the biomass steam gasification process☆. *Fuel* **2003,** *82*, 835-842.

(73) Heidi C. Butterman, M. J. C., CO2 Enhanced Steam Gasification of Biomass Fuels. In *16th Annual North American Waste-to-Energy Conference*, Philadelphia, Pennsylvania, USA, 2008; pp 157-172.

(74) Kumar, A.; Eskridge, K.; Jones, D. D.; Hanna, M. A., Steam–air fluidized bed gasification of distillers grains: Effects of steam to biomass ratio, equivalence ratio and gasification temperature. *Bioresour. Technol.* **2009,** *100*, 2062-2068.

(75) Gil, J.; Aznar, M. P.; Caballero, M. A.; Francés, E.; Corella, J., Biomass Gasification in Fluidized Bed at Pilot Scale with Steam−Oxygen Mixtures. Product Distribution for Very Different Operating Conditions. *Energy Fuels* **1997,** *11*, 1109-1118.

(76) Corella, J.; Aznar, M. P.; Delgado, J.; Aldea, E., Steam gasification of cellulosic wastes in a fluidized bed with downstream vessels. *Ind. Eng. Chem. Res.* **1991,** *30*, 2252-2262.

(77) Pohořelý, M.; Jeremiáš, M.; Svoboda, K.; Kameníková, P.; Skoblia, S.; Beňo, Z., CO2 as moderator for biomass gasification. *Fuel* **2014,** *117, Part A*, 198-205.

(78) Chen, C.; Wang, J.; Liu, W.; Zhang, S.; Yin, J.; Luo, G.; Yao, H., Effect of pyrolysis conditions on the char gasification with mixtures of CO2 and H2O. *Proc. Combust. Inst.* **2013,** *34*, 2453-2460.

(79) Kumar, A.; Wang, L.; Dzenis, Y. A.; Jones, D. D.; Hanna, M. A., Thermogravimetric characterization of corn stover as gasification and pyrolysis feedstock. *Biomass Bioenergy* **2008,** *32*, 460-467.

(80) Fermoso, J.; Stevanov, C.; Moghtaderi, B.; Arias, B.; Pevida, C.; Plaza, M. G.; Rubiera, F.; Pis, J. J., High-pressure gasification reactivity of biomass chars produced at different temperatures. *J. Anal. Appl. Pyrolysis* **2009,** *85*, 287-293.

(81) Senneca, O., Kinetics of pyrolysis, combustion and gasification of three biomass fuels. *Fuel Process. Technol.* **2007,** *88*, 87-97.

(82) Chen, S.; Meng, A.; Long, Y.; Zhou, H.; Li, Q.; Zhang, Y., TGA pyrolysis and gasification of combustible municipal solid waste. *J. Energy Inst.* **2015,** *88*, 332-343.

(83) Shrestha, R. Experimental Analysis and Modeling of Biomass Gasification using a Downdraft Gasifier. Auburn University, 2014.

(84) Sarker, S.; Nielsen, H. K., Preliminary fixed-bed downdraft gasification of birch woodchips. *Int. J. Environ. Sci. Technol.* **2015,** *12*, 2119-2126.

(85) Hanaoka, T.; Hiasa, S.; Edashige, Y., Syngas production by CO2/O2 gasification of aquatic biomass. *Fuel Process. Technol.* **2013,** *116*, 9-15.

(86) Warnecke, R., Gasification of biomass: comparison of fixed bed and fluidized bed gasifier. *Biomass Bioenergy* **2000,** *18*, 489-497.

(87) Son, Y.-I.; Yoon, S. J.; Kim, Y. K.; Lee, J.-G., Gasification and power generation characteristics of woody biomass utilizing a downdraft gasifier. *Biomass Bioenergy* **2011,** *35*, 4215-4220.

(88) Yang, W.-C., *Handbook of Fluidization and Fluid-Particle Systems*. CRC Press New York, 2003; Vol. 10.

(89) Mastellone, M. L.; Zaccariello, L.; Santoro, D.; Arena, U., The O2-enriched air gasification of coal, plastics and wood in a fluidized bed reactor. *Waste Management* **2012,** *32*, 733-742.

(90) Kim, Y. D.; Yang, C. W.; Kim, B. J.; Kim, K. S.; Lee, J. W.; Moon, J. H.; Yang, W.; Yu, T. U.; Lee, U. D., Air-blown gasification of woody biomass in a bubbling fluidized bed gasifier. *Appl. Energy* **2013,** *112*, 414-420.

(91) Karatas, H.; Olgun, H.; Akgun, F., Experimental results of gasification of waste tire with air&CO2, air&steam and steam in a bubbling fluidized bed gasifier. *Fuel Process. Technol.* **2012,** *102*, 166-174.

(92) Campoy, M.; Gómez-Barea, A.; Vidal, F. B.; Ollero, P., Air–steam gasification of biomass in a fluidised bed: Process optimisation by enriched air. *Fuel Process. Technol.* **2009,** *90*, 677-685.

(93) Rapagnà, S.; Jand, N.; Kiennemann, A.; Foscolo, P. U., Steam-gasification of biomass in a fluidised-bed of olivine particles. *Biomass Bioenergy* **2000,** *19*, 187-197.

(94) Li, X. T.; Grace, J. R.; Lim, C. J.; Watkinson, A. P.; Chen, H. P.; Kim, J. R., Biomass gasification in a circulating fluidized bed. *Biomass Bioenergy* **2004,** *26*, 171-193.

(95) Li, K.; Zhang, R.; Bi, J., Experimental study on syngas production by co-gasification of coal and biomass in a fluidized bed. *Int. J. Hydrogen Energy* **2010,** *35*, 2722-2726.

(96) Pfeifer, C.; Puchner, B.; Hofbauer, H., Comparison of dual fluidized bed steam gasification of biomass with and without selective transport of CO2. *Chem. Eng. Sci.* **2009,** *64*, 5073-5083.

(97) Miccio, F.; Piriou, B.; Ruoppolo, G.; Chirone, R., Biomass gasification in a catalytic fluidized reactor with beds of different materials. *Chem. Eng. J. (Loughborough, Engl.)* **2009,** *154*, 369-374.

(98) Alauddin, Z. A. B. Z.; Lahijani, P.; Mohammadi, M.; Mohamed, A. R., Gasification of lignocellulosic biomass in fluidized beds for renewable energy development: A review. *Renewable Sustainable Energy Rev.* **2010,** *14*, 2852-2862.

(99) Roberts, D. G.; Harris, D. J., A Kinetic Analysis of Coal Char Gasification Reactions at High Pressures. *Energy Fuels* **2006,** *20*, 2314-2320.

(100) Iwaszenko, S., Using Mathematica software for coal gasification simulations – Selected kinetic model application. *Journal of Sustainable Mining* **2015,** *14*, 21-29.

(101) Bhatia, S. K.; Perlmutter, D. D., A random pore model for fluid-solid reactions: I. Isothermal, kinetic control. *AIChE J.* **1980,** *26*, 379-386.

(102) Zhang, Y.; Ashizawa, M.; Kajitani, S.; Miura, K., Proposal of a semi-empirical kinetic model to reconcile with gasification reactivity profiles of biomass chars. *Fuel* **2008,** *87*, 475-481.

(103) Fei, H.; Hu, S.; Shi, F.; Li, Y.; Jiang, D.; Xiang, J., A New Mathematical Model Study on CO2 Gasification Reaction of Typical Agricultural Residues. *Ind. Eng. Chem. Res.* **2012,** *51*, 13619-13626.

(104) Bhat, A.; Ram Bheemarasetti, J. V.; Rajeswara Rao, T., Kinetics of rice husk char gasification. *Energy Convers. Manage.* **2001,** *42*, 2061-2069.

(105) Cetin, E.; Moghtaderi, B.; Gupta, R.; Wall, T. F., BIOMASS GASIFICATION KINETICS: INFLUENCES OF PRESSURE AND CHAR STRUCTURE. *Combust. Sci. Technol.* **2005,** *177*, 765-791.

(106) Seo, D. K.; Lee, S. K.; Kang, M. W.; Hwang, J.; Yu, T.-U., Gasification reactivity of biomass chars with CO2. *Biomass Bioenergy* **2010,** *34*, 1946-1953.

(107) Ochoa, J.; Cassanello, M. C.; Bonelli, P. R.; Cukierman, A. L., CO2 gasification of Argentinean coal chars: a kinetic characterization. *Fuel Process. Technol.* **2001,** *74*, 161-176.

(108) Sircar, I.; Sane, A.; Wang, W.; Gore, J. P., Experimental and modeling study of pinewood char gasification with CO2. *Fuel* **2014,** *119*, 38-46.

(109) Yuan, S.; Chen, X.-l.; Li, J.; Wang, F.-c., CO2 Gasification Kinetics of Biomass Char Derived from High-Temperature Rapid Pyrolysis. *Energy Fuels* **2011,** *25*, 2314-2321.

(110) Miura, K.; Hashimoto, K.; Silveston, P. L., Factors affecting the reactivity of coal chars during gasification, and indices representing reactivity. *Fuel* **1989,** *68*, 1461-1475.

(111) Mayer, Z. A.; Apfelbacher, A.; Hornung, A., Effect of sample preparation on the thermal degradation of metal-added biomass. *J. Anal. Appl. Pyrolysis* **2012,** *94*, 170-176.

(112) Duman, G.; Uddin, M. A.; Yanik, J., The effect of char properties on gasification reactivity. *Fuel Process. Technol.* **2014,** *118,* 75-81.

(113) Lahijani, P.; Zainal, Z. A.; Mohammadi, M.; Mohamed, A. R., Conversion of the greenhouse gas CO2 to the fuel gas CO via the Boudouard reaction: A review. *Renewable Sustainable Energy Rev.* **2015,** *41*, 615-632.

(114) Hattingh, B. B.; Everson, R. C.; Neomagus, H. W. J. P.; Bunt, J. R., Assessing the catalytic effect of coal ash constituents on the CO2 gasification rate of high ash, South African coal. *Fuel Process. Technol.* **2011,** *92,* 2048-2054.

(115) Aho, A.; DeMartini, N.; Pranovich, A.; Krogell, J.; Kumar, N.; Eränen, K.; Holmbom, B.; Salmi, T.; Hupa, M.; Murzin, D. Y., Pyrolysis of pine and gasification of pine chars – Influence of organically bound metals. *Bioresour. Technol.* **2013,** *128,* 22-29.

(116) Hurley, S.; Li, H.; Xu, C., Effects of impregnated metal ions on air/CO2-gasification of woody biomass. *Bioresour. Technol.* **2010,** *101,* 9301-9307.

(117) Huang, Y.; Yin, X.; Wu, C.; Wang, C.; Xie, J.; Zhou, Z.; Ma, L.; Li, H., Effects of metal catalysts on CO2 gasification reactivity of biomass char. *Biotechnol. Adv.* **2009,** *27*, 568-572.

(118) Moulijn, J. A.; Cerfontain, M. B.; Kapteijn, F., Mechanism of the potassium catalysed gasification of carbon in CO2. *Fuel* **1984,** *63,* 1043-1047.

(119) Lahijani, P.; Zainal, Z. A.; Mohamed, A. R.; Mohammadi, M., CO2 gasification reactivity of biomass char: Catalytic influence of alkali, alkaline earth and transition metal salts. *Bioresour. Technol.* **2013,** *144,* 288-295.

(120) Zhou, Z.-j.; Hu, Q.-j.; Liu, X.; Yu, G.-s.; Wang, F.-c., Effect of Iron Species and Calcium Hydroxide on High-Sulfur Petroleum Coke CO2 Gasification. *Energy Fuels* **2012,** *26,* 1489-1495.

(121) Lee, J. S.; Kim, S. D., Gasification kinetics of waste tire-char with CO2 in a thermobalance reactor. *Energy* **1996,** *21,* 343-352.

(122) Xu, K.; Hu, S.; Su, S.; Xu, C.; Sun, L.; Shuai, C.; Jiang, L.; Xiang, J., Study on Char Surface Active Sites and Their Relationship to Gasification Reactivity. *Energy Fuels* **2013,** *27,* 118-125.

(123) Min, F.; Zhang, M.; Zhang, Y.; Cao, Y.; Pan, W.-P., An experimental investigation into the gasification reactivity and structure of agricultural waste chars. *J. Anal. Appl. Pyrolysis* **2011,** *92*, 250-257.

(124) Gómez-Barea, A.; Ollero, P.; Fernández-Baco, C., Diffusional Effects in CO2 Gasification Experiments with Single Biomass Char Particles. 1. Experimental Investigation. *Energy Fuels* **2006,** *20*, 2202-2210.

(125) Rapagnà, S.; Latif, A., Steam gasification of almond shells in a fluidised bed reactor: the influence of temperature and particle size on product yield and distribution. *Biomass Bioenergy* **1997,** *12*, 281-288.

(126) Baruah, D.; Baruah, D. C., Modeling of biomass gasification: A review. *Renewable Sustainable Energy Rev.* **2014,** *39*, 806-815.

(127) Ravikiran, A.; Renganathan, T.; Pushpavanam, S.; Voolapalli, R. K.; Cho, Y. S., Generalized Analysis of Gasifier Performance using Equilibrium Modeling. *Ind. Eng. Chem. Res.* **2012,** *51*, 1601-1611.

(128) Nguyen, T. D. B.; Ngo, S. I.; Lim, Y.-I.; Lee, J. W.; Lee, U.-D.; Song, B.-H., Three-stage steady-state model for biomass gasification in a dual circulating fluidized-bed. *Energy Convers. Manage.* **2012,** *54*, 100-112.

(129) Ruggiero, M.; Manfrida, G., An equilibrium model for biomass gasification processes. *Renewable Energy* **1999,** *16*, 1106-1109.

(130) Yoshida, H.; Kiyono, F.; Tajima, H.; Yamasaki, A.; Ogasawara, K.; Masuyama, T., Two-stage equilibrium model for a coal gasifier to predict the accurate carbon conversion in hydrogen production. *Fuel* **2008,** *87*, 2186-2193.

(131) Li, X.; Grace, J. R.; Watkinson, A. P.; Lim, C. J.; Ergüdenler, A., Equilibrium modeling of gasification: a free energy minimization approach and its application to a circulating fluidized bed coal gasifier. *Fuel* **2001,** *80*, 195-207.

(132) Jarungthammachote, S.; Dutta, A., Equilibrium modeling of gasification: Gibbs free energy minimization approach and its application to spouted bed and spout-fluid bed gasifiers. *Energy Convers. Manage.* **2008,** *49*, 1345-1356.

(133) Puig-Arnavat, M.; Hernández, J. A.; Bruno, J. C.; Coronas, A., Artificial neural network models for biomass gasification in fluidized bed gasifiers. *Biomass Bioenergy* **2013,** *49*, 279-289.

(134) Nikoo, M. B.; Mahinpey, N., Simulation of biomass gasification in fluidized bed reactor using ASPEN PLUS. *Biomass Bioenergy* **2008,** *32*, 1245-1254.

(135) Yan, H. M.; Rudolph, V., Modelling a compartmented fluidised bed coal gasifier process using aspen plus. *Chem. Eng. Commun.* **2000,** *183*, 1-38.

(136) Puig-Arnavat, M.; Bruno, J. C.; Coronas, A., Review and analysis of biomass gasification models. *Renewable Sustainable Energy Rev.* **2010,** *14*, 2841-2851.

(137) Doherty, W.; Reynolds, A.; Kennedy, D., The effect of air preheating in a biomass CFB gasifier using ASPEN Plus simulation. *Biomass Bioenergy* **2009,** *33*, 1158-1167.

(138) Kaushal, P.; Abedi, J.; Mahinpey, N., A comprehensive mathematical model for biomass gasification in a bubbling fluidized bed reactor. *Fuel* **2010,** *89*, 3650-3661.

(139) Beheshti, S. M.; Ghassemi, H.; Shahsavan-Markadeh, R., Process simulation of biomass gasification in a bubbling fluidized bed reactor. *Energy Convers. Manage.* **2015,** *94*, 345-352.

(140) Jakobs, T.; Djordjevic, N.; Fleck, S.; Mancini, M.; Weber, R.; Kolb, T., Gasification of high viscous slurry R&D on atomization and numerical simulation. *Appl. Energy* **2012,** *93*, 449-456.

(141) Wang, L.; Weller, C. L.; Jones, D. D.; Hanna, M. A., Contemporary issues in thermal gasification of biomass and its application to electricity and fuel production. *Biomass Bioenergy* **2008,** *32*, 573-581.

(142) Ravindranath, N. H., Biomass gasification: Environmentally sound technology for decentralized power generation, a case study from India. *Biomass Bioenergy* **1993,** *4*, 49-60.

(143) Dornburg, V.; Faaij, A. P. C., Efficiency and economy of wood-fired biomass energy systems in relation to scale regarding heat and power generation using combustion and gasification technologies. *Biomass Bioenergy* **2001,** *21*, 91-108.

(144) Voets, T.; Kuppens, T.; Cornelissen, T.; Thewys, T., Economics of electricity and heat production by gasification or flash pyrolysis of short rotation coppice in Flanders (Belgium). *Biomass Bioenergy* **2011,** *35*, 1912-1924.

(145) Administration, U. E. i. https://www.eia.gov/petroleum/weekly/crude.cfm#tabs-contract4.

(146) Sharma, A. K., Experimental investigations on a 20 kWe, solid biomass gasification system. *Biomass Bioenergy* **2011,** *35*, 421-428.

(147) Massoudi Farid, M.; Jeong, H. J.; Hwang, J., Co-gasification of coal–biomass blended char with CO2 and H2O: Effect of partial pressure of the gasifying agent on reaction kinetics. *Fuel* **2015,** *162*, 234-238.

(148) Tursun, Y.; Xu, S.; Wang, C.; Xiao, Y.; Wang, G., Steam co-gasification of biomass and coal in decoupled reactors. *Fuel Process. Technol.* **2016,** *141, Part 1*, 61-67.

(149) Kuo, P.-C.; Wu, W., Thermodynamic analysis of a combined heat and power system with CO2 utilization based on co-gasification of biomass and coal. *Chem. Eng. Sci.*

(150) Giuffrida, A.; Romano, M. C.; Lozza, G., Thermodynamic analysis of air-blown gasification for IGCC applications. *Appl. Energy* **2011,** *88*, 3949-3958.

(151) Tijmensen, M. J. A.; Faaij, A. P. C.; Hamelinck, C. N.; van Hardeveld, M. R. M., Exploration of the possibilities for production of Fischer Tropsch liquids and power via biomass gasification. *Biomass Bioenergy* **2002,** *23*, 129-152.

(152) Sari, A., Investigation of the supercritical conditions for Fischer–Tropsch reaction over an industrial Co–Ru/γ-Al2O3 catalyst. *Chem. Eng. J. (Loughborough, Engl.)* **2014,** *244*, 317-326.

(153) Munasinghe, P. C.; Khanal, S. K., Biomass-derived syngas fermentation into biofuels: Opportunities and challenges. *Bioresour. Technol.* **2010,** *101*, 5013-5022.

(154) Wender, I., Reactions of synthesis gas. *Fuel Process. Technol.* **1996,** *48*, 189-297.

(155) Sadhwani, N.; Adhikari, S.; Eden, M. R., Biomass Gasification Using Carbon Dioxide: Effect of Temperature, CO2/C Ratio, and the Study of Reactions Influencing the Process. *Ind. Eng. Chem. Res.* **2016,** *55*, 2883-2891.

(156) Herguido, J.; Corella, J.; Gonzalez-Saiz, J., Steam gasification of lignocellulosic residues in a fluidized bed at a small pilot scale. Effect of the type of feedstock. *Ind. Eng. Chem. Res.* **1992,** *31*, 1274-1282.

(157) Demirbaş, A., Mechanisms of liquefaction and pyrolysis reactions of biomass. *Energy Convers. Manage.* **2000,** *41*, 633-646.

(158) Guizani, C.; Escudero Sanz, F. J.; Salvador, S., Effects of CO2 on biomass fast pyrolysis: Reaction rate, gas yields and char reactive properties. *Fuel* **2014,** *116*, 310-320.

(159) Sadhwani, N.; Adhikari, S.; Eden, M. R.; Wang, Z.; Baker, R., Southern pines char gasification with CO2—Kinetics and effect of alkali and alkaline earth metals. *Fuel Process. Technol.* **2016,** *150*, 64-70.

(160) Bassyouni, M.; ul Hasan, S. W.; Abdel-Aziz, M. H.; Abdel-hamid, S. M. S.; Naveed, S.; Hussain, A.; Ani, F. N., Date palm waste gasification in downdraft gasifier and simulation using ASPEN HYSYS. *Energy Convers. Manage.* **2014,** *88*, 693-699.

(161) Sadhwani, N.; Liu, Z.; Eden, M. R.; Adhikari, S., Simulation, Analysis, and Assessment of CO2 Enhanced Biomass Gasification. In *Computer Aided Chemical Engineering*, Andrzej, K.; Ilkka, T., Eds. Elsevier: 2013; Vol. Volume 32, pp 421-426.

(162) Adeyemi, I.; Janajreh, I., Modeling of the entrained flow gasification: Kinetics-based ASPEN Plus model. *Renewable Energy* **2015,** *82*, 77-84.

(163) Rajul Nayak, R. K. M., Simulation of Coal Gasification Process using ASPEN PLUS. In *International Conference On Current Trends in Technology, "Nuicone – 2011"*, Institute of Technology, Nirma University, Ahmedabad, 2011.

(164) Pala, L. P. R.; Wang, Q.; Kolb, G.; Hessel, V., Steam gasification of biomass with subsequent syngas adjustment using shift reaction for syngas production: An Aspen Plus model. *Renewable Energy* **2017,** *101*, 484-492.

(165) Chaiwatanodom, P.; Vivanpatarakij, S.; Assabumrungrat, S., Thermodynamic analysis of biomass gasification with CO2 recycle for synthesis gas production. *Appl. Energy* **2014,** *114*, 10-17.

(166) Prabowo, B.; Aziz, M.; Umeki, K.; Susanto, H.; Yan, M.; Yoshikawa, K., CO2-recycling biomass gasification system for highly efficient and carbon-negative power generation. *Appl. Energy* **2015,** *158*, 97-106.

(167) Chutichai, B.; Patcharavorachot, Y.; Assabumrungrat, S.; Arpornwichanop, A., Parametric analysis of a circulating fluidized bed biomass gasifier for hydrogen production. *Energy* **2015,** *82*, 406-413.

(168) Hansen, V.; Müller-Stöver, D.; Ahrenfeldt, J.; Holm, J. K.; Henriksen, U. B.; Hauggaard-Nielsen, H., Gasification biochar as a valuable by-product for carbon sequestration and soil amendment. *Biomass Bioenergy* **2015,** *72*, 300-308.

(169) Klinghoffer, N. Utilization of char from biomass gasification in catalytic applications. COLUMBIA UNIVERSITY, 2013.

(170) Massoudi Farid, M.; Kang, M. S.; Hwang, J., The effect of CO on coal–biomass co-gasification with CO2. *Fuel* **2017,** *188*, 98-101.

(171) Zhang, Y.; Zheng, Y., Co-gasification of coal and biomass in a fixed bed reactor with separate and mixed bed configurations. *Fuel* **2016,** *183*, 132-138.

(172) Yu, M. M.; Masnadi, M. S.; Grace, J. R.; Bi, X. T.; Lim, C. J.; Li, Y., Co-gasification of biosolids with biomass: Thermogravimetric analysis and pilot scale study in a bubbling fluidized bed reactor. *Bioresour. Technol.* **2015,** *175*, 51-58.

(173) Yang, W.-C.; Chitester, D. C.; Kornosky, R. M.; Keairns, D. L., A generalized methodology for estimating minimum fluidization velocity at elevated pressure and temperature. *AIChE J.* **1985,** *31*, 1086-1092.

(174) Li, J.; Cheng, Z.; Fang, Y.; Wang, H.; Nie, W.; Huang, J.; Wang, Y., Minimum and terminal velocity in fluidization of coal gasification materials and coal blending of gasification under pressure. *Fuel* **2013,** *110*, 153-161.

(175) Pattipati, R. R.; Wen, C. Y., Minimum fluidization velocity at high temperatures. *Industrial & Engineering Chemistry Process Design and Development* **1981,** *20*, 705-707.

(176) Reschmeier, R.; Karl, J., Experimental study of wood char gasification kinetics in fluidized beds. *Biomass Bioenergy* **2016,** *85*, 288-299.

(177) van den Aarsen, F. G.; Beenackers, A. A. C. M.; van Swaaij, W. P. M., Wood Pyrolysis and Carbon Dioxide Char Gasification Kinetics in a Fluidized Bed. In *Fundamentals of Thermochemical Biomass Conversion*, Overend, R. P.; Milne, T. A.; Mudge, L. K., Eds. Springer Netherlands: 1985; pp 691-715.

(178) Fatehi, H.; Bai, X.-S., Effect of Pore Size on the Gasification of Biomass Char. *Energy Procedia* **2015,** *75*, 779-785.

Appendix A: Investigative study using Thermo Gravimetric Analysis

Before diving into detailed research about CO_2 gasification, an initial investigative study on the feedstock (pine) was done using a Thermo Gravimetric Analyzer (Shimadzu – TGA 50H) setup. 5 mg – 10 mg of pine sawdust was placed in a cylindrical alumina pan and heated at three different heating rates (5^{O}C/min, 10^{O}C/min, and 20^{O}C/min) to a temperature of 800^{o}C in a CO_2 atmosphere. The flow rate of CO_2 was maintained at 100 ml /min. The mass loss and differential mass loss were quantified and are shown in Figure A- 1.

The figure clearly shows two distinct regions of mass decay. After the initial 'bump' close to 100^{o}C which corresponds to drying, the first region of significant mass decay starts at around 250^{o}C and ends at 410^{o}C for all the three heating rates. This region corresponds to the devolatilization phase of the process. During this step, thermal degradation of cellulose and hemicellulose portions of the biomass takes place. Also, lignin with its aromatic and highly complex structure begins to degrade. The second mass decay region is seen to occur at different temperatures for the heating rates. This region corresponds to gasification step of the process where the complex gasification reactions occur and char is converted into product. These plots, especially the mass loss temperatures for 10^{o}C/min are in great agreement with studies in literature[17].

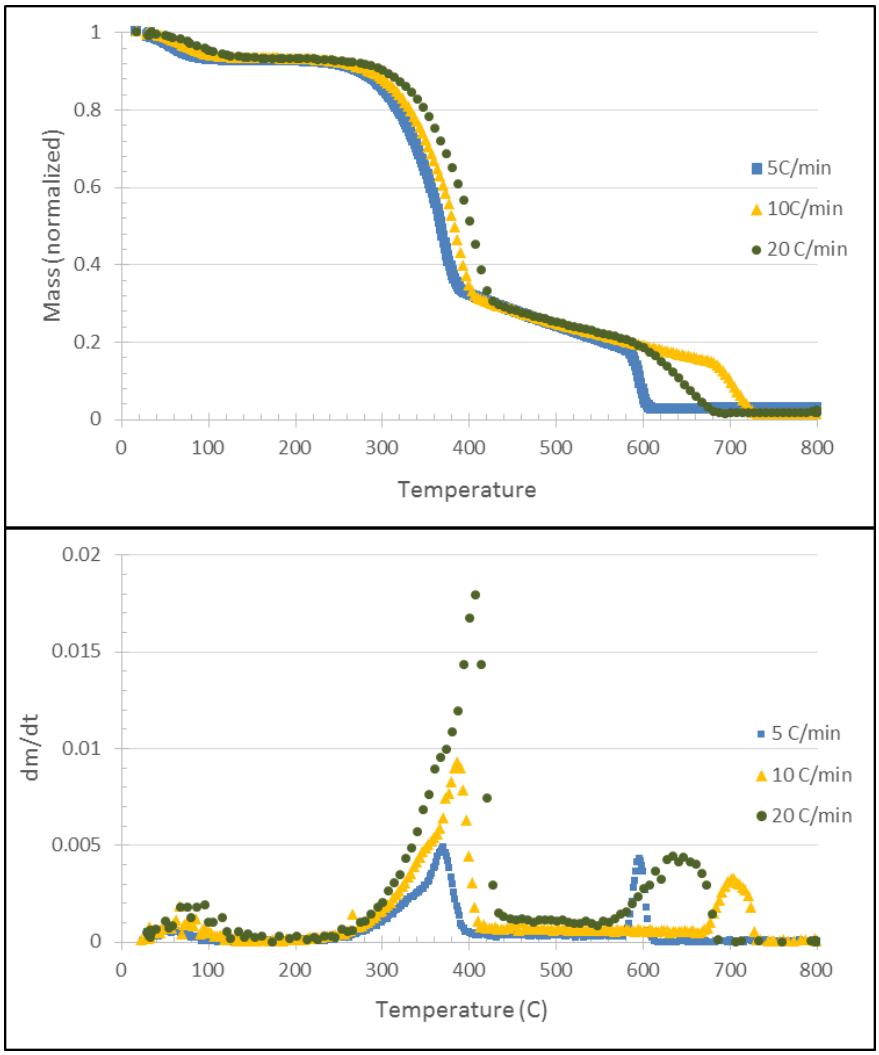

Figure A- 1 Mass loss and differential mass loss with temperature

Appendix B: Calculations for minimum fluidization velocity

Ergun's correlation for pressure drop per unit length across packed of solid particles is shown in equation [B.1][173].

$$\frac{\Delta P}{L} = \frac{150\,(1-\varepsilon)^2}{\phi^2\varepsilon^2}\frac{\mu u}{dp^2} + \frac{1.75(1-\varepsilon)u^2\,\rho\,g}{\varepsilon^3\phi dp} \qquad [B.1]$$

Where, ε is the void fraction (porosity), ϕ is the sphericity of the bed solids, μ is the dynamic viscosity, and ρ g the gas density. However, when the particle of bed fluidizes, the drag forces equal the buoyancy of the particle, thus the drag force is given by [B.2]

$$F_D = \Delta PA = AL\,(1-\varepsilon)(\,\rho\,p\,-\,\rho\,g)g \qquad [B.2]$$

These equations are solved simultaneously to obtain the minimum fluidization velocity, Umf, as defined in equation [B.3][174]:

$$Re_{mf} = [C_1^2 - C_2Ar]^{0.5} - C_1 \qquad [B.3]$$

$$Ar = \frac{\rho\,g(\,\rho\,p - \rho\,g)gdp^3}{\mu^2} \qquad [B.4]$$

The values of C_1 and C_2 have been approximated in literature[175] over a wide range of fluid properties and particle sizes and the equation is written as:

$$Re_{mf} = [33.7^2 + 0.0408Ar]^{0.5} - 33.7 \qquad [B.5]$$

For sand (ρp =2776 kg/m^3 & mean particle size dp= 263 μm), the minimum fluidization velocity was found out to be 0.0636 m/s.

For the bench scale fluidized bed gasifier used in the current research, the minimum fluidization velocity of 0.0636 m/s equals a flow rate of 7.74 liters per minute.

Appendix C: Intra particle mass transfer limitation calculations

Thiele modulus (ϕ) is the measurement of reaction rate with respect to the rate of diffusion. Lower values of ϕ (less than 0.3) imply that the rate of diffusion is high and the process is kinetically controlled whereas higher values imply that the system shows mass transfer resistance. Simplifying, the value of ϕ can be calculated using equation [C.1][176].

$$\phi = \frac{d_p}{6}\sqrt{\frac{R_{obs}}{De_{CO_2}}} \qquad [C.1]$$

Where dp = particle diameter, R_{obs} = observed reaction rate, and De = effective diffusivity which is calculated using equation [C.2].

$$De = \frac{D_{CO_2}\phi_p\,\sigma_c}{\tau} \qquad [C.2]$$

Where ϕ_p = particle porosity calculated to be 0.32, σ_c = Constriction factor and τ = tortuosity. The value of R_{obs} is calculated using the specific reaction rate obtained from a study by Van Dan Aarsen, et al. as mentioned in Appendix B. The calculated values of De and R_{obs} are plugged in equation [C.1] to yield the value of ϕ = 0.106. This implies that the process is kinetically controlled and the influence of mass transfer can be neglected.

Appendix D: Heat transfer limitations between bulk phase and particle for fluidized bed experiments

A heat balance between the particle and surrounding medium at the particle surface can be written as:

$$h * A_p * (T - T_s) = \Delta H * R_r \qquad [D.1]$$

Where h is the heat transfer coefficient (W/m^2K), A_p is the surface area of the particle (m^2), T and T_s are the temperatures (K) of the surrounding medium and the particle respectively, ΔH is the heat of reaction (kJ/mol) taking place inside the particle and R_r is the rate of reaction (mol/s). The value of h is determined using the correlation [D.2]:

$$Nu = 0.3\ Re^{1.3} \qquad [D.2]$$

Parameters in this study:

dp (biomass) = $315*10^{-6}$ m; u = 0.11 m/s; Viscosity = $1.76*10^{-5}$ Pa s; ρ_g = 1.251 kg/m^3; K = 0.024 W/mK

The value of h obtained from this correlation = 76.4 W/m^2K

Due to presence of multiple reactions in the current process, ΔH and R_r cannot be specified. Considering Boudouard reaction, ΔH = 172 kJ/mol. Van Dan Aarsen, et al.[177] studied the char – CO_2 gasification in a fluidized bed and reported the following values at 815°C:

R" (specific reaction rate) = $75.9*10^{-6}$(mol/m^2s); S_o (specific surface area) = $1.05*10^8$ (m^2/m^3). Equation [C.1] becomes:

$$h * A_p * (T - T_s) = \Delta H * R'' * S_o * V_p \quad [D.3]$$

From the above correlation, the value of (T-Ts) obtained = 1.1. Therefore, the bulk temperature of the particle has to be corrected by 1.1^{o}C

Appendix E: Sample gasification calculations and data analysis

[Objective 1] Sample calculation for fluidized bed gasification at 934^{O}C and CO_2/C ratio 1.04.

Data collected during experimental run.

Moisture content	8.03%	**Run duration**	60 min
Biomass fed	304 g (dry)	**Temperature**	934^{O}C
N_2 flow rate	10 l/min	**CO_2 flow rate**	1.6 l/min
Char	41 g	**Liquid**	32 g
CO, vol %	10.6	**H_2, vol %**	6.9
CH_4, vol %	4.9	**CO_2, vol %**	9.8
C_2H_2, vol %	0.04	**C_2H_4, vol %**	1.6

Product stream yields:

Char yield (%) = $\frac{Weight\ of\ Char\ collected}{Weight\ of\ biomass\ fed}$ X 100 = 41/304 = 13.4%

Liquid yield (%) = $\frac{Weight\ of\ Liquid\ collected}{Weight\ of\ biomass\ fed}$ X 100 = 32/304 = 10.5%

Gas yield (%) = 100 – (Char yield + liquid yield) = 100 – (13.4+10.5) = 76.1 %

Individual component yields:

Calculations for component Ci; where Ci = CO, CO_2, H_2, CH_4, C_2H_2 and C_2H_4

Flow rate of Ci = $\frac{(\text{Flow rate of } N_2) \text{ X (Vol \% Ci)}}{(Vol\% \ N_2)}$; Mass flow rate of Ci = (Flow rate of Ci) X (density of Ci)

Yield of Ci [g/kg dry biomass] = $\frac{\text{Mass flow rate of Ci}}{Feed\ rate\ of\ dry\ biomass}$ X 1000

Sample calculation for CO:

Flow rate of CO = $\frac{(\text{Flow rate of } N_2) \text{ X (Vol \% CO)}}{(Vol\% \ N_2)}$ = 10*10.6/66.16 = 1.61 l/min

Mass flow rate of CO = 1.61 * 1.25 (g/l) = 2.02 g/min

Yield of CO = 2.02 / 5.07 (g/min biomass) X 1000 = 398.5 g/kg dry biomass

Carbon conversion to gases:

C conversion to gases = $\frac{\sum Carbon\ out\ from\ CO,CO_2,CH_4,C_2H_4,C_2H_2}{\sum Carbon\ in\ from\ CO_2\ and\ biomass}$ X 100

Carbon out from gases = $\sum C\ content\ of\ CO, CO_2, CH_4, C_2H_4, C_2H_2$ X syngas yield (mol) X 12

= [(10.6 + 9.8 + 4.9 + 2*0.04+ 2*1.6)/100] * 0.12 * 12

= 0.49 kg/kg dry biomass

Carbon in from CO_2 & biomass = {[CO_2 flow rate X Density X (12/44)]/dry biomass feed rate] + Carbon % in biomass /100}

= [1.6 * 1.84 * (12/44)/ 5.06] + 47.49/100

= 0.63 kg/kg dry biomass

Carbon conversion to gases = (0.49/0.63) * 100

= 76.53%

Overall Carbon conversion = carbon conversion to gases + $\frac{\sum Carbon\ out\ from\ Char}{\sum Carbon\ in\ from\ CO_2\ and\ biomass}$

Carbon out from char = Amount of char collected X carbon % in char

= 41 * (81.14/100)

Carbon out from char = 33.27 g

Carbon yield from char = 0.11 kg/kg dry biomass

Carbon conversion to char = (0.11/0.63) * 100

= 17.27%

Overall carbon conversion = 76.53 + 17.27

= 93.8 %

Syngas heating value HHV = $\sum[volume\ fraction\ of\ Ci * Individual\ heating\ value\ of\ Ci]$

Individual heating values: CO =12.68 MJ/Nm^3; H_2 = 12.81 MJ/Nm^3; CH_4 = 39.78 MJ/Nm^3

HHV = [10.6 * 12.68 + 6.9 * 12.81 + 4.9 * 39.78] / 100

= [134.4 + 150.49 + 194.93] / 100

= 4.79 MJ/Nm^3

[Objective 2] Sample calculation for fixed bed reactor at 850^{O}C.

RPM predicted surface area calculation

RPM predicts that the surface area of the particle increases during the initial conversion phase due to the expansion of pores. The surface area of the particle can be correlated to conversion using equation below[178].

$$S = S_0(1-X)\sqrt{1-\ \Psi \ln(1-X)}$$

Where S_0 = initial char pore area (measured), Ψ = initial pore structure parameter(fitted) and X = conversion

Initial char pore surface area = 197.06 m^2/g

Value of Ψ = 15.54

Sample conversion value X = 0.25

$$S = 197.06 * (1-0.25) * \sqrt{1 - 15.54 * \ln(1 - 0.25)}$$

$$= 197 * 0.75 * 2.34$$

$$= 345.58\ m^2/g$$

[Objective 2] Arrhenius plots and calculation for activation energy (E_a)

Arrhenius equation: $K = A * \exp(-E_a/RT)$

Where K = rate constant, A = pre-exponential or frequency factor, Ea = Activation energy and R = universal gas constant = 8.314 J/mol K

Taking natural log of both sides;

$$\ln K = \ln A + [-E_a/R] * (1/T)$$

The value of activation energy and pre-exponential factor (frequency factor) is calculated by plotting ln K against the inverse of temperature.

Arrhenius plots for unloaded chars (using rate constant from three different models)

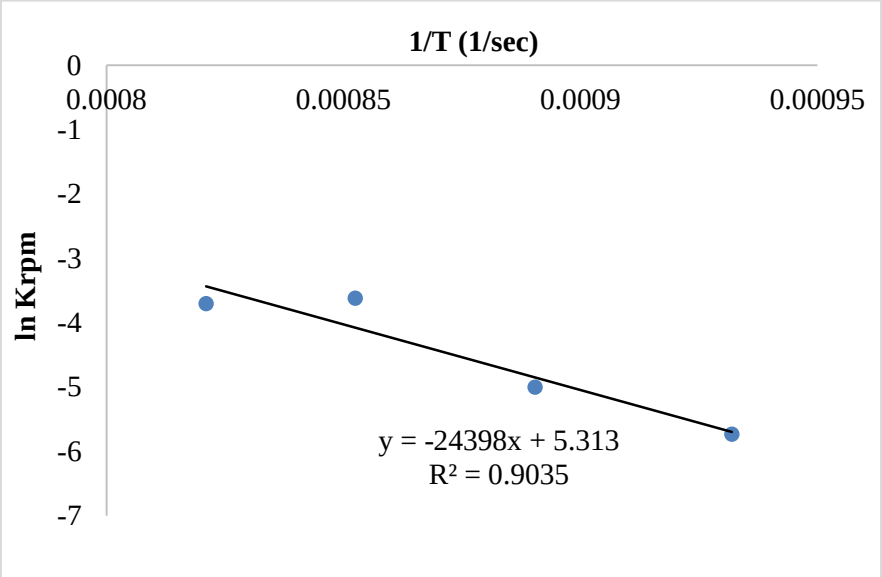

Figure E- 1 Arrhenius plot for unloaded char (RPM)

Calculations for unloaded char (RPM)

Slope = $[-E_a/R]$ = -24398

Ea = 24398 * 8.314 = 202.85 kJ/mol

ln A = 5.31

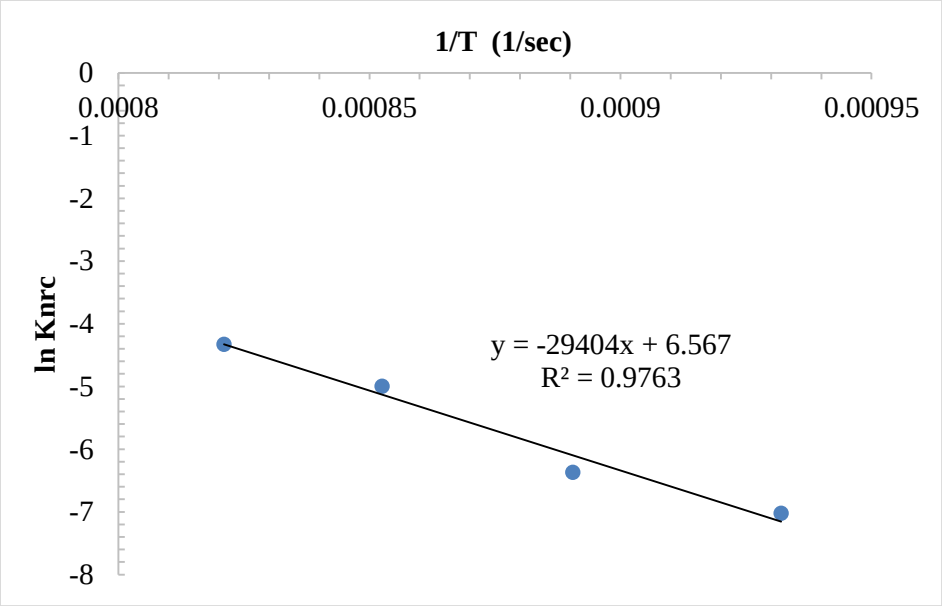

Figure E- 2 Arrhenius plot for unloaded char (NRC)

Calculations for unloaded char (NRC)

Slope = $[-E_a/R]$ = -29404

Ea = 29404 * 8.314 = 244.64 kJ/mol

ln A = 6.57

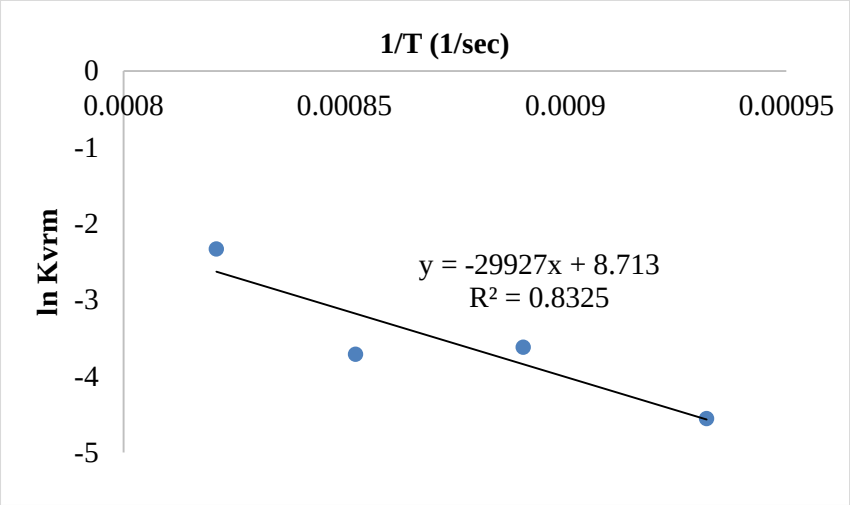

Figure E- 3 Arrhenius plot for unloaded char (VRM)

Calculations for unloaded char (VRM))

Slope = $[-E_a/R]$ = -29927

Ea = 29927 * 8.314 = 248.82 kJ/mol

ln A = 8.71

Arrhenius plots for loaded chars (using rate constant from RPM)

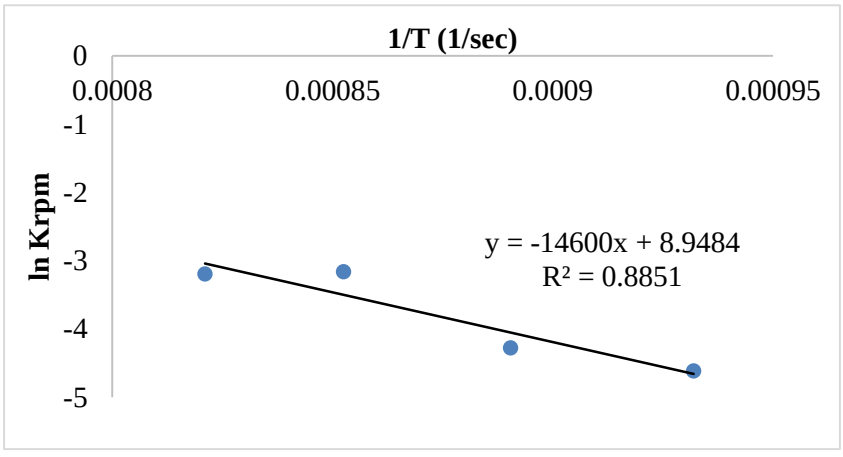

Figure E- 4 Arrhenius plot for K-loaded char

Calculations for K-loaded char

Slope = [$-E_a/R$] = -14600

Ea = 14600 * 8.314 = 121.39 kJ/mol

ln A = 8.95

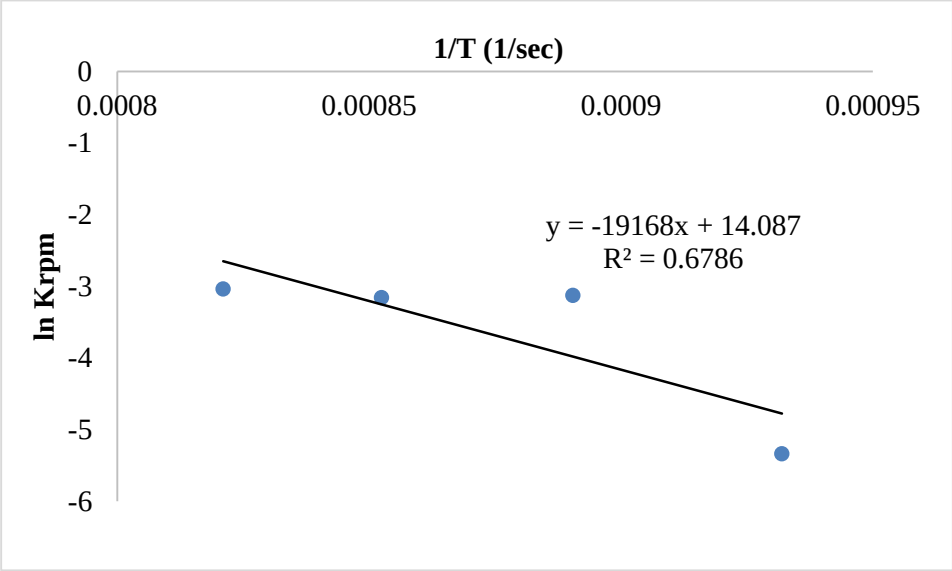

Figure E- 5 Arrhenius plot for Na-loaded char

Calculations for Na-loaded char

Slope = [$-E_a/R$] = -19168

Ea = 19168 * 8.314 = 159.36 kJ/mol

ln A = 14.087

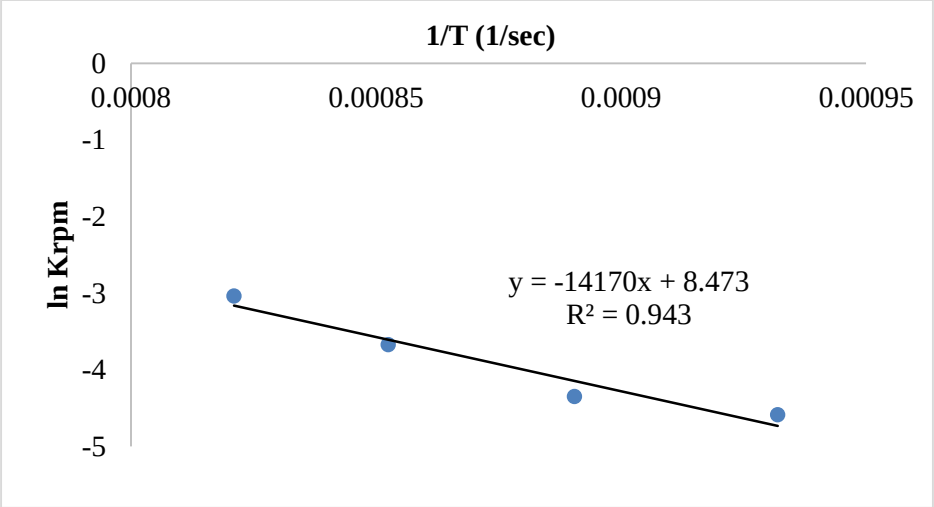

Figure E- 6 Arrhenius plot for Ca-loaded char

Calculations for Ca-loaded char

Slope = $[-E_a/R]$ = -14170

Ea = 14170 * 8.314 = 117.81 kJ/mol

ln A = 8.47

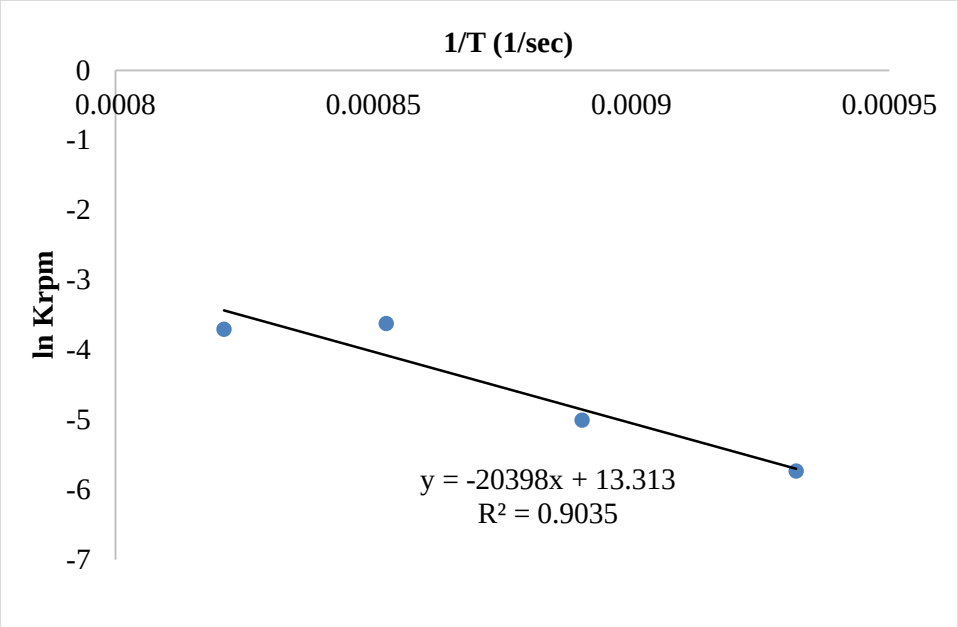

Figure E- 7 Arrhenius plot for Mg-loaded char

Calculations for Mg-loaded char

Slope = $[-E_a/R]$ = -20398

Ea = 20398 * 8.314 = 169.59 kJ/mol

ln A = 13.313

Data Analysis:

One-way Analysis of Variance of the Effect of Temperature on individual gas yields

Table E. 1 One-way ANOVA table for CO yield variation with temperature

Source	DF	SS	MS	F	P
Between groups	3	81205	27068	44.87	0.002
Within groups	4	2413	603		
Total	7	83618			

Table E. 2 One-way ANOVA table for H_2 yield variation with temperature

Source	DF	SS	MS	F	P
Between groups	3	263.66	87.89	28.35	0.004
Within groups	4	12.4	3.1		
Total	7	276.06			

Table E. 3 One-way ANOVA table for CH_4 yield variation with temperature

Source	DF	SS	MS	F	P
Between groups	3	2517	839	5.64	0.064
Within groups	4	595	149		
Total	7	3111			

Table E. 4 One-way ANOVA table for C_2H_4 yield variation with temperature

Source	DF	SS	MS	F	P
Between groups	3	1980	660	1.66	0.311
Within groups	4	1590	397		
Total	7	3570			

Table E. 5 One-way ANOVA table for C_2H_2 yield variation with temperature

Source	DF	SS	MS	F	P
Between groups	3	5.96	1.99	5.83	0.061
Within groups	4	1.36	0.34		
Total	7	7.32			

One-way Analysis of Variance of the Effect of Temperature on product stream yields

Table E. 6 One-way ANOVA table for char yield variation with temperature

Source	DF	SS	MS	F	P
Between groups	3	699.1	233.1	83.58	0.005
Within groups	4	11.15	2.79		
Total	7	710.28			

Table E. 7 One-way ANOVA table for liquid yield variation with temperature

Source	DF	SS	MS	F	P
Between groups	3	49.97	16.65	42.32	0.002
Within groups	4	1.57	0.39		
Total	7	51.55			

Table E. 8 One-way ANOVA table for gas yield variation with temperature

Source	DF	SS	MS	F	P
Between groups	3	1093.7	364.6	173.7	0.0001
Within groups	4	8.39	2.10		
Total	7	1102.9			

One-way Analysis of Variance of the Effect of Temperature on syngas characteristics

Table E. 9 One-way ANOVA table for carbon conversion to gases variation with temperature

Source	DF	SS	MS	F	P
Between groups	3	365	122	0.83	0.541
Within groups	4	584	146		
Total	7	949			

Table E. 10 One-way ANOVA table for HHV of syngas variation with temperature

Source	DF	SS	MS	F	P
Between groups	3	4.83	1.61	4.51	0.09
Within groups	4	1.43	0.36		
Total	7	6.26			

One-way Analysis of Variance of the Effect of CO_2/C ratio on Individual gas yields

Table E. 11 One-way ANOVA table for CO yield variation with CO_2/C ratio

Source	DF	SS	MS	F	P
Between groups	3	48495	16165	14.83	0.016
Within groups	4	4359	1090		
Total	7	52854			

Table E. 12 One-way ANOVA table for H_2 yield variation with CO_2/C ratio

Source	DF	SS	MS	F	P
Between groups	3	120.2	40.1	61	0.011
Within groups	4	2.6	0.6		
Total	7	122.8			

Table E. 13 One-way ANOVA table for CH_4 yield variation with CO_2/C ratio

Source	DF	SS	MS	F	P
Between groups	3	4303	1434	13.8	0.013
Within groups	4	416	104		
Total	7	4719			

Table E. 14 One-way ANOVA table for C_2H_4 yield variation with CO_2/C ratio

Source	DF	SS	MS	F	P
Between groups	3	454.8	151.6	24.5	0.005
Within groups	4	24.7	6.2		
Total	7	479.5			

Table E. 15 One-way ANOVA table for C_2H_2 yield variation with CO_2/C ratio

Source	DF	SS	MS	F	P
Between groups	3	0.78	0.26	11.78	0.019
Within groups	4	0.09	0.02		
Total	7	0.87			

One-way Analysis of Variance of the Effect of CO_2/C ratio on syngas characteristics

Table E. 16 One-way ANOVA table for syngas yield variation with CO_2/C ratio

Source	DF	SS	MS	F	P
Between groups	3	0.18	0.06	18.81	0.008
Within groups	4	0.01	0.01		
Total	7	0.19			

Table E. 17 One-way ANOVA table for carbon conversion to gases variation with CO_2/C ratio

Source	DF	SS	MS	F	P
Between groups	3	149.9	50.0	4.89	0.08
Within groups	4	40.8	10.2		
Total	7	190.8			

Table E. 18 One-way ANOVA table for syngas HHV variation with CO_2/C ratio

Source	DF	SS	MS	F	P
Between groups	3	11.43	3.81	4.20	0.10
Within groups	4	3.63	0.91		
Total	7	15.06			

Appendix F: Heat transfer limitations between bulk phase and particle for fixed bed experiments

A heat balance between the particle and surrounding medium at the particle surface can be written as:

$$h * A_p * (T - T_s) = \Delta H * R_r \qquad [F.1]$$

Where h is the heat transfer coefficient (W/m^2K), A_p is the surface area of the particle (m^2), T and T_s are the temperatures (K) of the surrounding medium and the particle respectively, ΔH is the heat of reaction (kJ/mol) taking place inside the particle and R_r is the rate of reaction (mol/s). The value of h is determined using the correlation F.2 for forced convection at low Re values.

$$Nu = 0.3\ Re^{1.3} \qquad [F.2]$$

Parameters in this study:

dp (biomass) = $275*10^{-6}$ m; u = 0.11 m/s; Viscosity = $1.53*10^{-5}$ Pa s; ρ_g = 1.842 kg/m^3; K = 0.015 W/mK

The value of h obtained from this correlation [F.2] = 76.4 W/m^2K

For Boudouard reaction, ΔH = 172 kJ/mol. Using equation [F.1] and values of reaction rates at different temperatures, the difference between particle and bulk temperature are obtained as shown in table F.1.

Table F. 1 Temperature correction for particles at different temperatures

Temperature (^oC)	$T - T_s$ (^oC)
800	0.85
850	2.6
900	3.4
945	5.2
975	6.9

Appendix G: SEM-EDX analysis on metal-loaded chars

Chars loaded with metal catalysts were subjected to ICP-MS analysis for accurate measurement of the amount loaded. These chars were further subjected to Energy-dispersive X-ray spectroscopy analysis (EDX) to understand the distribution of the metals on the char surface.

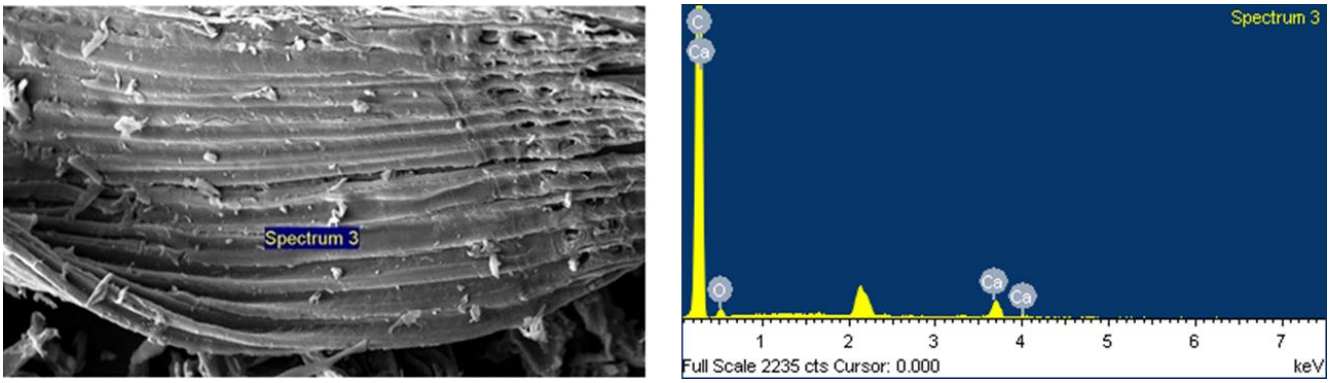

Figure G- 1 EDX analysis of calcium loaded char

Figure G-1 shows the EDX analysis performed on a calcium loaded char particle. In the image, the "chunks" on the char surface showed higher concentration of metal than the rest of the surface. It was postulated that these "chunks" act as anchor points for the metal to adhere to the surface of the char. Such points were distributed evenly throughout the char surface implying even distribution of the metal on the char surface.

Appendix H: Preliminary ASPEN plus model considering only Gibbs free energy minimization

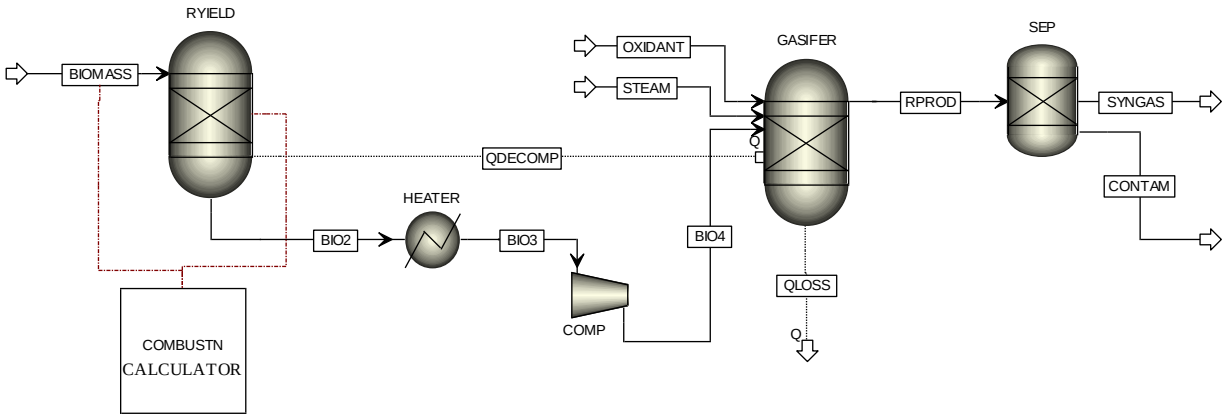

Figure H- 1 Thermodynamic equilibrium model for biomass gasification

A preliminary model based on thermodynamic equilibrium using ASPEN plus was developed in the initial stages of the current research. The model employed RYIELD reactor for splitting biomass into components; and RGIBBS reactor for the gasification step which uses a Gibbs free energy minimization routine to identify all possible products from gasification of the input materials. Various input streams containing carbon dioxide, biomass components and steam entered the RGIBBS reactor. The effect of temperature, pressure and steam addition on the output syngas composition was tested and reported[161].

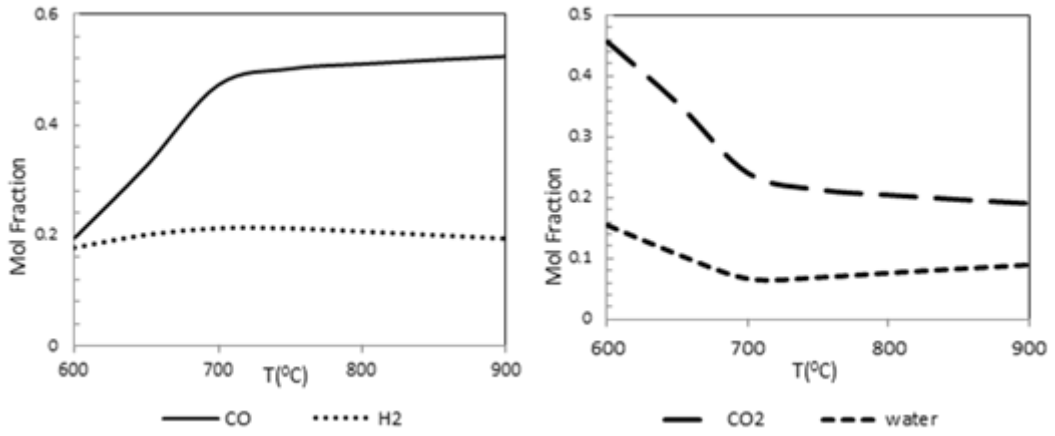

Figure H- 2 Effect of temperature on CO-H_2 conc. (left), CO_2-H_2O conc. (right)

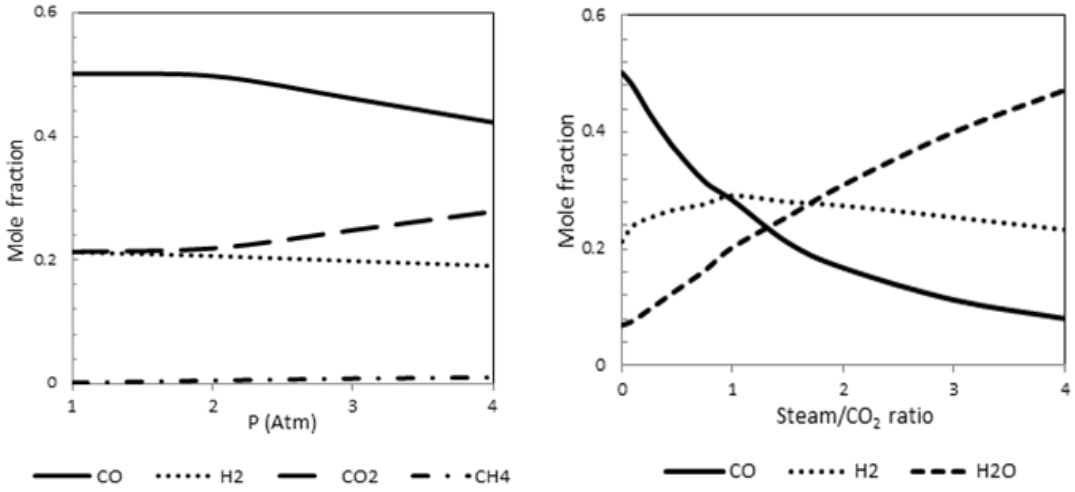

Figure H- 3 Effect of pressure and steam addition on syngas composition

Appendix I: List of components specified for the ASPEN Plus model

Table I. 1 List of components specified for the ASPEN plus model

Component ID	Type	Component name	Alias
C	Solid	CARBON-GRAPHITE	C
CO2	Conventional	CARBON-DIOXIDE	CO2
CO	Conventional	CARBON-MONOXIDE	CO
N2	Conventional	NITROGEN	N2
O2	Conventional	OXYGEN	O2
BIOMASS	Nonconventional		
H2	Conventional	HYDROGEN	H2
CH4	Conventional	METHANE	CH4
ASH	Nonconventional		
COS	Conventional	CARBONYL-SULFIDE	COS
H2S	Conventional	HYDROGEN-SULFIDE	H2S
NH3	Conventional	AMMONIA	H3N
HCL	Conventional	HYDROGEN-CHLORIDE	HCL
HCN	Conventional	HYDROGEN-CYANIDE	CHN
CL2	Conventional	CHLORINE	CL2
S	Conventional	SULFUR	S
TOLUENE	Conventional	TOLUENE	C7H8
C8H10-01	Conventional	O-XYLENE	C8H10-1
C8H10-02	Conventional	P-XYLENE	C8H10-3
NAPHTHAL	Conventional	NAPHTHALENE	C10H8
PHENOL	Conventional	PHENOL	C6H6O
STYRENE	Conventional	STYRENE	C8H8

INDENE	Conventional	INDENE	C9H8
ETHYLBEN	Conventional	ETHYLBENZENE	C8H10-4
C7H8O-01	Conventional	M-CRESOL	C7H8O-4
C9H8O	Conventional	2-METHYLBENZOFURAN	C9H8O
C9H10-01	Conventional	M-METHYL-STYRENE	C9H10-E2
H2O	Conventional	WATER	H2O
C2H2	Conventional	ACETYLENE	C2H2
C2H4	Conventional	ETHYLENE	C2H4

Appendix J: Fortran subroutine code for inclusion of kinetics in the ASPEN plus model

```
      SUBROUTINE KINTCS (SOUT,   NSUBS,  IDXSUB,   ITYPE,  NINT,
     2                   INT,    NREAL,  REAL,     IDS,    NPO,
     3                   NBOPST, NIWORK, IWORK,    NWORK,  WORK,
     4                   NC,     NR,     STOIC,    RATES,  FLUXM,
     5                   FLUXS,  XCURR,  NTCAT,    RATCAT, NTSSAT,
     6                   RATSSA, KCALL,  KFAIL,    KFLASH, NCOMP,
     7                   IDX,    Y,      X,        X1,     X2,
     8                   NRALL,  RATALL, NUSERV,   USERV,  NINTR,
     9                   INTR,   NREALR, REALR,    NIWR,   IWR,
     *                   NWR,    WR,     NRL,      RATEL,  NRV,
     1                   RATEV)
C
      IMPLICIT NONE

      INTEGER NSUBS, NINT,  NPO,   NIWORK,NWORK,
     +        NC,    NR,    NTCAT, NTSSAT,NCOMP,
     +        NRALL, NUSERV,NINTR, NREALR,NIWR,
     +        NWR
C
C
#include "ppexec_user.cmn"
      EQUIVALENCE (RMISS, USER_RUMISS)
      EQUIVALENCE (IMISS, USER_IUMISS)
C.....RCSTR...
#include "rcst_rcstri.cmn"
#include "rxn_rcstrr.cmn"
C
C
      EQUIVALENCE (TEMP, RPROPS_UTEMP)
      EQUIVALENCE (PRES, RPROPS_UPRES)
      EQUIVALENCE (VFRAC, RPROPS_UVFRAC)
      EQUIVALENCE (BETA, RPROPS_UBETA)
      EQUIVALENCE (VVAP, RPROPS_UVVAP)
      EQUIVALENCE (VLIQ, RPROPS_UVLIQ)
      EQUIVALENCE (VLIQS, RPROPS_UVLIQS)
C
C     DECLARE ARGUMENTS
      INTEGER IDXSUB(NSUBS),ITYPE(NSUBS), INT(NINT),
```

```
     +       IDS(2),NBOPST(6,NPO),IWORK(NIWORK),
     +       IDX(NCOMP),   INTR(NINTR),  IWR(NIWR),
     +       NREAL, KCALL, KFAIL, KFLASH,NRL,
     +       NRV,   I
      REAL*8 SOUT(1),     WORK(NWORK),
     +      STOIC(NC,NSUBS,NR),  RATES(1),
     +      FLUXM(1),    FLUXS(1),    RATCAT(NTCAT),
     +      RATSSA(NTSSAT),     Y(NCOMP),
     +      X(NCOMP),    X1(NCOMP),   X2(NCOMP)
      REAL*8 RATALL(NRALL),USERV(NUSERV),
     +      REALR(NREALR),WR(NWR),     RATEL(1),
     +      RATEV(1),    XCURR

C
C    DECLARE LOCAL VARIABLES
C
      INTEGER IMISS
      REAL*8 REAL(NREAL),  RMISS, XLEN,  DIAM,  TEMP,
     +      PRES,  VFRAC, BETA,  VVAP,  VLIQ,
     +      VLIQS

      INTEGER J, KDIAG, KV, KER
      REAL*8 xmolar(NC), VMX, DVMX, Si,
     +      vel(1), Eac, Kfor, Rg, LNx(NC)

C          DECLARE MOLAR FRACTION AS A FUNCTION OF TOTAL COMPONENTS

      DO J=1, NC
       xmolar(J) = (SOUT(J)/SOUT(NC+1))
      END DO

C          SPECIFY VARIABLES AND FUNCTIONS

      DO J=1, NC
         LNx(J) = LOG(1-xmolar(J))
      END DO

      KV = 1
      KDIAG = 2
      CALL PPMON_VOLV (TEMP, PRES, xmolar, NC, IDX, NBOPST, KDIAG, KV,
     +              VMX, DVMX, KER)

C DECLARE INDIVIDUAL RATES FOR C, CO2, CO
C DECLARE RPM RATE EXPRESSION

      Rg = 8.314
      Eac = 219.0
      Kfor = 5.13
```

```
vel(1)=VLIQ*Kfor*EXP(-Eac/Rg/TEMP)*(1-xmolar(1))*(1-((Si)*LNx(1)))

RATES(1) = -(vel(1))
RATES(2) = -(vel(1))
RATES(3) = 2.0*vel(1)

RETURN
END
```

Appendix K: Publications

The research carried out for this dissertation has resulted in three peer-reviewed publications which are mentioned here. In addition, the research has led to a number of oral and poster presentations at various national conferences.

1. **N. Sadhwani**, M.R. Eden, S. Adhikari, Z. Wang, R. Baker (2016), **"**Southern pines char gasification with CO_2 - Kinetics and effect of alkali and alkaline earth metals", Fuel Processing Technology, Elsevier, vol. 150, pages 64-70.

2. **N. Sadhwani**, M.R. Eden, S. Adhikari (2016), **"**Biomass gasification using carbon dioxide: Effect of temperature, CO_2/C ratio and the study of reactions influencing the process", Industrial and Engineering Chemistry Research, ACS publications, vol. 55, pages 2883–2891.

3. **N. Sadhwani**, Z. Liu, M.R. Eden, S. Adhikari (2013), "Simulation, Analysis and Assessment of CO_2 Enhanced Biomass Gasification", Computer Aided Chemical Engineering, Elsevier, volume 32, pages 421–426.

4. **N. Sadhwani**, M.R. Eden, S. Adhikari (2017), "Process Modeling of Fluidized Bed Biomass-CO_2 Gasification using ASPEN Plus", submitted to Computer Aided Chemical Engineering, for ESCAPE-2017.